Development and Investigation of High-Performance Fire Retardant Polypropylene Nanocomposites via High Energy Electrons

DISSERTATION

Zur Erlangung des akademischen Grades

Doktor rerum naturalium

(Dr. rer. nat.)

Vorgelegt

der Fakultät Mathematik und Naturwissenschaften

der Technischen Universität Dresden

von

M.Sc. Dan Xiao

geboren am 24 Januar 1987 in Hunan, China

Eingereicht am: 17/07/2017

Die Dissertation wurde in der Zeit von Februar 2014 bis Februar 2017 im Leibniz-Institut für Polymerforschung Dresden e. V. angefertigt.

Abstract

Polypropylene (PP) has excellent mechanical and chemical properties. Thus, it is used in a wide range of applications. However, like for most polymers, the high flammability of PP limits its application in various fields requiring specific flame-retardant standards. Some of halogenated flame retardants are restricted by European Community directives ROHs, WEEE and REACH. Now metallic hydroxides flame retardants are widely used in industry, but the high loading (about 60 wt %) seriously destroys the mechanical properties of polymeric materials. To improve the performance of flame retardant polymers, an environment-friendly electron beam (EB) technology has been successfully used in modifying flame retardant and polymer matrix.

In this work, high efficient functional intumescent flame retardants and functional surfactant are designed and prepared for EB technology. In-depth studies the thermal stability, fire behavior and mechanical properties of these flame retardant PP composites have been studied. The possible graft-linking and cross-linking mechanisms of such EB modified composites can be well established. Specially, it is shown that the novel surfactant has better thermal stability in comparison to traditionally used modifiers.

Another part of this work deals with the exploration of novel allylamine polyphosphate (AAPP) as flame retardant crosslinker for PP by electron beam (EB) treatment. Multifunctional AAPP showed unique efficient intumescent flame retardant properties. The limiting oxygen index (LOI) value and the effective melt drop resistance in UL-94 test of multifunctional flame retardant PP composites is greatly enhanced. In the cone calorimeter test, a reduction of peak heat release rate, total heat release and smoke production is achieved. Moreover, EB treatment increased the thermal stability of these designed flame retardant PP composites. Furthermore, AAPP provided an excellent quality of char residue in the combustion stage due to P−N−C and P−O−C structure. In addition, synergistic mechanism of AAPP with montmorillonite (MMT) was explored.

Finally, different EB parameters have been used to modify fire retardant polymer nanocomposites. The effects of EB treatment on thermal stability, fire behavior and mechanical properties of fire retardant PP nanocomposites have been discussed. The heat release, the production of toxic gases and the mass loss of EB modified fire retardant PP nanocomposites are delayed in accordance to the result of cone calorimeter test. Based on these results high performance fire retardant polymer nanocomposites can be developed for industrial applications such as insulated material of wire, cable, etc.

Acknowledgement

First of all, I would like to express my sincerest and heartfelt gratitude to Prof. Dr. Brigitte Voit for providing me with the opportunity at Leibniz-Institut für Polymerforschung (IPF) and for her valuable comments and discussions.

I am extremely indebted to Prof. Dr. De-Yi Wang and Dr. Uwe Gohs for their encouragement, supervision, and support. Their affection and love let me go through the most difficult time. Without their help, this topic would not be a reality. They are very nice persons and their humble and friendly personality are touched other aspects of my life. Besides, I am deeply thankful to Prof. Gert Heinrich and Prof. Udo Wagenknecht for giving me all necessary support. Futhermore, I thank Dr. Andreas Leuteritz for his scientific inputs.

I thankfully acknowledge the support of M.Eng. Carsten Zschech for helping me in carrying out electron beam experiments and Mrs. Anne Hofmann for her assistance. I would like to thank all of the technical staffs in IPF included Mrs. Sabine Krause for thermal analysis, Dr. Dieter Jehnichen for X-ray diffraction, Dr. Hartmut Komber for NMR characterization, Dr. Mikhail Malanin for FTIR characterization, Mr. Bernd Kretzschmar for processing work, Mrs. Regine Boldt for TEM analysis, Mrs. Maria Auf der Landwehr for MCC tests and SEM-EDX characterization as well as Mr. Joachim Gensch for blending process. I also have to thank Mr. Zhi Li for the cone calorimeter and mechanical properties tests at IMDEA Materials Institute in Madrid, Mr. Sergio De Juan for injection molding, and Ms. Xiao-min Zhao for morphology of the char residues. In particular, I sincerely appreciate Prof. Dr. De-Yi Wang providing me an opportunity to visit IMDEA and supervising me for the synthesis of AAPP at his research group in IMDEA Materials Institute in Spain.

In addition, I would like to express my sincere thanks and gratitude to Dr. Debdipta Basu, Dr. Shang-Lin Gao, Dr. Yao-Ming Zhang, Ms. Xiao-Ling Liu, Dr. Mimi Hetti, Mr. Natarajan Tamil Selvan, Ms. Alexandra Irina Lazar, and Mr. Peng-Cheng Zhao during my stay in Germany. Moreover, my deep and humble appreciation goes to my family, in particular my parents, for their unconditional support, encouragement and love.

Finally and but not the least, I acknowledge financial support from the China Scholarship Council (PhD program Nr.201308530045), the STSM support from COST MP1105 (MP1105-090315-053686) and IPF sholarship.

List of symbols

σ	Stress
ε	Strain
d	Interlayer distance
θ	Angle between incident beam and planes
λ	Wavelength
C=C	Carbon carbon double bond
$T_{-1\ \%}$	1 wt % of weight loss
$T_{-3\ \%}$	3 wt % of weight loss
$T_{-5\ \%}$	5 wt % of weight loss
T_{max}	Maximum decomposition temperature
R_{max}	Rate of maximum mass loss
D	Dose
E	Energy
E_{pol}	Energy absorbed per polymer chain
m	Mass
m_{pol}	Average mass of the polymer chain
N_r	Average number of radicals per PP molecule
N_A	Advogadro constant
G_t	Total number of radicals generated per 100 eV of absorbed energy
$N^{PP}{}_r$	Overall number of PP radicals
N^{FR}	Overall number of FR molecules
N	Number of molecules
N.R.	No rating
n	Amount of substance
c	Concentration
M_n	Number average molecular mass
wt %	Weight percent

List of abbreviations

AAPP	Allylamine polyphosphate
$Al(OH)_3$	Aluminum hydroxide
APP	Ammonium polyphosphate
ASTM	American society for testing and materials
CC	Cone calorimeter
CEC	Cation exchange capacity
CO	Carbon monoxide
CO_2	Carbon dioxide
DIN	Deutsches Institut für Normung
DSC	Differential scanning calorimetry
DTG	Derivative thermogravimetry
DPA	N^1- (5,5-dimethyl-1,3,2-dioxaphosphinyl-2-yl)-acrylamide
EB	Electron beam (state of the art technology)
EDX	Energy-dispersive X-ray spectroscopy
EELS	Electron energy-loss spectroscopy
EOC	Ethylene octene copolymer
EPDM	Ethylene propylene diene terpolymer
EPR	Electron paramagnanetic resonance spectroscopy
EIReP	Electron induced reactive processing
EU	European Union
EVA	Ethylene-vinyl acetate copolymer
FO-MMT	Functional organically modified montmorillonite
FR	Flame retardant
FTIR	Fourier transform infrared spectroscopy
HRR	Heat release rate
IFR	Intumescent flame retardant
IFR1	Weight ratio of DPA and APP was 1:2
IFR2	Weight ratio of SPSA and APP was 1:2
ISO	International organization for standardization
LDH	Layered double hydroxides
LLDPE	Linear low density polyethylene

LOI	Limiting oxygen index
$Mg(OH)_2$	Magnesium hydroxide
ML	Mass loss
MMT	Montmorillonite
O-MMT	Surface of montmorillonite was coated with bis(2-hydroxyethyl)-methyl-octadecyl-ammonium group
MMT-Na	Sodium montmorillonite
NMR	Nuclear magnetic resonance spectroscopy
NR	Natural rubber
N_2	Nitrogen
PE	Polyethylene
PER	Pentaerythritol
PFM	Polyfunctional monomer
PHRR	Peak heat release rate
PP	Polypropylene
ROHs	Restriction of hazardous substaces directive
REACH	Registration, Evaluation, Authorisation and restriction of Chemicals
SEM	Scanning electron microscopy
SPR	Smoke production rate
SPSA	Spirocylic pentaerythritol bisphosphorate disphosphoryl-di-prop-2-en-1-amine
TAC	Triallyl cyanurate
TEM	Transmission electron microscopy
TG-FTIR	Thermogravimetry – fourier transform infrared spectroscopy
THR	Total heat release
TPB	Thetriphenyl(undec-10-enyl)phosphonium bromide
TSP	Total smoke production
UL94	Standard for safety of flammability of plastic materials for parts in devices and appliances testing
UV	Ultraviolet
WAXS	Wide angle X-ray scattering
WEEE	Waste electrical and electronic equipment

Contents

Chapter 1

Introduction

1.1 Brief overview of polymer combustion

Synthetic and natural polymers play an essential and ubiquitous role in our life. However, when enough heat energy is exposed, most of them are generating flammable volatiles. If these combustible gases mix with air and undergo ignition, it starts to burn. There are three essential factors for the whole combustion process. These are heat, fuel and oxygen [1]. When enough heat is transfered to polymers to start the pyrolysis, the polymers can spontaneously burn [2]. The proposed combustion cycle is established in Fig. 1.1.

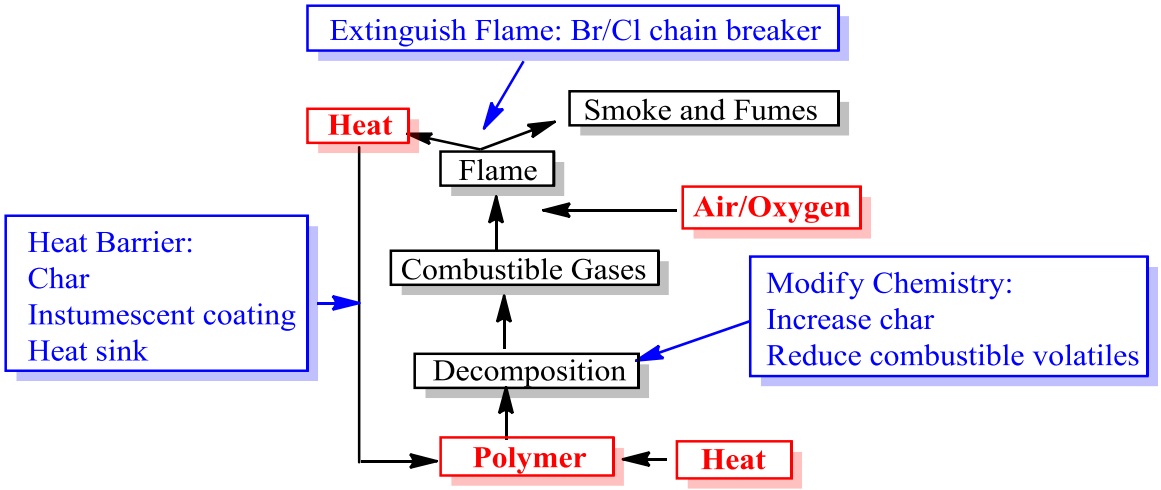

Fig. 1.1 Polymer combustion cycle [2]

The fire scenario can basically be split into three phases: the ignition, development and fully developed fire, like Fig. 1.2 [3]. The ignition stage usually starts when the temperature of combustible materials (e.g. furniture, computer, cable, etc.) reaches the ignition temperature and reacts with air. The development of fire pressure, heat flux, temperature, toxic gases and combustible degradation products is increased via the spread of other igniting materials. If the overall temperature is high enough and sufficient oxygen is available, there is a sudden transition to a growth stage to a fully developed fire with a total surface involvement of all combustible materials. In addition, the heat release achieves the highest value. Finally, the spread of fire maybe quickly threaten possession, livelihood, wealth and life [4]. Due to this high potential fire risk, more and more fire protection standards are formulated.

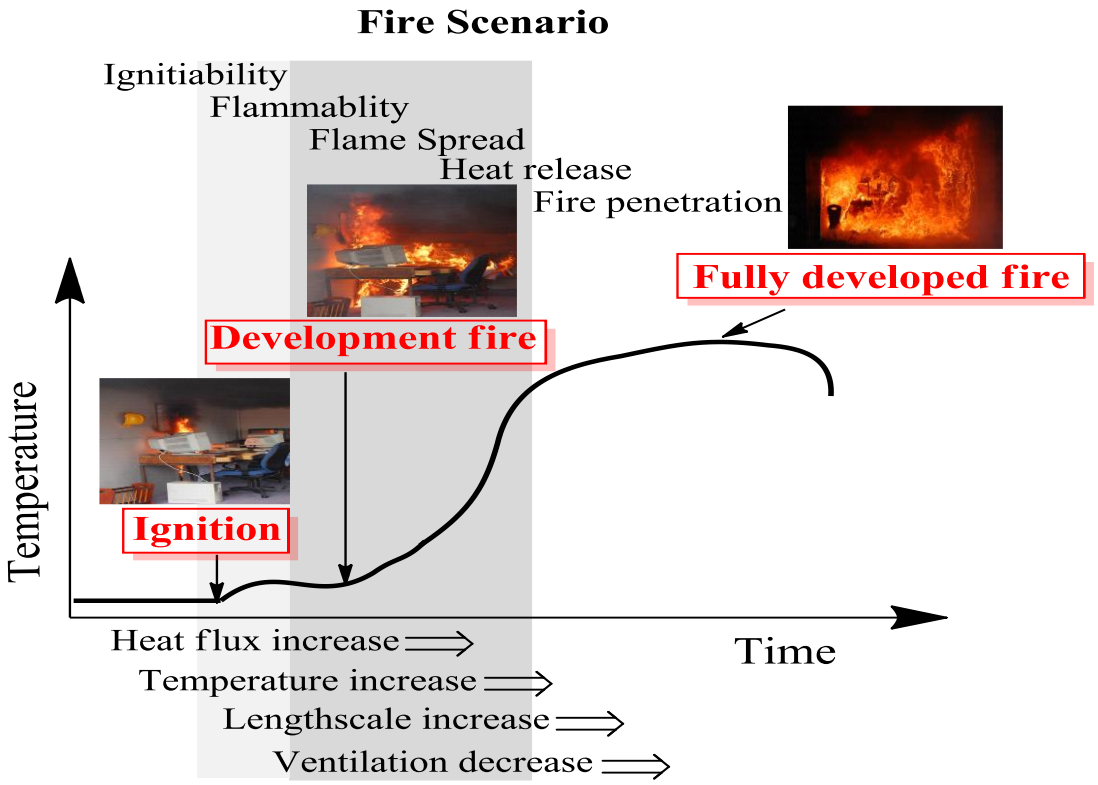

Fig. 1.2 Polymer combustion the relationship between temperature and time [3]

1.2 Challenges of flame retardant and montmorillonite in PP

Thus, the flame retardants (FR) are necessarily used in order to fit the required flame-retardant standard fields, which utilize different effects to stop fire such as extinguish flame, modify chemistry and heat barrier (Fig. 1.1). At first, halogenated FR were used due to their highly efficient flame retardancy and low price. However, a campaign of national and international environmental and consumer's agencies against the use of halogenated FR led to growing concern for possible side effects of these compounds [5, 6]. Consequently, mostly halogenated FR were restricted under the European Community directives ROHs, WEEE, and REACH [7, 8, 9]. Up to now, metallic hydroxides (aluminum hydroxide ($Al(OH)_3$), magnesium hydroxide ($Mg(OH)_2$) are widely used in industry, but the required high loading (about 60 wt %) seriously destroys the mechanical properties of polymeric materials.

To reduce the overall filler content and to enhance the fire retardancy of polymer, ammonium polyphosphate (APP) is one of most widely used flame retardant material in both industry and academia due to its high contents of phosphorus and nitrogen [10-14]. However, APP is not an efficient flame retardant for PP when it is used alone because of missing a carbon source. Recently, modified APP was prepared by incorporation of ethanolamine and/or piperazine in APP via ion exchange reaction [15, 16]. Modified APP could greatly improve the

stability of char layer and led to much better flame retardancy than that of unmodified APP. However, their thermal stability is reduced due to the use of organic substances. Moreover, due to missing of any chemical bonds between these flame retardant and polypropylene it might undergo migration. All of this greatly limits the efficiency of flame retardants and their further application. Therefore, different kinds of charring agents combining with APP as novel IFR were developed in this study. One the other hand, the novel multifunctional allylamine polyphosphate (AAPP) was designed and synthesized via a one-step method to replace the $Mg(OH)_2$.

With the development of nanotechnology, a small amount of nanofiller (e.g. montmorillonite (MMT), etc.) is often used as a synergistic agent for the preparation of polymer nanocomposites [17] showing significant enhancement of their properties, such as modulus [18], strength [19], heat resistance [20], gas permeability [21] and flame resistance [22-24]. To increase the compatibility of hydrophilic MMT surface with the hydrophobic polymer, the pristine MMT is modified by special surfactants. Surface energy, interlayer distance and thermal stability of these organoclays strongly depend on the chemical structure, packing density and type of cation included in the surfactant. For example, alkylammonium salts are commonly used [25, 26]. However, the main disadvantage is their low thermal stability [27-30] due to a Hofmann (β-elimination) process, which might lead to restacking of silicate layers during melt compounding under the industrial condition of compounding as well as injection molding or extrusion due to accelerated decomposition of traditional surfactants [31]. In addition, most of these surfactants (e,g. alkylammonium salts) are flammable. All of these disadvantages greatly limit their flame retardant efficiency as well as a broader application of MMT. Thus, in this work, a novel phosphonium compound (high thermal stability and flame retardancy) was designed, synthesized, analyzed and used for preparation of functional organically modified MMT (FO-MMT), which is used for increased thermal stability and synergistic effect on the flame retardancy of flame retarded PP composites.

1.3 Description of electron beam processing of flame retardant PP composites

Electron beam (EB) technology is a sustainable method fulfilling several principles of 'The Twelve Principles of Green Chemistry' in industry for about 50 years. Its main advantage is the spatial and temporal precise generation of polymer radicals in accordance to the requirement of the subsequent chemical reactions. In EB technology free radicals are mainly generated by the energy input of accelerated electrons. The electron induced chemical reactions lead to a modified structure of the polymer as well as altered biological, chemical, mechanical and

thermal properties of the modified polymer [32, 33]. Since EB processing has unique characteristics and advantages, more than 30 % of cables and wires are modified by EB technology [34, 35]. Nevertheless, the use of this state of the art technology is mostly limited to form parts (after molding) in solid state and at room temperature (stationary conditions). Recently, Electron Induced Reactive Processing (EIReP) was used as an efficient and pollution-free novel processing at IPF (Fig. 1.3) [36, 37], which modify filler and polymers during their melt mixing by high energy electrons in order to increase the interfacial adhesion between filler and matrix as well as between composite components [38-40].

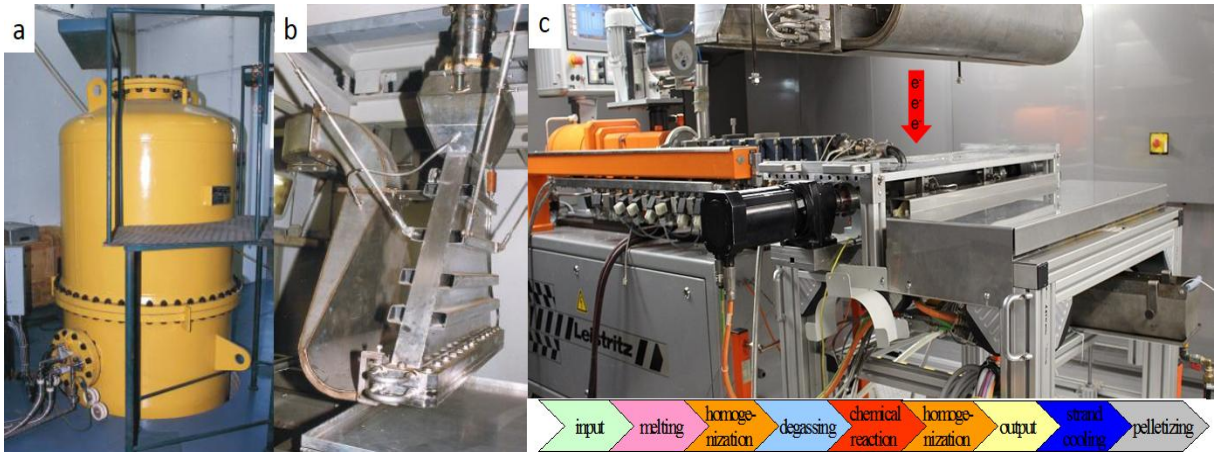

Fig. 1.3 Assembly of electron irradiation facility high voltage generator (a), electron beam scanner (b), and continuous EIReP (c)

According to previous studies [41, 42, 43], different polyolefin/surface modified $Mg(OH)_2$ composites were prepared by EB and EIReP without any use of additional compatibilizer. As shown in Fig. 1.4, the unmodified PP/60 wt % $Mg(OH)_2$ composites show poor tensile strength (22 MPa) and low elongations at break (1 %). State of the EB treatment has no significant influence on the tensile properties. In contrast, EIReP modified PP/60 wt % $Mg(OH)_2$ composites show best values of tensile strength (33 MPa) and elongation at break (5 %) of PP/$Mg(OH)_2$. This indicates an improved interfacial adhesion between $Mg(OH)_2$ and PP. Nevertheless, 60 wt % of filler is too high even using EIReP. Consequently, we have to develop new FR with lower loading to be used for EB technology.

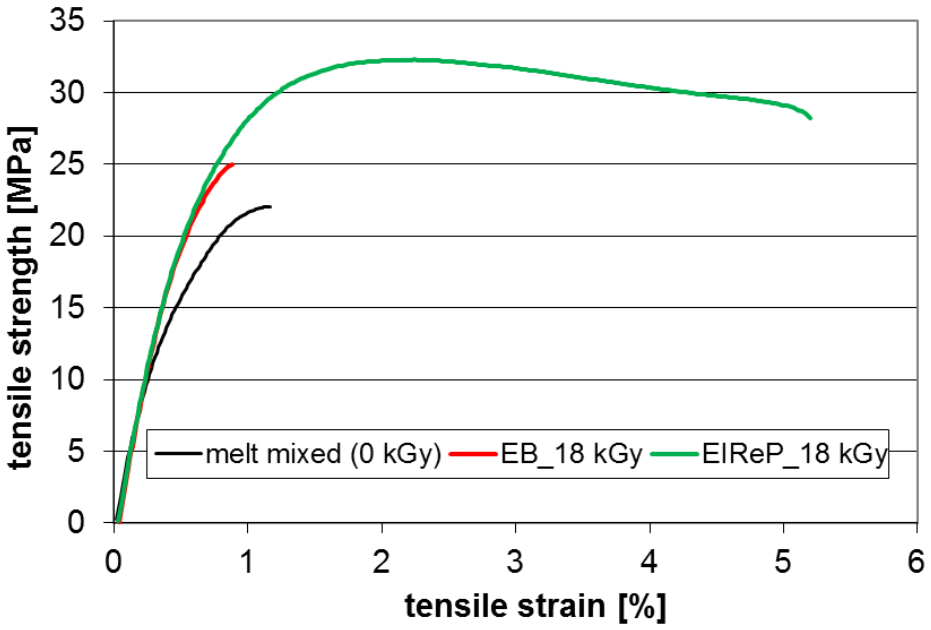

Fig. 1.4 Comparison of stress-strain-behavior of PP/60 wt % $Mg(OH)_2$ composites [43]

In this research, more efficient novel flame retardants and nanomaterial for PP were designed and developed. Afterwards, the multifunctional modifiers and flame retardants were stabilized by EB treatment (state of the art technology) in order to improve the thermal and flame retardant properties of flame retarded PP composites. The details are as follows:

- Design and synthesis of novel environmentally friendly functional IFR
- Preparation of functional surfactant for MMT (FO-MMT)
- Fire retardant polymer nanocomposites modified by EB treatment and EIReP
- Material-process-structure-property-relationships and related mechanisms

1.4 Synopsis of this thesis

The thesis comprises various chapters to give compact information on the theoretical background of the work, the scientific findings and discussions in a structured way.

In **Chapter 2**, a comprehensive overview about the state of the art of fire retardant, nanofiller and EB technology is presented. It mainly focusses on following questions. Why do polymers need fire retardancy? What is the relationship between polymer and fire? What are main fire retardants and mechanisms? What are IFR and nanofillers? What is EB technology?

In **Chapter 3**, the aims and objectives of this present work are clearly stated. Finally, a strategy is developed to successfully solve the tasks of the whole project.

In **Chapter 4**, the experimental details for this thesis are described in detail. These are raw materials used, experimental techniques for synthesization of the novel fire retardants and surfactants, preparation of flame retardant PP as well as characterization methods used to analyze and interpret the experimental data.

In **Chapter 5**, all experimental results including discussions are presented. It is divided into 6 subchapters. The first and second subchapter contains synthesis and characterization of novel charring agents N^1-(5,5-dimethyl-1,3,2-dioxaphosphinyl-2-yl)-acrylamide (DPA) and spirocylic pentaerythritol bisphosphorate disphosphoryl-di-prop-2-en-1-amine (SPSA) containing functional double bonds (C=C) together with APP as novel IFR1 and IFR2, respectively. In-depth studies, the thermal stability and fire behavior of these flame retardant PP composites are investigated. In addition, detailed mechanisms of graft-linking and cross-linking of these charring agents by EB treatment are discussed. In the 3th subchapter, an efficient and multifunctional AAPP has been designed and synthesized via a simple one-step method to be used as flame retardant cross-linker to polymers by EB treatment. Finally, the relevant cross-linking and flame-retardant mechanisms of PP/AAPP composites are investigated. Subchapter 4 reports the flame retardancy, thermal degradation and mechanical properties of intumescent flame retardant AAPP with MMT. In addition, the relevant synergistic mechanism is discussed. The fifth subchapter describes fire retardant polymer nanocomposites produced by radical induced chemical reactions at different EB parameters. First of all, surfactant thetriphenyl (undec-10-enyl) phosphonium bromide (TPB) is synthesized and characterized. Its initial decomposition temperature amounts to about 270 °C. Consequently, it is used to prepare FO-MMT by ion exchange reaction. The interlayer distance of novel FO-MMT increases to 1.85 nm. Finally, PP with AAPP and FO-MMT composites was irradiated at various doses. The interfacial adhesion between the nanomaterials and polymer matrix as well as the reaction between the fire retardant and polymer are studied systemically. Both structure-property relationship and flame retardant mechanisms are discussed. Subchapter 6 reports flame retardant PP nanocomposites processed by melt compounding and EIReP. The flame-retardant properties of PP/AAPP/FO-MMT nanocomposites with different dose values are studied. The results suggest that EIReP is a novel, fast and environment-friendly technology to reduce the heat and smoke toxicity release of flame retardant PP nanocomposites.

The Ph.D. ends with a summary and a brief outlook on future task. Finally, a comparison between AAPP and $Mg(OH)_2$ are added in order to demonstrate the result of this work.

Chapter 2

State of the art

2.1 Overview of flame retardant

Generally, fire is a chain degradation reaction that depends on several factors: radical initiation, chain propagation and chain termination in Fig. 2.1. During the combination, the degradation of polymer releases reactive species, i.e. hydrogen radicals ($H^{\bullet}$) and hydroxyl radicals ($OH^{\bullet}$). In chain propagation, oxidation can lead to acceleration by recombination reactions of macromolecular radicals [44]. In addition, these radicals proceed to undergo abstraction, fragmentation and combination reactions, both with the original polymer and other products from the decomposition [45].

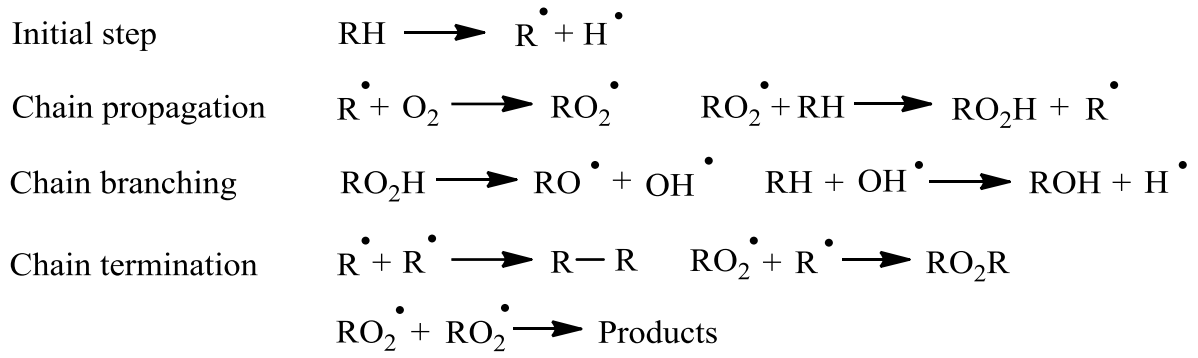

Fig. 2.1 The general mechanism for the oxidation of polymers [45]

In the case of polypropylene, the required thermal energy for the scission of hydrogen-carbon bonding of tertiary carbon is less compared to other bonds. As shown in Fig. 2.2, first of all, the scission of carbon-hydrogen bond is thermodynamically favored which produces many radicals. Then, in the presence of oxygen, oxidative dehydrogenation can compete with chain scission as well as with the formation of unsaturation and conjugated unsaturation [46, 47]. Since PP is a linear polymer, it is difficult to form cyclization by cross-linking fragmentation. With the development of burning, the degradation produces gases, such as carbon dioxide (CO_2), carbon monoxide (CO), etc. In the end there is no residual after the combustion process. Therefore, PP has a high flammability and flame retardant additives are one of the most efficient methods to reduce the high fire risk.

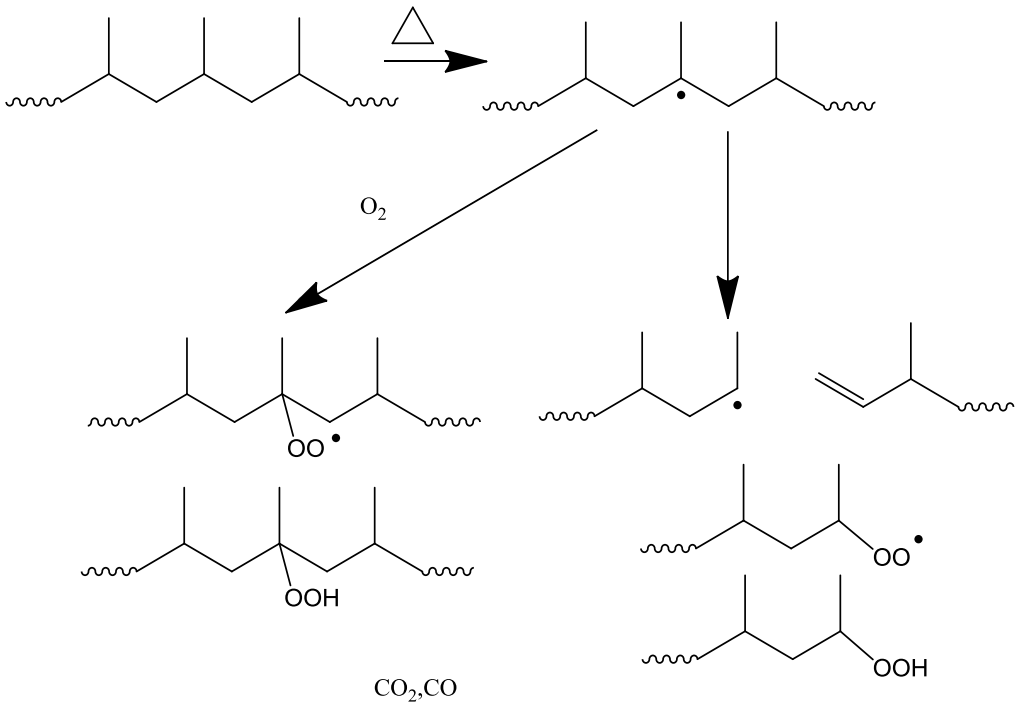

Fig. 2.2 The general thermal scission of PP [47]

2.1.1 Flame retardant mechanism

There are two main flame retardant mechanisms [44, 45]. One is the gas phase mechanism; the other is the condensed phase mechanism. These details are shown in Fig. 2.3.

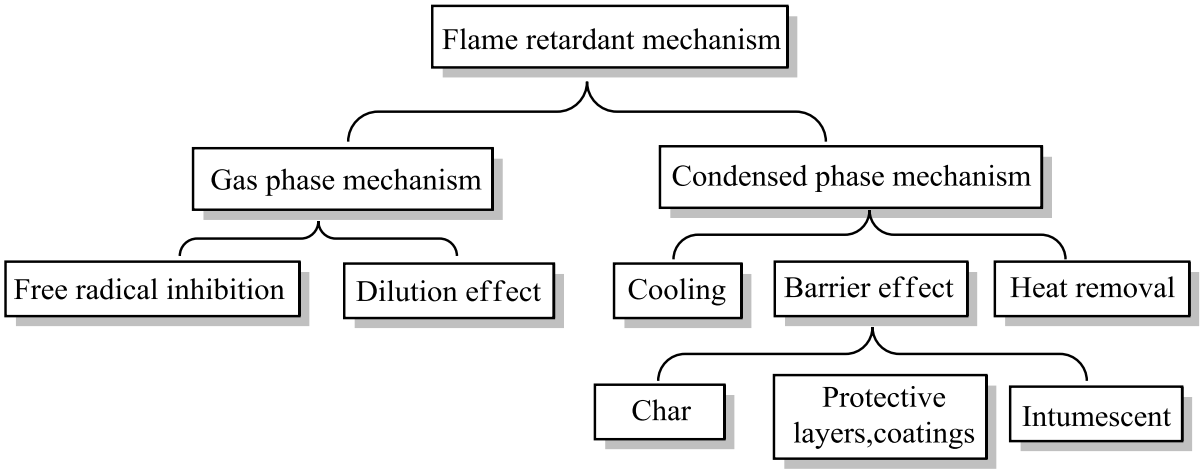

Fig. 2.3 Mechanism of flame retardant

Gas phase mechanism

Free radical inhibition proceeds by usual action of chlorine radicals (Cl·) or bromine radicals (Br·). Halogenated FR releases hydrogen halides which are effective in quenching free radicals during the combustion process [48, 49].

Dilution effect involves the addition of additives which produce inert gases during decomposition, such as CO_2 (calcium carbonate), water vapor (metal hydroxides), resulting in the dilution of fuel in the solid phase and the reduction of concentration of decomposition gases in gaseous phase [50, 51].

Condensed phase mechanism

Cooling below the polymer combustion temperature influences the energy balance of combustion. In this case, the decomposition of metal hydroxides ($Mg(OH)_2$, $Al(OH)_3$) are end other micreaction acting as a heat sink [52, 53].

The **barrier effect** not only acts as a trap for gaseous products of polymer decomposition, but also as a barrier for heat, oxygen and pyrolysis products [54, 55]. Usually, charring, intumescent system and a protective layer as coatings are using this way to stop the fire. Charring as a barrier is formed through cross-linking or aromatization to inhibit further degradation, starves the flame of fuel and protects the polymer surface [56, 57]. Intumescent system can engender the expanded carbonized or vitreous layer at the surface of the polymer via chemical transformation of degrading polymer chains [54, 58]. Intumescent systems generally are phosphorus-containing and nitrogen-containing compounds. Protective layer as coating happens between the gaseous phase and the solid phase where thermal degradation takes place [59]. Such a layer (solid or gaseous) limits the transfer of combustible volatile gases, oxygen, and heat. LDH, MMT, etc. work this way.

Heat removal is a portion of heat and fuel from the flame action zone. One type of heat removal is melt dripping [60]. Theoretically, the melt dripping decreases flammability but this dripping can also help to spread the fire.

Combustion is a complex process. The flame retardant additives may function in the condensed phase and/or in the gas phase. In the case of $Mg(OH)_2$, water vapor is generated that dilutes the concentration of decomposition gases in gaseous phase as well as reduces the temperature and the heat in condensed phase.

2.1.2 Classification of flame retardants

Traditionally, halogenated FR with antimony trioxide are the main flame retardants for polymer. However, more and more halogen-free flame retardants have been developed in the recent 10 years. These are metal hydroxides, boron-containing compounds, silicon-containing

compounds, nitrogen-containing compounds, phosphorus-containing compounds as well as nanocomposites [61]. Detailed information is given in the following part.

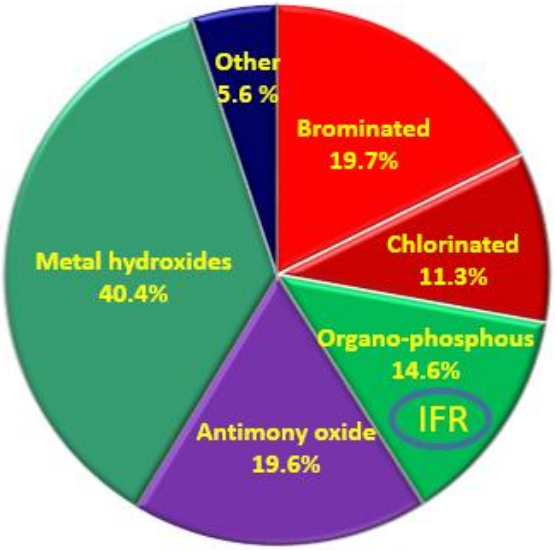

Fig. 2.4 Global consumption of FR in plastics by type, tonnes (2011) [61]

Halogenated FR

The main mechanism of halogenated FR is flame inhibition (Fig. 2.5). Bromine and chlorine radicals stop the combustion and HCl and HBr are covered with the polymer surface. Brominated FR such as decabromodiphenylether® (deca-BDE), bis(2'3-dibromopropyl ether) of tetrabromobisphenol® A (TBBPA-DBPE) or stabilized hexabromocyclododecane® (HBCD) from a price-performance stand point are used in combinations with antimony oxide [44, 62]. However, some of halogenated FR are restricted because of environmental issues.

$$HX + H^{\bullet} \longrightarrow H_2 + X^{\bullet}$$
$$HX + OH^{\bullet} \longrightarrow H_2O + X^{\bullet}$$

X is halogenated element

Fig. 2.5 Mechanism of halogenated FR

Metal hydroxides

Metal hydroxides are the most commonly used halogen-free flame retardants which decompose endothermically and release water molecules into the gas phase during the burning process (Fig. 2.6). $Al(OH)_3$ and $Mg(OH)_2$ are widely used in industry due to their lower cost and less smoke production [45, 56]. Nevertheless, $Al(OH)_3$ has lower thermal stability and

therefore it is less suitable to be processed with PP [51, 63]. In order to obtain UL94 V-0 rate in PP, a significant high amount has to be used which seriously reduces the mechanical properties of PP/$Mg(OH)_2$ composites in comparison to neat PP.

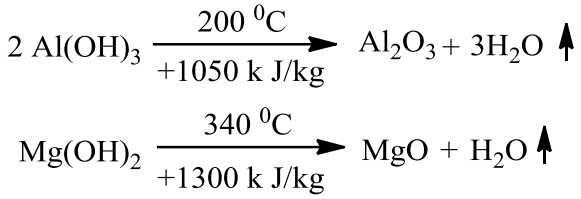

Fig. 2.6 Mechanism of metal hydroxide

Boron-containing compounds

Boron-containing compounds act as a flame retardant in both the condensed and vapor phase. In the boron-alumina trihydrate system, boron trihalides play a role as Lewis acids, promote cross-linking and minimize the decomposition of polymer into volatile flammable gases [64]. However, boron-containing FR is not effective alone in PP.

Silicon-containing compounds

Silicon-containing compounds may act in the gas (trapping of radicals) and condensed phase (char formation). They are considered to have good dielectric and gloss properties, improved moldability, anti-dripping properties, processability and impact resistance, thermal stability and non-corrosive smoke evolution [65, 66]. However, only few of them have been used in PP alone that passed UL94 V-0 rate.

Nitrogen-containing compounds

Nitrogen-containing flame retardants release inert nitrogen gas which dilutes the flammable gases and oxygen. Normally, nitrogen-containing FR is mixed with phosphorus-containing compounds, like melamine phosphate.

Phosphorus-containing compounds based on intumescent flame retardant (IFR)

Phosphorus-containing compounds are widely used as flame retardants for thermoplastics, mastics, coatings and textiles [2, 44, 54]. They influence the burning process mainly in the solid or gas phase. IFR is one of the most popular phosphorus-containing compounds. At high temperatures, the IFR reacts to a polymeric form of phosphoric acid, inducing endothermic dehydration reactions. This causes the formation of char, a glassy layer. This inhibits the usual

pyrolysis process which is otherwise feeding the flames. Therefore, char rather than combustible gas is formed, and thus the amount of fuel produced is significantly reduced. This intumescent char plays a particular role in the flame retardant process, because it acts as a two way barrier, hindering the passage of combustible gases and molten polymer towards the flame as well as shielding the polymer from the heat of the flame. However, most of the phosphorus-containing FR have poor thermal stability, processability and volatility problems.

Nanocomposites

With the development of nanotechnology, nanocomposites containing nanoparticles such as MMT [27, 65-69], LDH [70], carbon nanotubes [71], polyhedral oligomeric silsesquioxanes [72], etc, have gained a special attention in the flame retardant polymer. For instance, MMT has been mainly used due to its small particle size, high aspect ratio and high swelling capacity. The main flame retardant mechanisms of layered nanocomposites are barrier, migrant and catalyzing carbonization [73] (Fig. 2.7). The barrier mechanism suggests that layered MMT is based on physical effects preventing the transition of heat and degradation products during the combustion process. Gradually, inorganic-rich layer is formed by a combination of migration of layer and ablative reassembling to provide thermal and oxygen flow insulation in the condensed and gas phase. Meanwhile, the nanoparticles can strengthen the char or catalyze the carbonization with reduction of the releases of pyrolytic products and promotion of the crosslinking of polymer. The high hydrophobicity of the clays requires further modification of such material in order to be more miscible and compatible with the polymer matrix. The modification is usually conducted by ion exchange with a long-chain amine or ammonium salt compounds which lower the surface energy and improve wettability of the clay making it more hydrophilic. However, the poor thermal stability of surfactants might result in agglomerates, bubbles and aging.

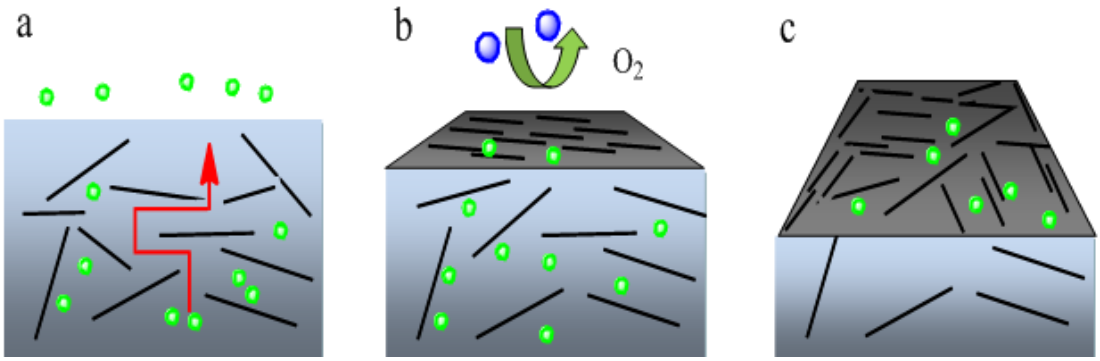

Fig. 2.7 Mechanism of nanocomposites systems barrier (a), migrant (b), and catalyzing carbonization (c)

Based on the above examples, a wide variety of FR systems is available for polymers. The advantages and disadvantages of commonly used FR system are summarized in Table 2.1. Among them, phosphorus-containing compounds and nanocomposites are the most promising halogen-free flame retardant in polyolefins. Until now, IFR additives of phosphorus-containing compounds are one of the most popular approaches for polyolefins. However, it is worth noting that some synergistic agents like MMT, LDH, etc. have been used to improve further the flame retardancy of PP/IFR systems.

Table 2.1 Advantages and disadvantages of FR in PP

Types	Advantages	Disadvantages	Note	Ref.
Halogenated FR	Low cost Efficient at low loadings with synergists Easy to process	Emissions of smoke and toxic gases Corrosive emissions	Regulations and Rules (RoHs, WEEE, REACH, etc.)	[4, 7, 8, 9]
Metal hydroxide	No acidic gas emissions Effective smoke reduction Non-toxic Low price	Very high loading (ca. 60 wt %) Decrease mechanical properties	The most widely used in cable, wire, tyre, etc.	[4, 41, 42]
Boron-containing compound	Environmentally friendly Anti-dripping properties	Few structures effective in PP	-	[65, 66]
Silicon-containing compound	Environmentally friendly Anti-dripping properties	Few structures effective in PP	-	[4, 54]
Nitrogen-ontaining compound	Halogen-free Low smoke occurring Low toxicity	Poor processability Few structures effective in PP	-	[44, 45]
Phosphorus-containing compound	Halogen-free Low smoke occurring Low toxicity	Poor processability Volatility problem	IFR is one of the most popular FR	[44, 54]
Nanocomposites	Synergistic effect with other FR Reduce dripping Improved quality of char	Poor thermal stability Difficult to incorporate High cost	One of the most attractive topics in FR field (MMT, LDH, etc.)	[17, 20, 70, 73]

2.2 Intumescent flame retardant in polyolefin

PP and PE are the most commonly utilized polyolefins. However, both of them have a high flammability. As reported in the reviews of Hamerton [4], Wilkie [44], Bourbigot [54], Weil [74] and Camino [75], commercial FR polyolefins based on intumescent flame retardant came out very recently and provided the latest development on the market [44, 54]. In the combustion process, IFR polyolefins show unique expanded charring to slow down heat, smoke emission, oxygen and mass transfer by intumescent char in Fig. 2.8.

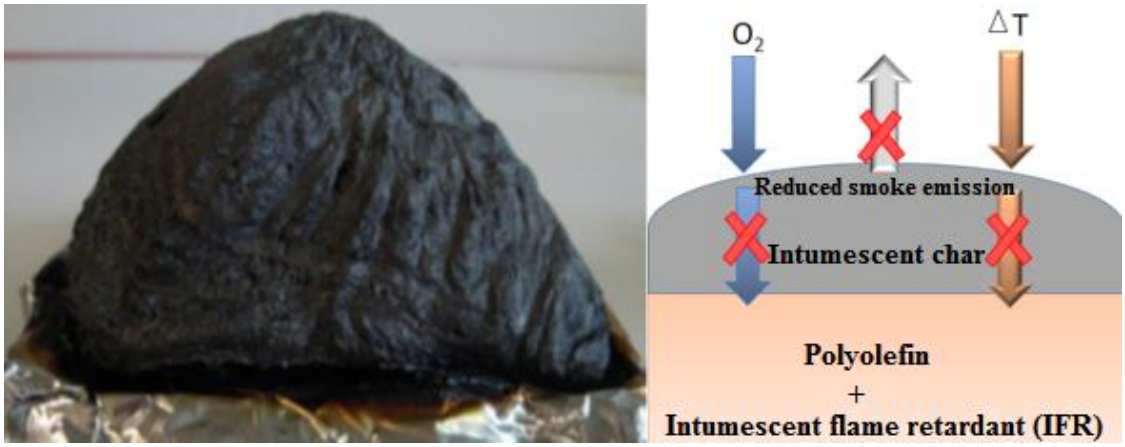

Fig. 2.8 Example of an IFR in polyolefin [54]

2.2.1 Mechanism of intumescent flame retardant

Flame-retarding polymers by intumescence are essentially a special case of a condensed phase mechanism [76]. Intumescent systems were reviewed by Camino et al. [77], which interrupt the self-sustained combustion of the polymer at its earliest stage. Typically, as shown in Fig. 2.9, the ingredients of IFR are composed of an acid source, carbonization agent and blowing agent. The intumescence process results from a combination of char and non-combustible gas at the surface of the burning polymer. The resulting foamed cellular charred layer, whose density decreases as a function of temperature, protects the underlying material from the action of the heat flux or the flame.

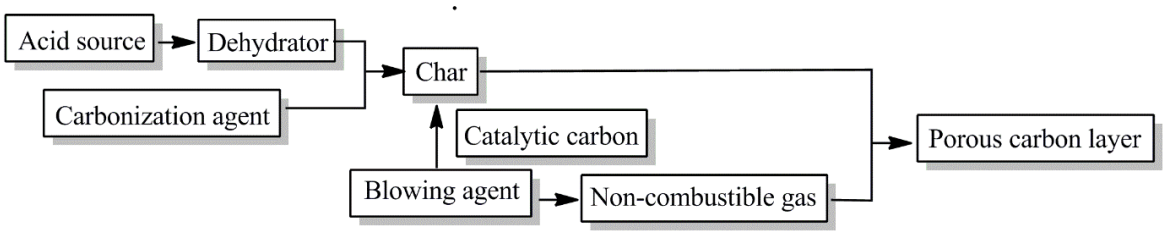

Fig. 2.9 Mechanism of IFR systems

2.2.2 Present status of intumescent flame retardant

APP acts both as the acid source and blowing agent in IFR systems, which is one of most widely used flame retardant material [54, 78, 79]. In order to prepare more effective IFR, two important methods can be used. Firstly, two types of novel charring agent were synthesized, like phosphate derivatives and triazine derivatives. Secondly, the microencapsulation with charring agent [80], melamine [81, 82], etc. at the surface of APP is also an efficient method to enhance its flame retardancy.

For phosphate derivatives, the main three types are caged phosphorus as shown in the Fig. 2.10. Wang et al. [83] proposed to use the catalytic action of a phosphotungstic acid in the synthesis of melamine salts of pentaerythritol phosphate in order to solve the problems of conventional preparation methods. Bourbigot et al. [84] investigated polyamide-6 clay nanocomposite hybrid (PA-6-nano) as a carbonization agent. Some phosphorus-containing and nitrogen-containing intumescents were synthesized, such as spiro and caged bicyclic phosphate (SBCPO) [85], spirocyclic pentaerythritol bisphosphorate disphosphoryl melamine (SPDPM) [86], poly(4,4-diaminodiphenyl methane spirocyclic pentaerythritol bisphosphonate) (PDSPB) [87], poly(2-hydroxy propylene spirocyclic pentaerythritol bisphosphonate) (PPPBP) [88], etc.

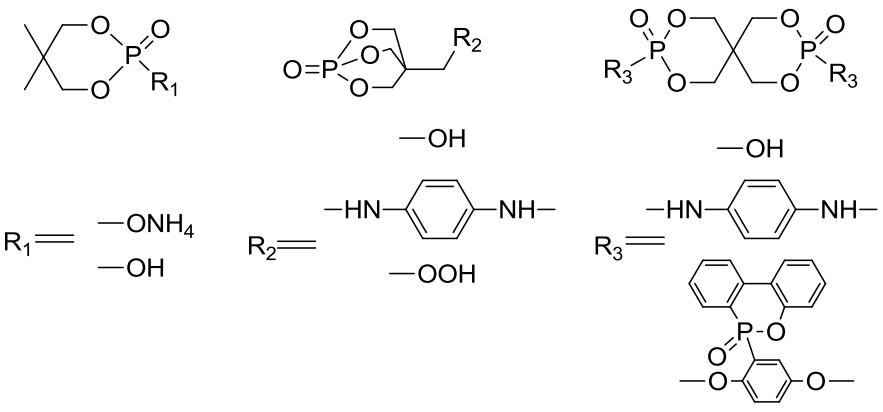

Fig. 2.10 Phosphate derivatives of charring agent IFR systems

Other authors suggested the synthesis of triazines derivatives (Fig. 2.11). They reported [89-91] triazines derivatives showed high initial temperature of the thermal degradation. These triazines derivatives in combination with APP are effective IFR in polyolefins.

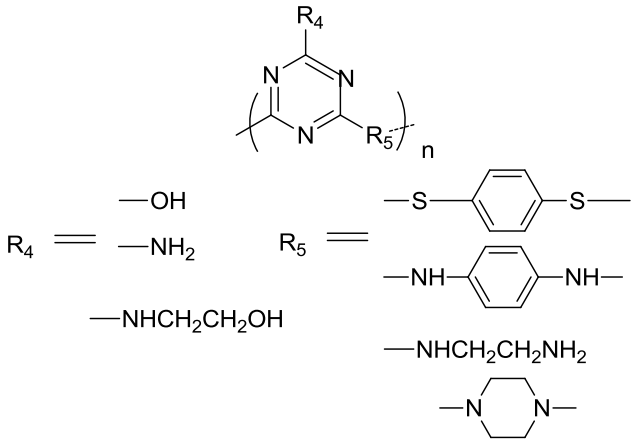

Fig. 2.11 Triazine derivatives of charring agent IFR systems

On the other hand, the microencapsulation with charring agent (carbon source) at the surface of APP is also an efficient method to enhance the application of APP in polyolefin [92-96], such as commercial AP®420, AP®760, OP®1230/1240 (Germany company), FR CROS®, Budit® 3167, Budit®310 (Budenheim Germany), Melapur® 200 (Switzerland), and GrafGuard®, GrafTech® (US), etc.

Unfortunately, most of novel of phosphate derivatives and triazine derivatives are developed from phosphorus oxychloride and cyanuric chloride. There are some risks to the environment [97-100]. In addition, the preparation process of microencapsulation is complicated [95]. Very recently, Wang et al [15, 16] prepared modified APP by incorporation of ethanolamine and/or piperazine in APP via ion exchange reaction. These modified APP had greatly improved the stability of char layer and led to much better flame retardancy than that of unmodified APP. Moreover, the flame retardant mechanism was confirmed. Stable char layer rich P−N−C structure and P−O−C structure were formed at the later stage of combustion. These modified APP were developed by ion exchange reaction. Their thermal stability is reduced due to the use of organic substances. Moreover, due to missing of any chemical bonds between these flame retardant and polypropylene it might undergo migration. All of this greatly limits the efficiency of flame retardants and their further application.

2.3 Montmorillonite based polymer nanocomposites

Among all nanofillers, montmorillonite (MMT) is the most commonly used layered silicate in nanocomposite preparation because of its low price, large surface area, good surface reactivity and adsorptive properties [102]. The flame retardancy of polymer nanocomposites can be enhanced significantly via addition of a small amount of MMT [102-104]. Consequently, clay

is added in polymer matrix. The carbonaceous-silicate layer is generally formed on the surface of burning nanocomposites. This stable layer as a barrier can remarkably retard flame spread and reduce heat release rate (HRR) [44, 102, 103]. Moreover, the self-extinguishing and anti-dripping promoters are provided by a conventional flame retardant polymer with MMT [18-21], which not only can improves flame retardancy, but also increases other properties, such as modulus, strength, heat resistance and gas permeability. It is well known that the dispersion of MMT within polymeric matrices is crucial for the performance of polymer/layer platelets nanocomposites [104]. In Fig. 2.12 the three main states are shown. These are phase separated, intercalated and exfoliated nanocomposites. In the case of exfoliation, layered platelets of MMT are uniformly separated and dispersed, which may significantly change properties of polymeric matrix.

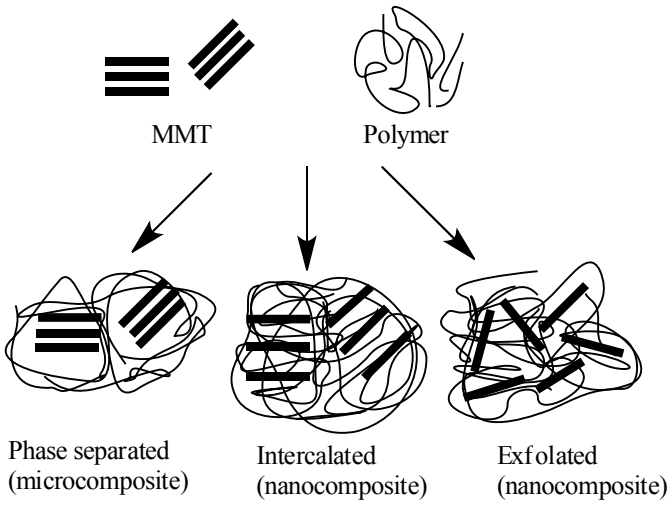

Fig. 2.12 Different structures of layered platelets/polymer nanocomposites

Thus, to increase the compatibility of hydrophilic MMT surface within the hydrophobic polymer matrices, the pristine MMT is modified by special surfactants. In the case of cations in the gallery gap of MMT, they can be replaced by small molecule ions of surfactants [104-107]. The alkylammonium surfactants are the mostly used for the modification of MMT. However, ammonium surfactants have a low thermal stability due to Hofmann (β-elimination) process [27-30, 66] (Fig. 2.13). Therefore, melt processing at higher temperature leads to degradation. The elimination reaction of modifiers accelerates the aging and decomposition of thermoplastics as well as leads to the restacking of the platelets. In addition, most of these surfactants (e.g. alkylammonium salts) are flammable. The choke points of low stability and flammability of clay's organic surfactants greatly limit their further applications.

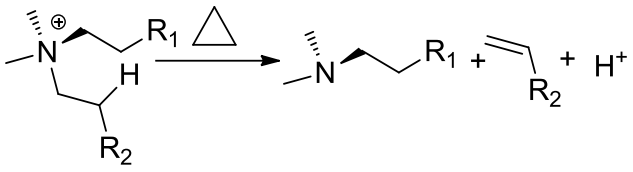

Fig. 2.13 Hofmann elimination reaction of alkyl ammonium organic treatment

2.4 Crosslinking of polyolefins

Polyolefins hold more than 50 % of plastic market share [108]. However, their use is restricted when fillers are added leading to in low heat resistance, poor solvent resistance, and weak resistance to environmental stress cracking. In order to overcome these items, crosslinking of polymersis an effective way to improve thermal and chemical properties. Usually, there are three mains crosslinking method: peroxide [109], UV [110] and radiation crosslinking [111].

Peroxide crosslinking

Before starting the crosslinking of polymer [112], the polymers and peroxides are blended under relatively low temperature in order to get a homogeneous distribution of peroxide in the polymer without starting its decomposition. Afterwards, the mixtures are heated above the decomopsition temperature of peroxides to produce a large number of free radicals [111]. Normally, these highly active free radicals can abstract hydrogen from polyolefins or react with double bonds. However, there are some disadvantages. For peroxide crosslinking, the peroxide and the polyolefins have to be mixed at relatively low temperature. This pre-processing temperature has to be below the decomposition temperature of peroxides as well as higher than the melting temperature of the polymer. In addition, the product is processed at high temperature and pressure for a long time. Therefore, the efficiency and quality of these compounded products are affected by heat treatment as well as the decay products of the peroxides.

UV cross-linking

Ultraviolet light (UV) crosslinking is a useful method for improving properties of polyolefin composites [113, 114]. Generally speaking, an appropriate amount of photoinitiator is incorporated into polyolefin. Afterwards, a photoinitiator specific wave length of UV light is absorbed resulting in the generation of initial radicals. The seradicals are generating macroradicals of polyolefins. Finally, the crosslinked structures are produced by the reaction of

macroradicals. Nevertheless, the penetration of UV is too low in order to modify thick polymer layers.

Radiation cross-linking

Radiation processing is widely used for cross-linking, curing, degrading, grafting, and polymerization of polymeric materials [35, 115, 116], e.g. PLA [117], PP [118], PP/EPDM [119], PP/NR [120], PP/EOC [121], etc. Free radicals are generated without any use of chemical additives. In addition, the generation of radicals does not depend on temperature as well as state of aggregation. In the case of high energy electrons, the radical generation can be spatially and temporally controlled by electron energy and electron current, respectively. In comparison to UV, accelerated electrons have a higher penetration depth.

2.5 Electron beam processing of polymers

Electron beam (EB) technology belongs to the group of chemical modification of polymers. The electron induced chemical reactions lead to a modified structure of the polymer as well as altered biological, chemical, mechanical and thermal properties of the modified polymer [111, 122-125].

2.5.1 Basic concept

Free electrons are generated in a high vacuum e. g. by a heated cathode. Then, the electrons are accelerated in a high-voltage or magnetic field. These accelerated focused electrons are scanned in order to generate of broad electron beam penetrating the thin beam exit window of electron accelerator. Afterwards, the high energy electrons passed through the air gap between beam exit window and polymer surface in order to transfer their kinetic energy to the polymeric material. As shown in Fig. 2.14, the interactions with atomic electrons result in the generation of ionization (1) as well as excited atoms or molecules (2). Finally, the thermalized electrons are captured by atoms (3). The basic reactions of high energy radiation processing are the ability of EB treatment to produce reactive cations, anions and free radicals in polymeric material (4). As the result of a large number of free radicals are generated for chain scission, crosslinking, functionalization, formation of small molecular products and structural rearrangement [122]. In EB technology, crosslinking, grafting and main chain scissions are the most important processes for polymer modification. The energy input per unit of mass and the total number of radicals can be controlled via the absorbed dose. Usually, polymer with a single chain ($-CH_2-$) is prone to crosslinking whereas those with backbone tertiary carbon (-CHR-) are revealing to main

chain scission [123, 124]. In both cases, crosslinking and degradation occur simultaneously because of secondary and tertiary carbon-hydrogen bond in different types of PP [47]. Compared to isotactic PP, atactic PP is more sensitive to crosslinking due to a predominantly amorphous structure. Nevertheless, regular PP inclines to be degraded by β-chain scission under high energy radiation [125]. To decrease degradation of PP, various polyfunctional monomers (PFM) generally are used. Their basic feature is that PFM contains multiple unsaturated bonds which can be rapidly reacted with macroradicals of polymer under EB treatment. Finally, the desired material properties are achieved by radical induced chemical reactions at suitable electron beam parameters (dose, dose rate, atmosphere, temperature, molecular weight…).

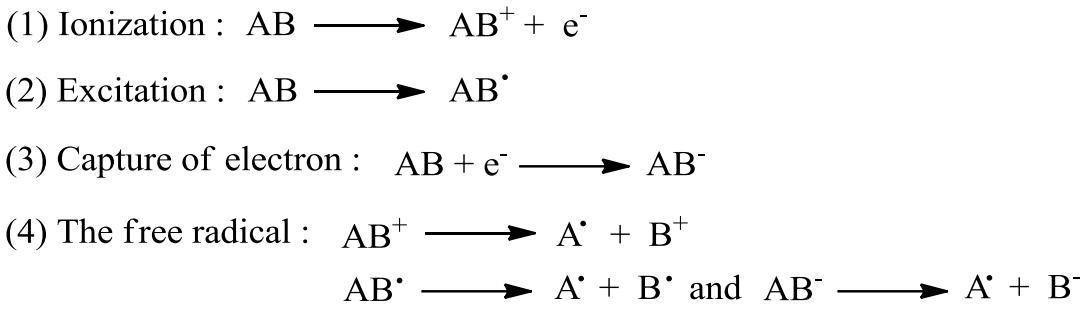

Fig. 2.14 Basic reactions induced by electron beam

2.5.2 Modifications of flame retardant PP composites

Since EB processing has unique characteristics and advantages, more than 30 % of cables and wires as well as about 95 % of tires in Japan are modified by EB technology [34, 35]. However, most of these raw materials are easy to burn. In order to obtain required flame-retardant standards, $Mg(OH)_2$ is used as halogen-free FR additive due to its high decomposition temperature and decomposition with the release of water. In Fig. 2.15, the SEM image of $Mg(OH)_2$ (60 mass %) filled PP demonstrates the low interfacial adhesion of this physical compound leading to reduced mechanical properties. Thus, surface modifications of $Mg(OH)_2$(MH_surface) are developed [126-128] to increase its compatibilization in polymer matrix, such as commercial Onyx Elite®431, Micral®532, Hymod®M632, HN® 100, MagChem®MH10, MagChem®S, MagChem® UF, FloMag® MHP, and CellGuard®MH, etc. However, the values of elongation at break of PP/MH_surface composites are still strongly reduced compared with neat PP (Fig. 2.16).

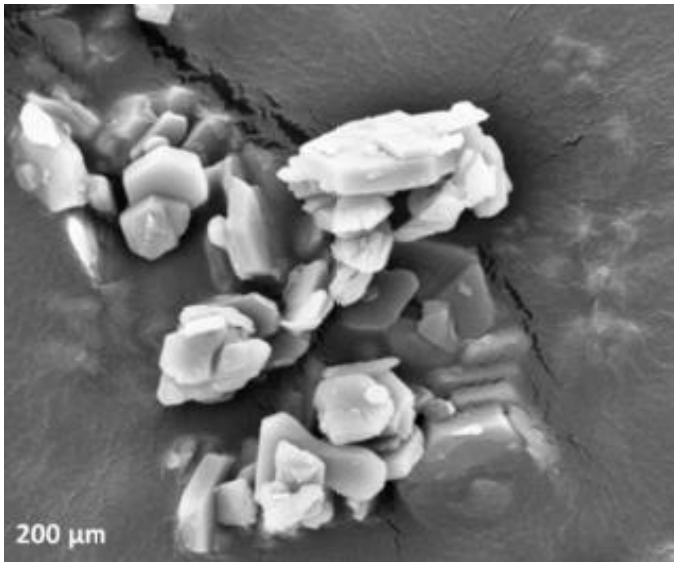

Fig. 2.15 SEM image for $Mg(OH)_2$ in PP [43]

EB treatment was used to improve interfacial adhesions between flame retardant and polymer. In recent years, polymer/$Mg(OH)_2$ composites have been modified by high energy electrons at different absorbed dose and treatment conditions to improve the mechanical properties of polyolefin/$Mg(OH)_2$ composites [41, 42]. Yasin et al [129] studied γ-rays irradiation of PE/$Mg(OH)_2$/sepiolite composites. The results showed that the modulus of irradiated composites at 150 kGy significantly increased from 616.1 to 1001.4 MPa. Fang and his co-worker studied [130] PE/EVA/$Mg(OH)_2$ composites via high energy electron beam for electric cables. It was reported that both tensile strength and modulus of irradiated PE/EVA/$Mg(OH)_2$ composites increased compared with non-irradiated PE/EVA/$Mg(OH)_2$ composites. Hence, the LOI of irradiated samples are higher than those of unirradiated composites. However, as shown in Fig. 2.16 (green bars), the mechanical performance of PP/$Mg(OH)_2$ composites prepared by electron induced reactive processing (EIReP) are still significantly reduced in comparison to virgin PP due to high filler loading as well as EB induced degradation of PP in the molten state.

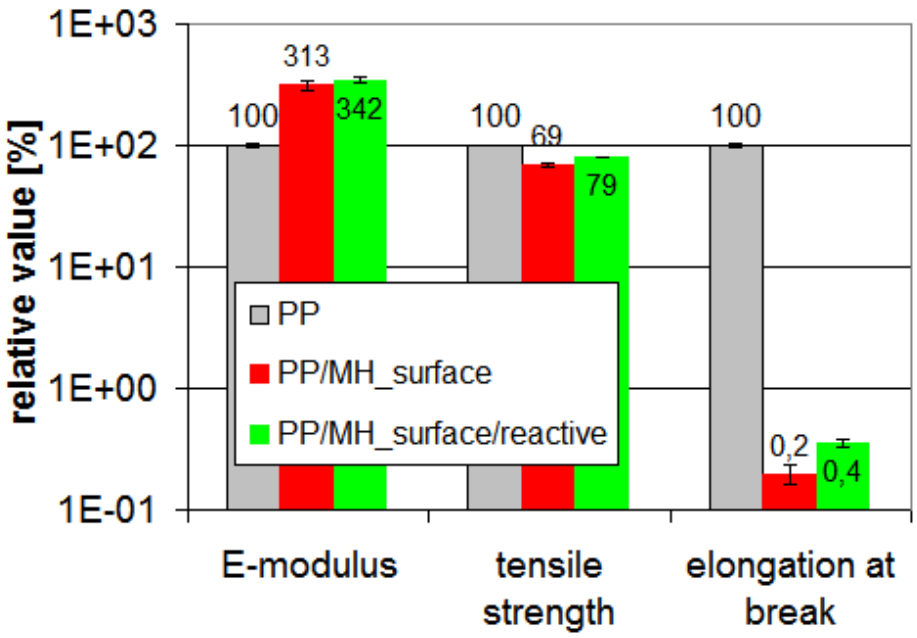

Fig. 2.16 Mechanical properties of PP, non-irradiated PP/60 wt % $Mg(OH)_2$ and EIReP modified PP/60 wt % $Mg(OH)_2$ composites [43]

2.5.3 EIReP processing of flame retardant PP composites

Recently, electron induced reactive processing (EIReP) has been developed at Leibniz Institut für Polymerforschung Dresden e.V. (IPF) where a high energy electron accelerator is coupled with an internal mixer (Fig.2.17). In this novel process, the chemical reactions of flame retardant PP composites are induced by EB treatment under the dynamic conditions of melt mixing. The total volume is modified due to the change of molten PP within the penetration depth of high energy electrons during the mixing process. Moreover, EB treatment time and electron energy not only control dose rate and penetration depth, respectively but also influences the ratio of radical generation rate and the ratio of modified volume. Mechanical, chemical and morphological characteristics of selected polyolefin were studied in order to evaluate the potential of EIReP [43]. The combination of physical (PP, $Mg(OH)_2$) and chemical (free radicals) modification of PP/60 wt % $Mg(OH)_2$ composites could be controlled by EIReP at fixed mixing rate, temperature, dose, electron current, and treatment time. Finally, the interfacial adhesion reactions between $Mg(OH)_2$ and different molecular weights PP were investigated using this novel technology (see Fig. 2.16).

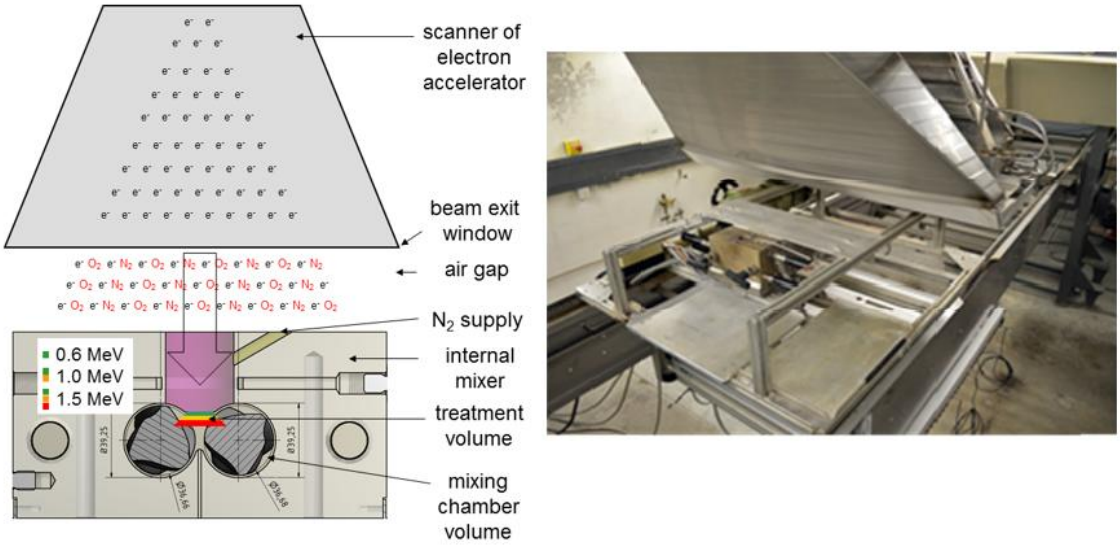

Fig. 2.17 Electron accelerator coupled with internal mixer [43]

It was confirmed that PP tends to degradation using EIReP at 185 °C. A lower molecular mass of PP (like PP120MO) was more favorable. In Fig. 2.18, SEM images displayed that EIReP modified PP120MO with 60 wt % $Mg(OH)_2$ composites had better interfacial adhesion between $Mg(OH)_2$ and PP matrix without any use of additional compatibilizer. Consequently, the tensile strength and elongation at break of EIReP modified PP/$Mg(OH)_2$ composites at 18 kGy were enhanced from 22 MPa and 1 % to 33 MPa and 5 %, respectively [43]. Nevertheless, loading of 60 wt % filler is too high.

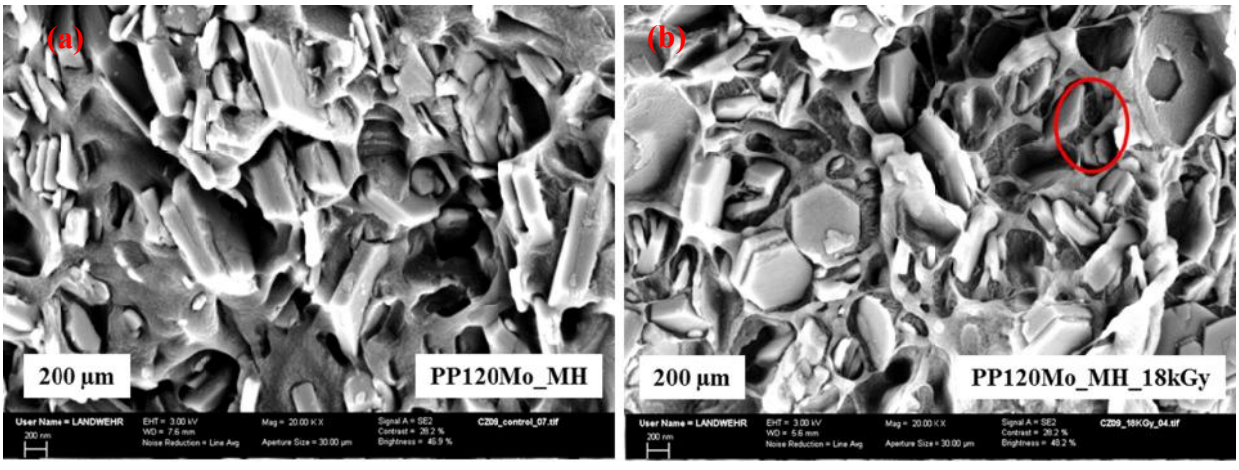

Fig. 2.18 SEM images for EIReP modified PP/60 wt % $Mg(OH)_2$ composites at 0 (a) and 18 kGy (b) [43]

Incorporation of layered nanofiller (LDH and MMT) into flame retarded polymer blends is one of the techniques to reduce the overall filler content and to enhance the fire retardancy

of polymer. Costa et al. [131] studied PE/LDH/$Mg(OH)_2$ composites. In comparison to PP/60%$Mg(OH)_2$ composites, a flammability rating of PP/50%$Mg(OH)_2$/10%LDH composites were achieved in UL94 testing. However, a further increase of LDH loading in a $Mg(OH)_2$/LDH combination is limited by the processibility and the mechanical properties of the composites. Hong et al. [132] investigated PP/$Mg(OH)_2$/MMT composites. The addition of 10 wt % MMT and 60 wt % $Mg(OH)_2$ increased the LOI 18 to 27 %. A reduction of peak heat release of PP/$Mg(OH)_2$/MMT composites was obtained compared to PP/$Mg(OH)_2$ composites in cone calorimeter test. However, the tensile strength and the elongation at break were altered to a level avoiding any use in cable insulating applications. Therefore, LDH and MMT can work as synergists, but $Mg(OH)_2$ has to be replaced by more efficient new flame retardant.

Chapter 3

Aim, objective, and strategy

3.1 Aim and objectives of this work

Up to now, metallic hydroxides flame retardants are used to replace some of halogenated FR, but the high loading seriously destroys the mechanical properties of polymeric materials. To reduce the overall filler content, APP is one of most widely used flame retardant material. However, APP is not an efficient flame retardant for PP when it is used alone because of missing a carbon source. To prepare more effective IFR, many novel charring agents were synthesized. Nevertheless, first of all, some components of traditional IFR are made from low molecular mass components which might undergo migration. Secondly, since IFR is a physical compound, it is resulting in low thermal stability of flame retardant polymer. On the other hand, MMT is often used as a synergistic agent for the preparation of polymer nanocomposites showing significant enhancement of their flame resistance properties. However, the main disadvantage of surfactants for MMT is their low thermal stability and flammable. All of these disadvantages greatly limit their flame retardant efficiency as well as a broader application of APP and MMT.

To overcome these disadvantages, EB technology is used as a pollution-free processing, which modify flame retardants, MMT and polymers by high energy electrons. The aim of this work is to develop and investigate high-performance fire retardant PP nanocomposites produced by EB technology. High efficient flame retardants and nanomaterial for PP are designed and prepared which are modified by high energy electrons afterwards to improve properties of flame retardant PP composites. There are two main tasks as follows:

- First task: development of new FR based on APP by modification with carbon source in order to get a highly efficient IFR which can be coupled by EB treatment to the polymer matrix.

Based on previous studies [41, 42, 43], PP/$Mg(OH)_2$ composites were modified by high energy electrons to increase its mechanical property. However, the high filler content of 60 wt % limited the enhancement of mechanical properties even after EIReP. In this study, a more efficient fire retardant has to be developed in order to replace $Mg(OH)_2$ and ensure a lower filler loading. In last decades, intumescent flame retardant (IFR) as environmentally friendly flame

retardant is used to prepare flame retardant PP. Nevertheless, there are no chemical bonds between IFR and PP, which leads to low thermal stability of the flame retardant PP. Consequently, the design and the processing of IFR have to be modified in order to reduce the migration behavior of IFR. In addition, the mechanisms of electron induced chemical reactions should be studied.

- Second task: Development of temperature stable functional (flame retardant) surfactant for MMT to be used for the modification of MMT as well as to be coupled to the polymer matrix by accelerated electrons.

Flame retardant polymer nanocomposites based on PP, FR and MMT are widely studied. However, the main disadvantage is the low thermal stability of surfactant used to modifiy MMT. Thus, a functional modifier for MMT (FO-MMT) is developed to enhance the thermal stability and to generate a synergistic effect for the flame retardancy. According to the patent EP 2643389B1 [133], FO-MMT was designed to EB modification to graft the surfactants to PP resulting in PP increased stress transfer to exfoliated MMT platelets. In this work, both of functional fire retardants and functional surfactants are designed for grafting and/or crosslinking by high energy electrons. The morphology, thermal stability, fire behavior, and mechanical properties of these flame retardant PP composites are investigated. Furthermore, the detailed mechanisms are discussed.

The modification of flame retardant PP by EB technology is studied in order to establish a relationship between raw materials, process, morphology, and nanocomposite properties.

3.2 Strategy for this thesis

This research approach is related to material science and engineering, covering a wide range of areas of organic chemistry, polymer chemistry, polymer modification with high energy electrons, polymer processing and fire chemistry. The structure property relationships and mechanism are studied in detail. The strategy for this thesis is shown in Fig. 3.1.

(1) Design and synthesis of novel functional modifier and fire retardant

According to the molecular design, functional fire retardants and functional modifiers are designed firstly. The additives contain unsaturated bonds (C=C) to be used for chemical reactions with generated PP macroradicals under well designed EB conditions in order to enhance the properties of fire retardant PP composites. The chemical structures of synthesized additives are characterized by NMR, FTIR, etc.

(2) Preparation of functional nanomaterials

In this study, MMT, one of the most attractive subclass of smectite, is used as basic nanofiller. The synthesized modifiers and fire retardants of section (1) are used to modify this nanofiller via the cation exchange, aiming to be reactive with the polymers during EB treatment. These functionalized nanomaterials are investigated by WAXS, SEM, TGA, etc.

(3) Preparation of fire retardant PP nanocomposites

Fire retardant polymer nanocomposites are prepared by melt compounding. The samples to be tested are produced by injection molding.

(4) Fire retardant PP nanocomposites modified by electron beam technology

The fire retardant (FR) PP nanocomposites based on functional fire retardants, FO-MMT and polypropylene. They are modified by EB technology to study the impact of high energy electron treatment on the properties of FR PP nanocomposites. The interfacial adhesion between the nanomaterials and polymer matrix as well as the reaction between the fire retardant and polymer matrix are studied systemically.

(5) Structural properties relationships and mechanism

On the one hand, structural properties relationship includes the full-scale properties of fire retardant polymer nanocomposites, like thermal behavior, burning behavior, mechanical properties etc. On the other hand, it includes the detailed study on the mechanisms, such as flame retardant mechanism as well as mechanism of reinforcement. The analytical techniques include cone calorimeter, LOI, UL94, MCC, FTIR, XRD, DSC, TGA, SEM, and TGA-FTIR.

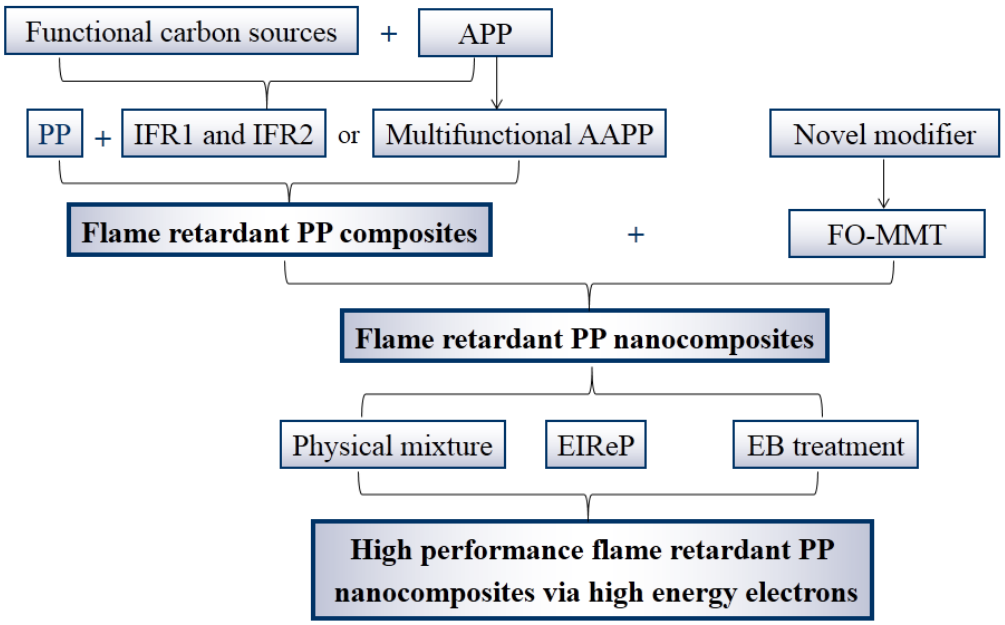

Fig. 3.1 Scheme for this thesis

Chapter 4

Experimental

4.1 Materials

Phosphorus oxychloride, pentaerythritol, neopentyl glycol, triethylamine, allylamine, 10-bromodec-1-ene, toluene, ethanol, triphenylphosphine, prop-2-en-1-amine, trichloromethane, sodium hydroxide and tetrahydrofuran were purchased from Sigma-Aldrich Chemical Reagent Co., Ltd. and used without further purification. The toluene was dried by 4Å molecular sieves. Sodium montmorillonite with trade names of MMT-Na and surface of montmorillonite coated by bis(2-hydroxyethyl)-methyl-octadecyl-ammonium group with trade names of O-MMT were purchased from BYK-Gardner GmbH. Its cation exchange capacity (CEC) amounts to 98.7 mEq per 100 g. Polypropylene (PP, HD 120MO, density = 0.908 g/cm^3, number average molar mass = 220200 ± 4500 g/mol) was purchased from Borealis, Porvoo, Finland. Ammonium polyphosphate (APP, density = 1.9 g/cm^3, degree of polymerization ≥ 1000, solubility ≤ 0.50 g/100ml (25 °C in wather)) was supplied by Budenheim company.

4.2 Synthesis section

4.2.1 Synthesis of DPA

N^1-(5,5-dimethyl-1,3,2-dioxaphosphinyl-2-yl)-acrylamide (DPA) was prepared from neopentyl glycol and phosphoryl chloride, leading to 2,2-dimethyl-1,3-propanediol phosphoryl chloride, which reacted with prop-2-en-1-amine, as shown in Fig. 4.1. First of all, phosphorus oxychloride reacts with the alcohol group of neopentyl glycol to an intermediate is formed and the by-product hydrogen chloride is absorbed by sodium hydroxide. Subsequently, the nitrogen-phosphorus band of DPA is formed by reation of 2,2-dimethyl-1,3-propanediol phosphoryl chloride and the amino group of prop-2-en-1-amine.

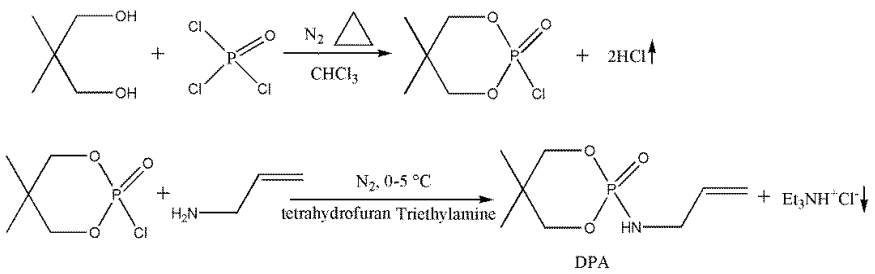

Fig. 4.1 Synthesis of DPA

4.2.1.1 Synthesis of 2,2-dimethyl-1,3-propanediol phosphoryl chloride

Neopentyl glycol (104 g, 1 mol) and 300 ml trichloromethane were charged to a 500 ml baked out and dry nitrogen filled flask with dropping funnel, a stirrer, reflux condenser, and rubber pipe to transport the generated hydrogen chloride into the sodium hydroxide solution (1 mol/L). Phosphorus oxychloride (153.6 g, 1 mol) was added slowly by drops and the temperature was kept at about 50 °C during the process. After adding phosphoryl chloride, the temperature was increased to 60 °C and kept constant for 6 h. Then trichloromethane was removed to obtain a white solid 2,2'-dimethyl-1,3'-propanediol phosphoryl chloride (89 %). Characterization: **^{1}H NMR** (500 MHz, d_6-DMSO) (ppm): 3.92 - 3.85 (d, -CCH_2O-PO-, 8H), 0.95 - 0.92 (s, -CH_3). **FTIR** (ATR) (cm^{-1}) (1310, 1180, 972).

4.2.1.2 Synthesis of DPA

In a baked-out and dry nitrogen filled three-neck round-bottom flask equipped with a magnetic stirrer, a thermometer, a cooling bath, a mixture of prop-2-en-1-amine (0.5 mol) and tri-ethylamine (0.55 mol) was added dropwise to a stirred solution of 2,2'-dimethyl-1,3'-propanediol phosphoryl chloride (0.5 mol) in anhydrous tetrahydrofuran (350 ml) under nitrogen gas at 0-5 °C. Then the resulting mixture was allowed to warm to room temperature and left stirring for 12 h under nitrogen. The mixture was then filtered off by a Buchner funnel and the filtrate concentrated under reduced pressure. Finally, the residue was washed with ethyl ether (100 ml, 3 times). The white solid DPA (82 %) was dried in a vacuum oven at 80 °C for 12 h. Characterization: **^{1}H NMR** (500 MHz, $CDCl_3$) (ppm): 5.83-5.13 (m, $CH=CH_2$, 3H), 4.48-4.23 (m, -CH_2-, 4H), 3.89-3.72 (m, -CH_2-, 2H), 0.93 (m, -CH_3, 6H). **FTIR** (ATR) (cm^{-1}) (3189, 2877, 1652, 1211, 1049, 817).

4.2.2 Synthesis of SPSA

Spirocylic pentaerythritol bisphosphorate disphosphoryl-di-prop-2-en-1-amine (SPSA) was prepared from pentaerythritol and phosphoryl oxychloride, leading to spirocylic pentaerythritol bisphosphorate diphosphoryl chloride, which then reacted with prop-2-en-1-amine, as outlined in Fig. 4.2. First of all, phosphorus oxychloride reacts with alcohol group of pentaerythritol to double intermediates are formed and the by-product hydrogen chloride is absorbed by sodium hydroxide. Subsequently, the nitrogen-phosphorus band of SPSA is formed by reation of spirocylic pentaerythritol bisphosphorate diphosphoryl chloride and the amino group of prop-2-en-1-amine. The leaving group hydrogen chloride is precipitated.

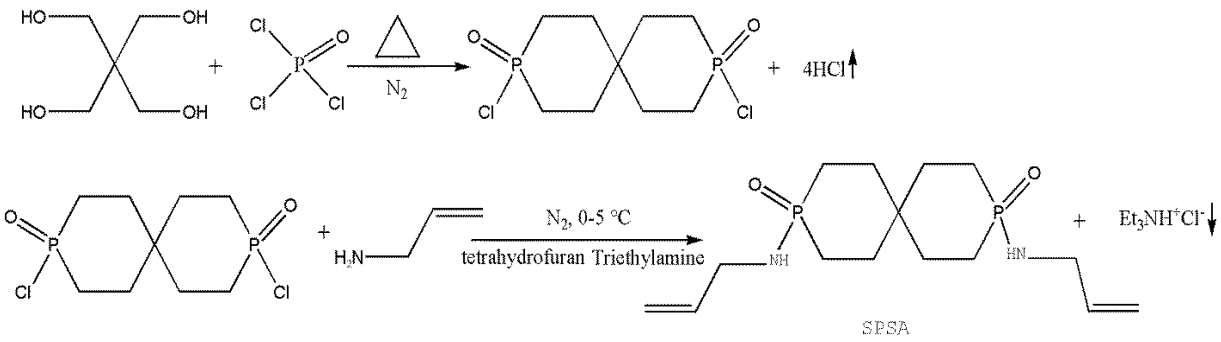

Fig. 4.2 Synthesis of SPSA

4.2.2.1 Synthesis of spirocylic pentaerythritol bisphosphorate diphosphoryl chloride

In a 500 ml glass flask equipped with a magnetic stirrer, a thermometer, a heating bath and circumference condenser, pentaerythritol (68 g, 0.5 mol) and phosphoryl chloride (618 g, 4 mol) were mixed. The mixture was stirred about 100 °C until HCl evolution subsided. Then, the mixture was gradually heated to about 105 °C and refluxed until no HCl gas was emitted. The raw product obtained was filtered and purified using a filter with chloroform (80 ml, 3 times) sequentially. The product was dried to constant mass at 55 °C in vacuum 12 h. Thus, spirocylic pentaerythritol bisphosphorate diphosphoryl chloride, a white solid powder, was obtained (108 g, yield: 73 %). Characterization: **^{1}H NMR** (500 MHz, *d_6*-DMSO) (ppm): 4.23-4.20 (d, -CCH_2O-PO-, 8H). **FTIR** (cm^{-1}): (1305, 1025).

4.2.2.2 Synthesis of SPSA

In a three-neck round-bottom flask equipped with a magnetic stirrer, a thermometer, a cooling bath, a mixture of prop-2-en-1-amine (28.5 g, 0.5 mol) and triethylamine (70 ml, 0.5 mol) were added dropwise to a stirred solution of spirocylic pentaerythritol bisphosphorate diphosphoryl chloride (60 g, 0.2 mol) in anhydrous tetrahydrofuran (100 ml) under nitrogen gas at 0 - 5 °C. The resulting mixture was allowed to warm to room temperature and left stirring for 12 h under nitrogen. Then the mixture was filtered off by a Buchner funnel. Finally, the filtrate was concentrated and and washed by ethyl ether (80 ml, 3 times). Thus, the product SPSA (57 g, yield: 85 %) was distilled at 38 °C under reduced pressure to provide the desired compounds. Characterization: **^{1}H NMR** (500 MHz, $CDCl_3$) (ppm): 5.80-5.11 (m, -CH=CH_2, 6H), 4.51-3.00 (m, -CH_2-, 14H), 0.93 (m, -CH_3, 6H). **FTIR** (ATR) (cm^{-1}) (3311, 2877, 1635, 897).

4.2.3 Synthesis of AAPP

Allylamine polyphosphate (AAPP) was prepared from APP and allylamine via ion exchange reation. At high temperatures, the ammonia gas was released from APP, leading to acidic APP is to be replaced by alkaline allylamine. The reaction is shown in Fig. 4.3.

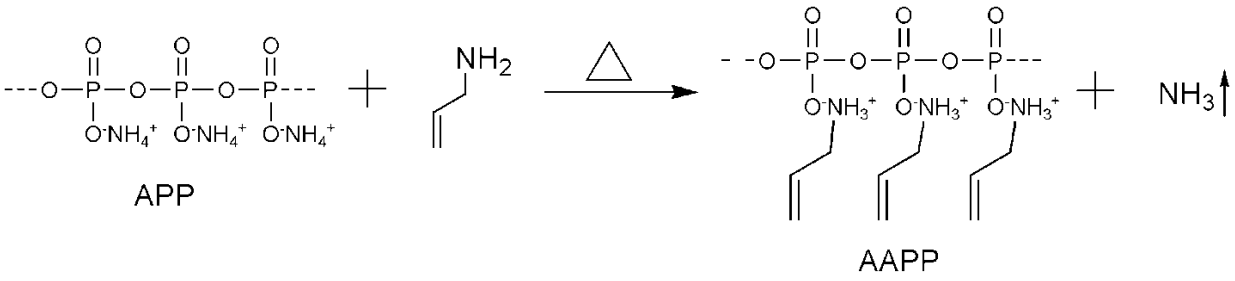

Fig. 4.3 Synthesis of AAPP

In a three-neck round-bottom flask equipped with a magnetic stirrer, a thermometer, a heating bath, allylamine (60 g) and APP (100 g) were added in the mixed solvent of water (1000 ml). Then, the mixture was heated up to 60 ºC under nitrogen. After 2h, the ammonia gas was released. Next, the reaction mixture was cooled down to room temperature. After that, the mixture was concentrated at reduced pressure and washed with ethanol (100 ml, 2 times). Then, white solid was filtered, and then the sample was dried in a vacuum oven at 80 ℃ for 12 h. Characterization: **^{1}H NMR** (500 MHz, D_2O) (ppm): 5.72-5.70 (m, CH=, 1H), 5.27-5.24 (m, CH_2=, 2 H), 3.47-3.47 (d, -CH_2-, 2H). **^{31}P NMR** (500 MHz, D_2O) (ppm): -24.1. **FTIR** (ATR) (cm^{-1}) (2654, 2150, 1631, 1260, 1228, 1063).

4.2.4 Synthesis of TPB

Triphenyl(undec-10-enyl)phosphonium bromide (TPB) was prepared from triphenylphosphine and 10-bromodec-1-ene, a similar ylide reagent in Wittig reation. The unshared pair electrons of triphenylphosphine reacts with electron withdraw group of alkyl halide 10-bromodec-1-ene. The reaction is shown in Fig. 4.4.

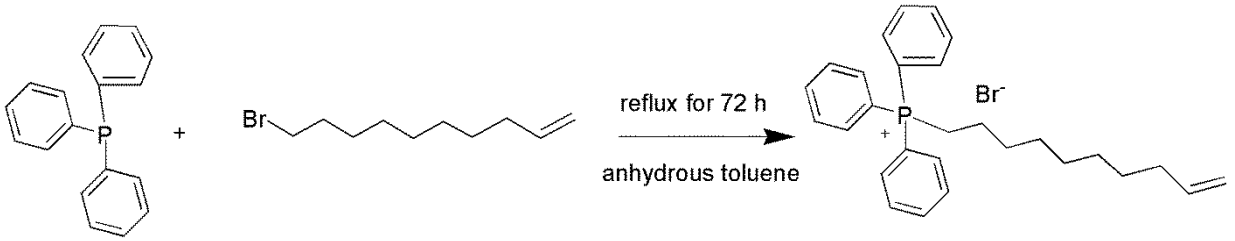

Fig. 4.4 The reaction of TPB

In a baked-out and dry nitrogen filled three-neck round-bottom flask equipped with a magnetic stirrer, a thermometer, a heating bath, finely ground triphenylphosphine (393 mg, 1.5 mmol) was added to a solution of 10-bromodec-1-ene (218 mg, 1 mmol) in anhydrous toluene (20 ml). Afterward, the mixture was heated at 113 °C at reflux for 72 h under nitrogen. The reaction mixture was cooled. Subsequently, all of the solution was slowly dropped in the petroleum ether at 0 °C, the solid precipitate was collected. The resulting solid was dried under vacuum to get TPB (419 mg, yield: 85 %) as a pale yellow solid. Characterization: **^{1}H NMR** (500 MHz, d_6-DMSO) (ppm): 8.00-7.25 (m, H of benzene, 15H), 5.87-5.80 (m, -CH_2-, 2H), 4.98-4.11 (m, -CH=CH_2, 3H), 1.56-1.08 (m, -CH_2-, 16H). **FTIR** (ATR) (cm^{-1}) (2921, 1585, 1473, 1430, 1307, 1182, 738, 689).

4.2.5 Preparation of FO-MMT

Functional organically modified MMT (FO-MMT) was prepared by cation exchange method. The preparation procedures are shown in Fig. 4.5.

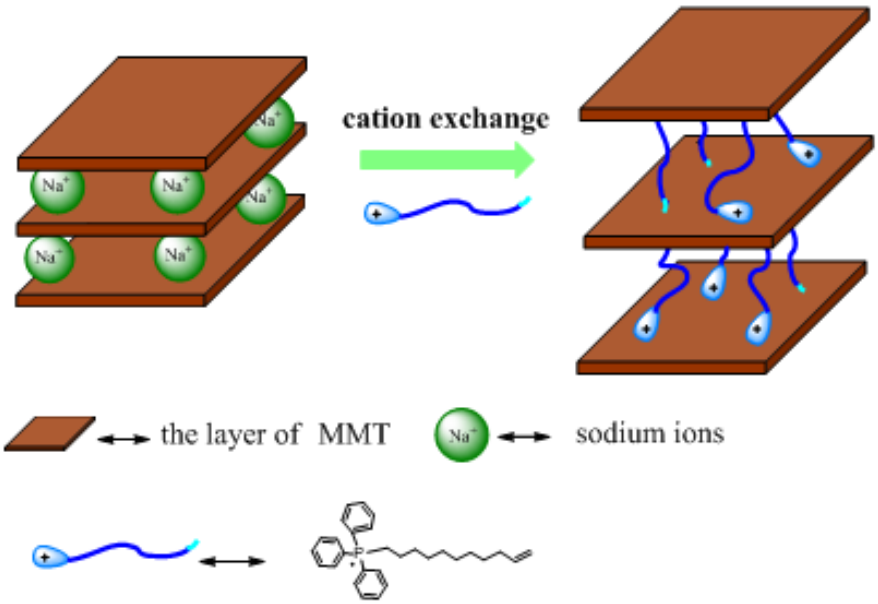

Fig. 4.5 Intercalated functionalized FO-MMT by cation exchange method

In a filled three-neck round-bottom flask equipped with a magnetic stirrer, a thermometer, a heating bath, MMT-Na (3 g) was dispersed in distilled water and ethanol (800 ml: 200 ml) at 80 °C. The amount of surfactant TPB was about 1.2 times of cation exchange capacity (CEC), based on CEC = 98 meq/100 g. The mixture was stirred over night at 80 °C. After cooling to room temperature, the FO-MMT was filtered using a Buchner funnel. The resulting FO-MMT

was washed with distilled water and ethanol (800 ml: 200 ml) several times until no bromide ions were detected by the silver nitrate test and then dried in vacuum at 70 °C over night. Characteristic reflections of MMT materials with a series of (001) reflections at a low angle, corresponding to the basal spacing and higher order reflections. In comparison, the unmodified MMT shows an interlayer distance of 0.98 nm. In the case of FO-MMT, the first reflection peak is shifted to 4.76º. Thus, the interlayer distance amounts to 1.85 nm according to the Bragg equation.

4.3 Preparation of flame retarded PP

4.3.1 Melt compounding

Flame retardants were dried in a vacuum oven at 80 °C for 8 h before used. At first, the preliminary formulations were investigated via microcompounder (15 mL, DSM Xplore, Geleen, Netherlands) at 190℃ and a rotor speed of 200 rpm for 10 min. Then, PP blends filled with different ratios of flame retardants (see Table 5.1, Table 5.4, Table 5.7, Table 5.11, Table 5.17, and Table 5.18) were prepared by extrusion (twin-screw extruder KETSE 20/40 EC, Brabender) with the rotation speed of 80 rpm. The following temperature protocol from the feed zone to the die: 175, 180, 180, 175, 175 and 170 ºC. PP/AAPP/FO-MMT composites (see Table 5.17 and Table 5.18) were done via the mixing chamber in 170 °C with 60 rpm by melt mixing for a total mixing time of 13 minutes.

4.3.2 Molding

The pellets were put into injection molding machine (Arburg 320 C) at a processing temperature of about 200 °C in order to produce the samples with suitable dimensions for UL-94, LOI and tensile tests. In addition, some samples (PP/IFR1 (100 × 100 × 4 mm^3), PP/IFR2 (100 × 100 × 4 mm^3), and PP/AAPP/O-MMT composites (100 × 100 × 4 mm^3) for cone calorimeter tests were molded by injection molding (Arburg 320 C). Others sheets (PP/AAPP (100 × 100 × 3 mm^3), PP/AAPP/FO-MMT for EB treatment (100 × 100 × 2 mm^3) and PP/AAPP/FO-MMT for EIReP (100 × 100 × 1 mm^3) composites) for cone calorimeter tests were compression molded by hot-plate press (LabPro 400, Fontijne Presses) at 210 ºC.

4.3.3 Electron beam irradiation

The FR contains double bonds in order to graft these FR by high-energy electrons to PP. The amount of FR depends strongly on the requirements of flame retardancy (LOI, UL 94, and CC

tests). Thus, the absorbed dose has to be determined in such a way, that the numbers of PP radicals are equal to the number molecules of FR in order to graft each FR to PP chain.

The number of radicals was determined using the definition of absorbed dose (eq. (4.1)). We used this definition and applied it to the polymer molecule by introducing the energy absorbed per polymer chain (E_{pol}) as well as average mass of the polymer chain (m_{pol}) (eq. (4.2)). E_{pol} amounts to the product of average number of radicals per PP molecule (N_r) and the energy required for the generation of one radical per PP molecule (E_r). The overall G-value (G_t) describes the average number of radicals generated per 100 eV of absorbed energy. In the case of PP, G_t amounts to 2.45 radicals per 100 eV (average value from literature). Thus, we calculated E_{pol} in accordance to eq. 4.3. Using the correlation between m_{pol} and number average molar mass (M_n) we got eq.4.4 for the calculation of absorbed dose for the generation of N_r.

$$D = \frac{E}{m} \quad \text{(eq. 4.1)}$$

$$D = \frac{E_{pol}}{m_{pol}} \quad \text{(eq. 4.2)}$$

$$E_{pol} = N_r * E_r = \frac{N_r}{G_t} \quad \text{(eq. 4.3)}$$

$$D = \frac{N_r * N_A}{M_n^{PP} * G_t} \Rightarrow N_r = \frac{D * M_n * G_t}{N_A} \quad \text{(eq. 4.4)}$$

The overall number of PP radicals (N^{PP}_r) should be equal to the overall number of FR molecules (N^{FR}) in order to graft all FR molecules to PP molecules (eq. 4.5). In eq. 4.5 we used the relationship that N^{PP}_r is equal to the product of average number of radicals per PP molecule and the number of PP molecules.

$$N^{PP}_r = N_r * N^{PP} = N^{FR} \Rightarrow N_r = \frac{N^{FR}}{N^{PP}} \quad \text{(eq. 4.5)}$$

The number of molecules (N) is proportional to the amount of substance (n) which is defined as ratio of mass for a pure sample (m) to the molar mass of this substance (eq. 4.6). In the case of compounds, we have to take into account the concentration of this substance (c) in the compound. Finally, we got the eq. 4.7 in order to calculate the required absorbed dose for the grafting of all FR to the PP molecules.

$$n = \frac{m}{M} \quad \text{(eq. 4.6)}$$

$$D = \frac{N_A}{M_n^{PP} * G_t} * \frac{N^{FR}}{N^{PP}} = \frac{N_A}{M_n^{PP} * G_t} * \frac{M_n^{PP} * c^{FR}}{M^{FR} * c^{PP}} = \frac{N_A}{G_t} * \frac{c^{FR}}{M^{FR} * c^{PP}} \quad \text{(eq. 4.7)}$$

Therefore, in this study, flame retardant PP composites were irradiated at room temperature in nitrogen atmosphere with different dose using an ELV-2 electron accelerator (BINP, Novosibirsk, Russia). The electron energy was 1.5 MeV, and the electron current amounted to 4 mA.

Flame retardant PP nanocomposites was developed by EIReP where a high energy electron accelerator is coupled with an internal mixer at 170 °C with 60 rpm by melt mixing for a total mixing time of 13 minutes. The electron energy was 1.5 MeV, and the electron current amounted to 4 mA.

4.4 Characterization techniques

4.4.1 Structural characterization

Fourier transform infrared spectra (FTIR) of the samples were recorded using a Bruker Vertex 80/80v spectrometer (Bruker, Germany) within the wave number range of 4000-600 cm^{-1}. The experiment was carried out in the attenuated total reflection (ATR) mode.

^{1}H nuclear magnetic resonance (^{1}H NMR) and ^{31}P nuclear magnetic resonance (^{31}P NMR) spectra of the samples were performed on Bruker spectrometer (DRX 500, Germany) using deuterium-oxide (D_2O), dimethyl sulfoxide-d_6 (DMSO-D_6), or deuterated chloroform ($CDCl_3$) as a solvent.

4.4.2 Morphological characterization

Wide angle X-ray scattering (WAXS) tests were obtained using 2-circle diffract meter XRD 3003 T/T (GE Inspection Technologies/Seifert-FPM, Germany) with Cu-K α radiation (λ = 0.1541 nm) generated at 40 kV and 30 mA in the range of 2 θ = 0.5 to 70° using 0.05° as step length (Δ 2θ).

High-resolution transmission electron microscopy (TEM) was observed using a Libra 200 with integrated Ω-type energy filter (Carl Zeiss Microscopy GmbH, Germany). Ultra-thin sections of the rubber specimens were placed by ultramicrotomy (Reichert Ultracut S, Austria)

at -130 °C with a thickness of a section 100 nm. The energy filter was tested for electron energy-loss spectroscopy and elemental mapping by energy-filtered imaging.

Scanning electron microscopy (SEM) with energy dispersive X-ray analysis (EDX) was observed using microscope model (Carl Zeiss SMT, Germany) to study morphological features of the powdered samples. The samples were prepared using conducting copper tape and then coated with a thin layer of platinum (layer thickness 3 nm) using a sputter coater (BAL-TEC SCD 500 sputter coater).

4.4.3 Thermal properties

The thermogravimetric analysis (TGA) was carried out for all the samples using a TGA Q 5000 (TA Instruments, Germany) in the range from 40 to 700℃ . The samples were heated at heating rate of 10 K/min under nitrogen atmosphere.

Differential scanning calorimetry (DSC) was observed using TA Instruments coupled with an autosampler in the temperature range of -50 to 150 °C at the scanning rate of 10 K/min under nitrogen atmosphere.

4.4.4 Fire behavior

Limiting oxygen index (LOI) is definited as the minimum concentration of oxygen that can support the combustion of polymer. LOI is tested by passing a mixture of oxygen (O_2) and nitrogen (N_2) over a burning specimen, and reducing the oxygen level until a critical level is reached. The value of LOI is expressed in the oxygen/(nitrogen+oxygen) (see eq. 4.8) that either maintains flame combustion of the sample for 3 min or consumes a length of 5 cm of the material, with the material placed in a vertical position (the top of the test sample is inflamed with a burner).

$$LOI(\%) = \frac{[O_2]}{[O_2] + [N_2]} \times 100\% \quad \text{(eq. 4.8)}$$

In this study, the LOI was measured using an Oxygen Index Instrument (Fire Testing Technology, UK) with the sample dimensions (120 × 6.5 × 3 mm^3), according to the standard DIN EN ISO 4589-1 and 4589-2.

UL-94 vertical burning test is a plastics flammability standard [134] which is proposed by Underwriters Laboratories for safety of flammability of polymer for parts in devices and appliances testing. UL-94 suspended vertically above a cotton patch is performed. The flame is applied for 10 s and then removed. The after flame time t_1 (the time required for the flame to

extinguish) is noted. After extinction, the flame is applied for another 10 s. The after flame time t_2 is noted, together with the after glow time t_3 (the time required for the fire glow to disappear). The standard specifies that five specimens must be tested. The specimen is classified as V-0, V-1 or V-2 according to the criteria listed in Table 4.1.

In this study, the UL-94 tests were performed using a vertical burning instrument (Fire Testing Technology, UK), and the specimens in this work for testing were of dimensions (130 × 13 × 3.2 mm^3) according to the standard ASTM D 3801.

Table 4.1 UL94 vertical burning test classification [134]

Criteria conditions	V-0	V-1	V-2
After flame time for each individual specimen t1 or t2	≤ 10 s	≤ 30 s	≤ 30 s
Total after flame time for any condition set (t1 plus t2 for the 5 specimens) for 5 specimens	≤ 50 s	≤ 250 s	≤ 250 s
After flame plus afterglow time for each individual specimen after the second flame application (t2+t3)	≤ 30 s	≤ 60 s	≤ 60 s
Flame or glowing up to the clamp	No	No	No
Cotton ignition	No	No	Yes

The cone calorimeter (CC) is regarded as one of most powerful bench-scale fire facilities. Its principle is based on oxygen consumption in the combustion of polymer. Conical radiant electrical heater uniformly irradiates the sample from above. The combustion is triggered by an electric spark [135, 136]. The measurements of the gas flow and oxygen concentration are used to calculate the quantity of heat released per unit of time and surface area: heat release rate (HRR) expressed in kW/m^2. The evolution of the HRR over time, in particular the value of its peak heat release rate (PHRR), is usually taken into account in order to evaluate the fire properties. Key parameters measured in one or both of the cone calorimeter and smoke density tests include HRR, total heat release (THR), mass loss (ML), time to ignition (TTI), carbon monoxide (CO) and carbon dioxide (CO_2) production, total smoke production (TSP), smoke production rate (SPR), smoke toxicity index and specific optical density, etc.

In this study, the cone calorimeter test was carried out on a cone calorimeter (Fire Testing Technology, UK) by following ISO 5660-1. The squared specimens (100 × 100 × 1 ~ 4 mm^3)

were wrapped in aluminum foil and placed in a frame without the grid. The specimens were irradiated at a heat flux of 50 kW/m^2, corresponding to a medium fire scenario.

4.4.5 Mechanical properties

Tensile test (TS) was carried out according to ISO 527/1BA/10 on dumb bell-shaped specimens using a tensile testing machine (Zwick 8195.05, Germany) at a constant cross-head speed of 10 mm/min. The E modulus was determined in between 0.1 and 0.25 % tensile strain.

The PP/AAPP/FO-MMT composites were carried out according to DIN EN ISO 527-2/1BA/ 50 on dumb bell-shaped specimens using a tensile testing machine (Zwick 8195.05, Germany) at a constant cross-head speed of 50 mm/min. The E modulus was determined in between 0.05 and 0.25 % tensile strain.

4.4.6 Mechanism studies

Thermogravimetry-infrared spectroscopy (TG-FTIR) was done with a Q5000 (TA Instruments, USA) coupled with fourier-transformed infrared spectrometer Nicolet 380 (Thermo Electron, USA) from 40 to 700 ℃ at a heating rate of 10 K/min and under nitrogen atmosphere (25 ml/min). The FTIR spectra of the gas evolved were acquired from 8 scans with a resolution of 4 cm^{-1}.

Scanning electron microscopy (SEM) (microscope model: Ultra Plus, Carl Zeiss SMT) with energy dispersive X-ray analysis (EDX) was used to study morphological features of the powdered samples. The samples were placed on a sample holder using conducting copper tape and then coated with a thin layer of platinum (layer thickness 3 nm) using a sputter coater (BAL-TEC SCD 500 sputter coater).

Chapter 5

Results and discussion

5.1 DPA based PP/IFR1 composites

APP is an efficient phosphorus-containing FR due to its high contents of phosphorus and nitrogen. However, APP is not an efficient FR for PP when it is used alone because of missing a carbon source. To increase the flame retardancy of APP, a novel charring agents physically combined with APP (it was not coupled to APP by chemical bonds) were prepared. However, traditional charring agent has low thermal stability since there is not chemical coupling between charring agent and polymer. Therefore, the novel carbon source N^1-(5,5-dimethyl-1,3,2-dioxaphosphinyl-2-yl)-acrylamide (DPA) together with APP as a novel IFR1 was developed and functionalized with a carbon-carbon double bond (=) for EB induced grafting with the polymer chain. In this part, first of all, DPA was synthesized according to the procedure reported in Fig. 4.1. DPA was physically combined with APP (mass ratio of DPA and APP was 1:2) to prepared a novel IFR1. PP mixed with APP as reference system and different ratios (see Table 5.1) of IFR1 were prepared by a twin-screw extruder. Then, the pellets were put into injection molding machine to produce the samples with suitable dimensions for flame retardancy test. Afterwads, these composites were irradiated using an ELV-2 electron accelerator with dose values of 32 kGy. The flame retardancy properties of PP, PP/APP and PP/IFR1 composites were studied by LOI, UL-94 and CC test. In addition, the morphology of char residues was investigated by SEM with EDX. Finally, the effect of high energy electron on the thermal stability of PP/IFR1 composites was investigated.

Table 5.1 Formulation of neat PP, PP/APP and PP/IFR1 composites

Sample	PP (wt %)	APP (wt %)	DPA (wt %)
Neat PP	100	0	0
PP/30%APP	70	30	0
PP/30%IFR1	70	20	10
PP/25%IFR1	75	16.7	8.3
PP/20%IFR1	80	13.3	6.7

5.1.1 Structural characterization of DPA

5.1.1.1 FTIR spectroscopy of DPA

The FTIR spectrum of DPA is presented in Fig. 5.1. The absorption band at 3189 cm^{-1} corresponds to vibration of N-H, and the band at 2877 cm^{-1} is assigned to CH_2 stretching. Moreover, the band at 1211 cm^{-1} is associated with the stretching mode of P=O and the absorption band at 1049 cm^{-1} is for P-O-C stretching band. The absorption band at 817 cm^{-1} is assigned to the skeleton vibration of caged bicycle phosphates. Also, the characteristic absorption band for carbon-carbon double bonds (1652 cm^{-1}) is clearly observed.

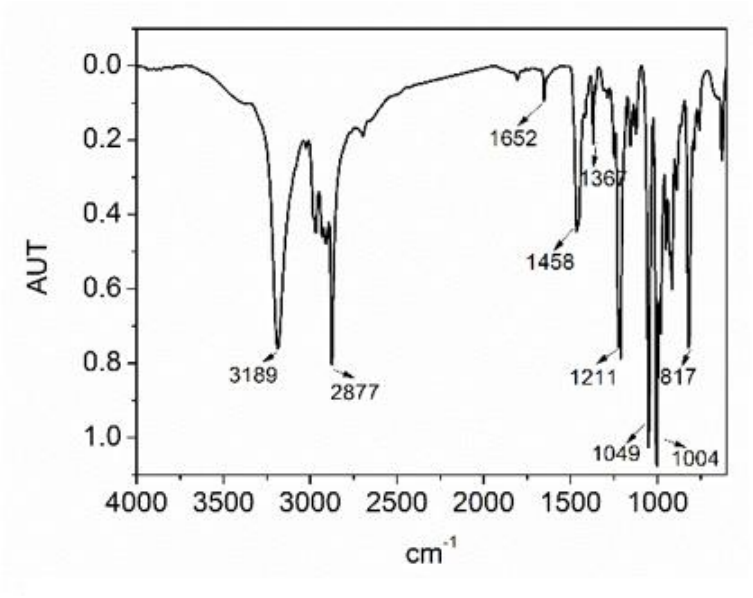

Fig. 5.1 FTIR spectra of DPA

5.1.1.2 ^{1}H-NMR spectroscopy of DPA

The ^{1}H NMR spectrum of DPA is shown in Fig. 5.2. The multiple peaks between 5.83 and 5.13 ppm (f, g) corresponds to the protons of the double bond. Signals from 4.48 to 4.23 ppm are attributed to the $–CH_2–$ protons (b) from the caged bicyclic phosphates, and the $–CH_2–$ protons (d) adjacent to the double bond resonate at 3.89 and 3.72 ppm. The band at 0.93 ppm is assigned to the protons on $–CH_3$ of the structure of DPA segments (corresponding to a in Fig. 5.2).

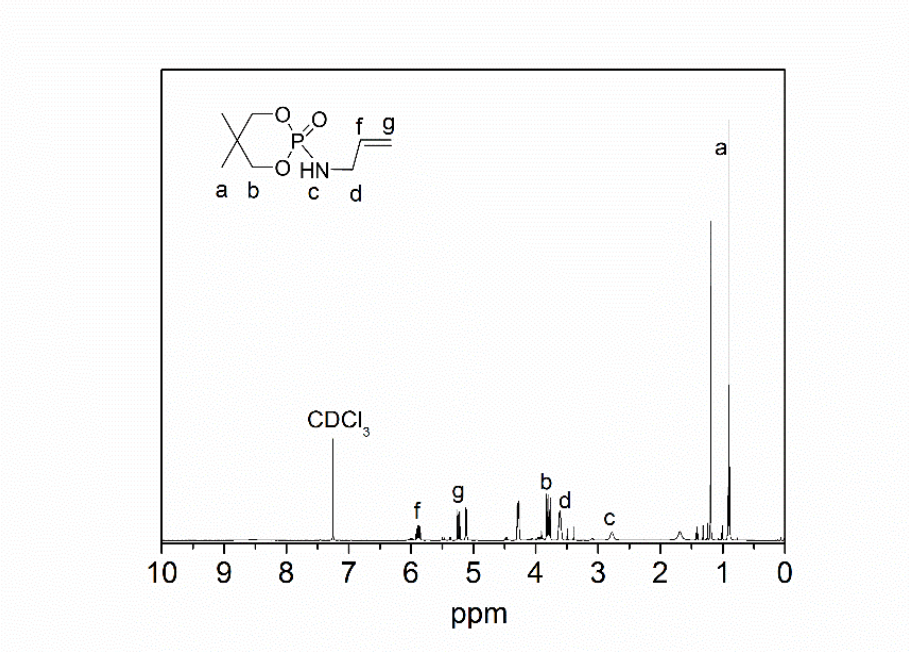

Fig. 5.2 ^{1}H NMR spectra of DPA

5.1.2 Fire behavior of PP/IFR1 composites

5.1.2.1 LOI and UL94

The LOI values and UL94 results for neat PP, PP/APP and PP/IFR1 composites are showed in Table 5.2. The LOI value of PP with 30 wt % APP is 20.4 %. Meanwhile, there is melt dripping in UL94 test. However, it is seen from Table 5.2 that the LOI value of PP containing 20, 25, and 30 wt % IFR1 are 21.3, 22.6 and 24.5 %, respectively. When the content of IFR1 reached 30 wt %, PP/IFR1 composites passes V-0 rating and has no dripping. These results indicate that IFR1 has a higher efficiency than APP alone.

Table 5.2 LOI values and UL94 results of neat PP, PP/APP and PP/IFR1 composites

Sample	LOI (%)	UL94	Dripping
PP	17.6	N.R.	Yes
PP/30%APP	20.4	N.R.	Yes
PP/30%IFR1	24.5	V-0	NO
PP/25%IFR1	22.6	N.R.	Yes
PP/20%IFR1	21.3	N.R.	Yes

N.R.: no rating

5.1.2.2 Cone calorimeter

The heat release rate (HRR) is recognized to have the greatest influence on the developing, spreading and intensity of fires [136]. The experimental results of neat PP, PP/APP and PP/IFR1 composites are shown in Fig. 5.3. It is detected that neat PP burnt easily after ignition at the range of 40 – 230 s. The peak heat release rate (PHRR) is 842 kW/m^2. The PHRR of PP with 30 wt % APP decreases to 490 kW/m^2. However, the PHRR of PP with 20, 25, and 30 wt % IFR1 are reduced to 418, 384 and 331 kW/m^2, respectively. It is found that there are some peaks at the HRR plots of PP/IFR1 composites. In this case, the first peak is identified as the development of the ceramic surface layer. After that, the HRR plots tend to a relatively steady state [44, 67, 85], which is proof that IFR1 is a more efficient flame retardant to PP compared with APP alone.

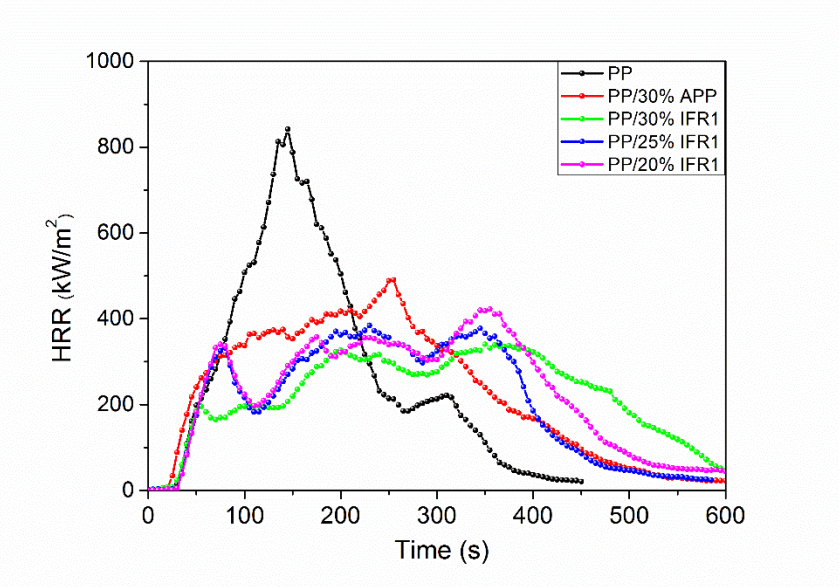

Fig. 5.3 HRR plots of neat PP, PP/APP and PP/IFR1 composites

Total heat release (THR) vs. times plots of neat PP, PP/APP and PP/IFR1 composites are presented in Fig. 5.4. As could be observed, the maximum (124 MJ/m^2) THR of neat PP is reached after 300 s. The growth THR rate of PP/IFR1 composites is much lower of than that of PP/30%APP composites. The reduction of THR in PP/30% IFR1 composites indicates that more PP chains participate in aromatization, carbonization, and therefore less combustible products go into the gas phase [44, 54].

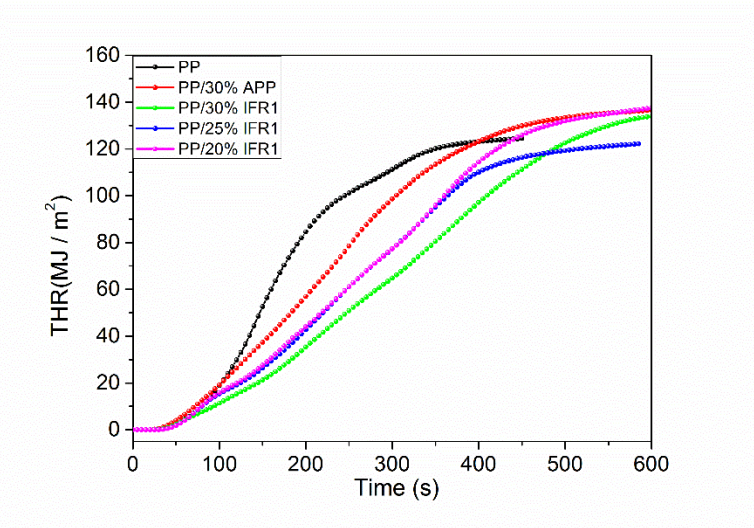

Fig. 5.4 THR plots of neat PP, PP/APP and PP/IFR1 composites

5.1.3 Morphology of burnt PP/IFR1 composites

Digital photos for the residues of neat PP, PP/APP and PP/IFR1 composites after CC tests are shown in Fig. 5.5. The residues of PP with 30 %APP are not expanded in Fig. 5.5 b_1, and Fig.5.5 b_2. For the PP/30%IFR1 composites, a thick and cohesive residual char is formed. It can be seen that there are some swollen residual char (Fig. 5.5 c_1, and Fig. 5.5 c_2) which might act as barrier to prevent the transmission of oxygen and heat.

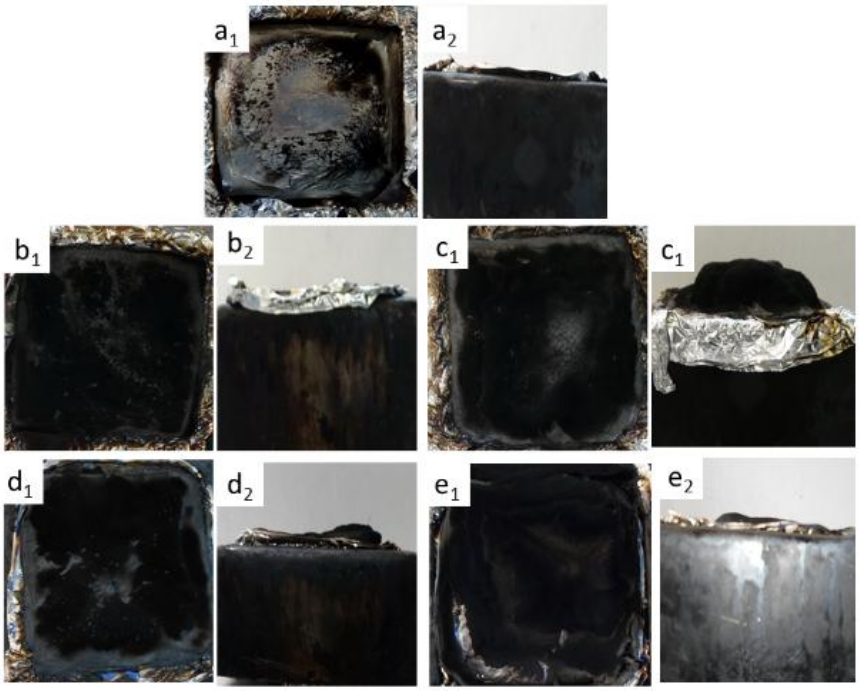

Fig. 5.5 Digital photographs for the residues of neat PP (a_1, a_2), PP/30% APP (b_1, b_2), PP/30% IFR1 (c_1, c_2), PP/25% IFR1 (d_1, d_2) and PP/20% IFR1 (e_1, e_2) after CC tests

To further evaluate the IFR1 residues structure, the microstructures of residues are tested by SEM and EDX. The SEM imagers for the residues of the outer and inner surface of PP/30% IFR1 composites are shown in Fig. 5.6. The outer surface of the PP/30% IFR1 composites char residues (Fig. 5.6a) is continuous, compact and unsmoothed during the combustion process. The inner surface of char residues (Fig. 5.6b) exhibits cell structure and the swollen chars are expanded as the calceolate structure. In addition, closed holes observed in the inner surface might be caused by the gases generated during the combustion. The results of EDX analysis for the char residues of PP with 30% IFR1 is given in Fig. 5.6c. The content of C, O, N and P element of the char residues of PP/30% IFR1 are 25.1, 3.8, 46.6, and 24.5 wt %, respectively. Consequently, rich P and N-based compounds are formed on the surface via varied decomposition and reconstruction processes.

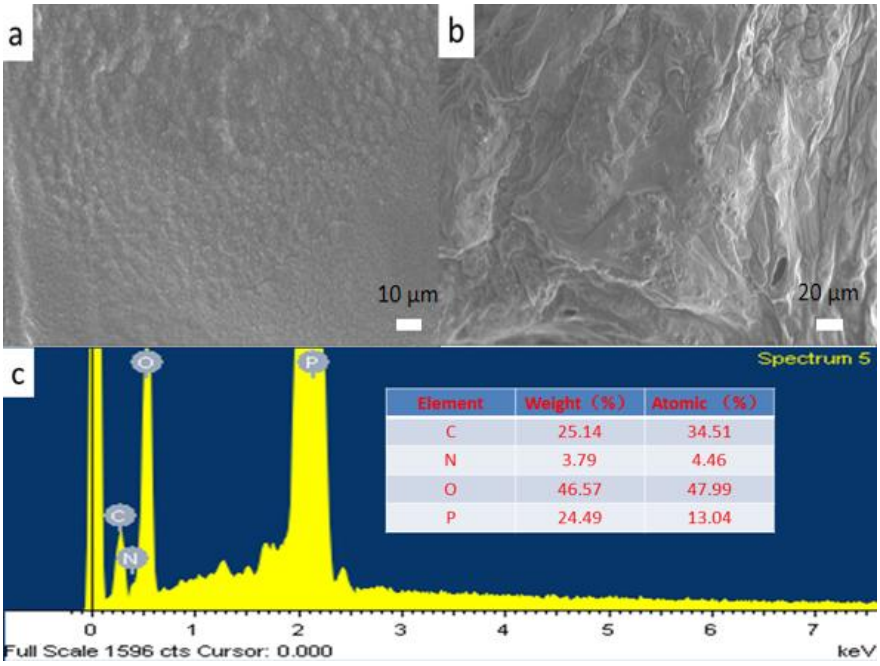

Fig. 5.6 SEM images for the outer residues surface (a) and the inner residues surface (b) of PP/30% IFR1; EDX spectra (c) for the char residues of PP/30% IFR1

5.1.4 Thermal properties of PP/IFR1 composites

The thermogravimetric analysis (TGA) and derivative thermogravimetric analysis (DTG) plots of non-irradiated as well as EB irradiated PP and PP/IFR1 composites under N_2 atmosphere are presented in Fig. 5.7. The data are summarized in Table 5.3. As shown in Fig. 5.7(a), there is only one degradation step for neat PP ranging from 350 to 450 °C. The thermal decomposition of PP/30%IFR1 composites is more complex with several decomposition steps. When the

heating temperature increases to 200 °C, the PP/30% IFR1 composites begins to decompose, where ammonia and water molecules release.

The $T_{-5\%}$ (5 wt % of mass loss) of neat PP is 371 °C in Fig 5.7(a). After irradiation, $T_{-5\%}$ value of EB PP is reduced to 348 °C due to EB induced chain scission. Obviously, the thermal stability of flame retardant PP composites is remarkably improved via EB treatment. For example, $T_{-5\%}$ value of PP/30%IFR1 composites is increased from 287 °C to 319 °C. Moreover, the T_{max} of flame retardant PP composites are also increased via EB treatment. These results illustrate that the thermal stability of PP/IFR1 composites is improved under high enery EB treatment. Herein, a possible grafting mechanism between DPA and PP is proposed in Fig. 5.8. As a result of the interaction of high energy electrons with PP matrix, the macroradicals are produced by inducing chemical reactions from the structure of tertiary hydrogen (C−H). Then, those macroradicals attached to the C=C group presented in the DPA to realize grafting reaction.

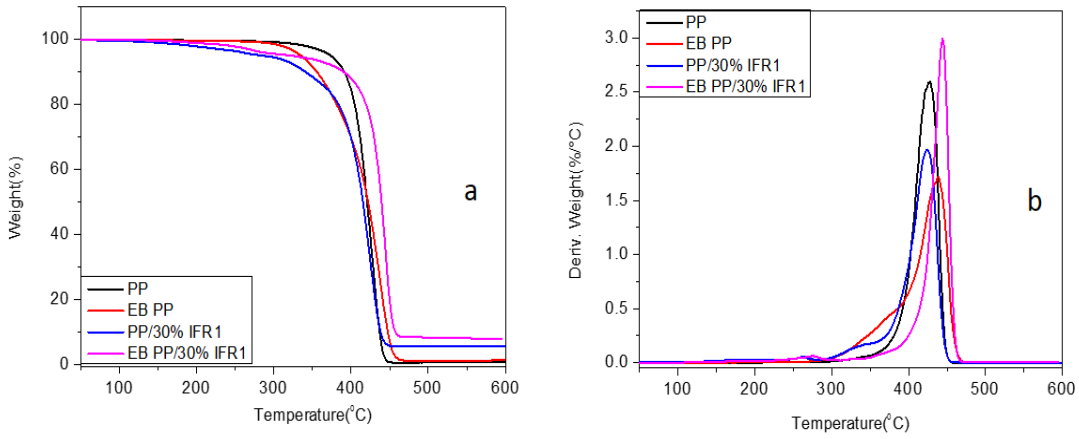

Fig. 5.7 The TGA (a) and DTG (b) plots of neat PP, PP/30%APP and PP/30%IFR1 composites

Table 5.3 Data obtained from TGA and DTG plots of neat PP, PP/30%APP and PP/30%IFR1 composites

Sample	$T_{-5\%}$ (°C)	T_{max} (°C)	R_{max} (%/K)
PP	371	428	2.6
EB PP †	348	426	1.5
PP/30% IFR1	287	423	2.0
EB PP/30% IFR1 †	319	442	3.0

† The composites were irradiated with a dose of 32 kGy

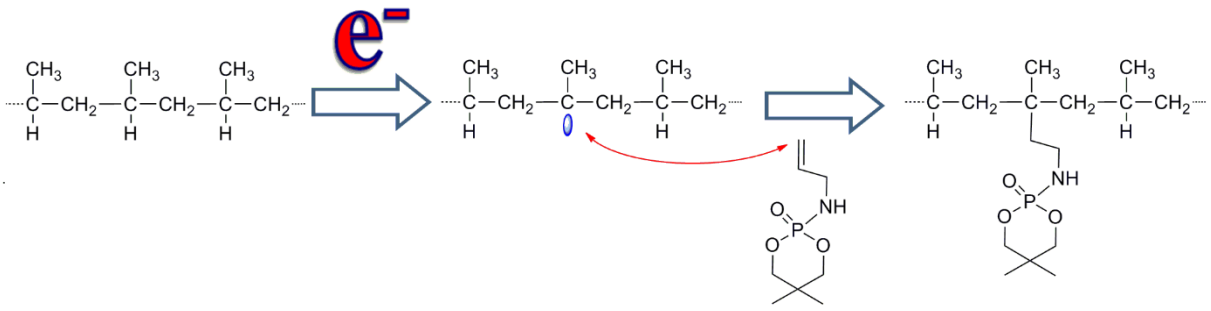

Fig. 5.8 Possible grafting mechanism via EB treatment

5.1.5 Conclusions

To increase the flame retardancy of APP in PP, the carbon source N^1-(5,-dimethyl-1,3,2-dioxaphosphinyl-2-yl)-acrylamide (DPA) functionalized with a carbon-carbon double bond was synthesized and characterized. The IFR1 based on APP and DPA was mixed with PP via twin-screw extruder. The PP with 30 wt % IFR1 composites passed the UL-94 V-0 rating (3.2 mm) and its LOI value reached 24.5 %. Moreover, the CC data showed that PP/IFR1 composites had a better contribution to the HRR and THR of PP/IFR1 composites compared to PP/APP composites. In addition, SEM micrographs illustrated that a compact and stable residues layer for PP/IFR1 composites was formed during the combustion process, which acted as good barrier to prevent the transmission of fuel and oxygen. Aiming to further increase the thermal stability of flame retardant PP composites, the thermal stability of PP/IFR1 composites was enhanced under EB treatment which might be a promising formulation to increase the low thermal stability of intumescent flame retardant polymer composites. Due to the structure of carbon sources influence the property of flame retardant PP composites, different kind of functional charring agent would be studied via EB treatment in the next part.

5.2 SPSA based PP/IFR2 composites

In subchapter 5.1, DPA consisting of acid sources, blowing agent, carbon source, and one carbon-carbon double bond was prepared. Nevertheless, different kinds of charring agents greatly influence the stable intumescent char in the flame retardant process. One of the most effective IFR formulations is the system consisting of APP and pentaerythritol (PER). Unfortunately, it has some disadvantage that the conventional APP-PER additives have lower thermal stability and worse flame retardancy compared with halogenated flame retardant. To deal with these problems, the acid source structures of double caged phosphorus (eg. spirocylic pentaerythritol bisphosphorate diphosphoryl) have been reported [84-88], which are reacted between phosphorus oxychloride and -OH group of PER. However, there is still not any chemical coupling between these charring agent and polymer, it leads to low thermal stability of flame retardant PP composites. Thus, in this part, the halogen-free functional charring agent containing caged phosphorus structure that may couple with PP by EB treatment, spirocyclic pentaerythritol bisphosphorate disphosphoryl-di-prop-2-en-1-amine (SPSA), was developed according to the procedure reported in Fig. 4.2. SPSA was used together with APP (mass ratio of SPSA and APP was 1:2) to prepared a novel IFR2. PP mixed with APP as reference system and different ratios (compositions see Table 5.4) of IFR2 were prepared by a twin-screw extruder. Then, the pellets were put into injection molding machine to produce the samples with suitable dimensions for on LOI, UL-94 sample, and CC test. Afterwards, these composites were irradiated with dose values of 32 kGy in N_2 at room temperature. SPSA was characterized by FTIR, and ^{1}H NMR. The flame retardancy properties of neat PP, PP/APP and PP/IFR2 composites were studied by LOI, UL-94, and CC test. The morphology of char residues was investigated by SEM with EDX. In addition, the influence of EB treatment on the thermal stability of PP/IFR2 composites was investigated.

Table 5.4 Formulation of neat PP, PP/APP and PP/IFR2 composites

Sample	PP (wt %)	APP (wt %)	SPSA (wt %)
PP	100	0	0
PP/30%APP	70	30	0
PP/30%IFR2	70	20	10
PP/25%IFR2	80	13.3	6.7
PP/20%IFR2	75	16.7	8.3

5.2.1 Structural characterization of SPSA

5.2.1.1 FTIR spectroscopy of SPSA

In order to identify the structure of SPSA, firstly, FTIR spectroscopy is used as shown in Fig. 5.9. The characteristic absorption band at 3311 cm^{-1} is attributed to the N-H bond segments in the structure of SPSA. Also, the characteristic absorption bands for carbon-carbon double bonds (1635 cm^{-1}) are clearly observed. The band at 987 cm^{-1} is assigned to P-O-C bond on the structure of SPSA segments.

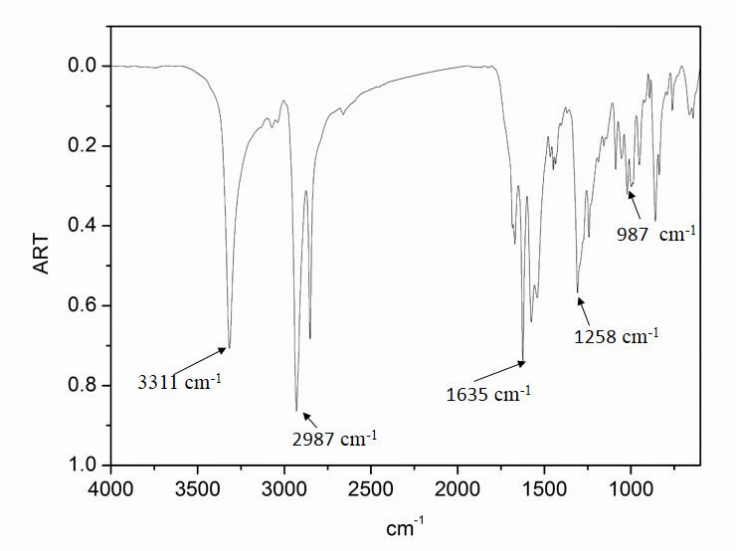

Fig. 5.9 FTIR spectrum of SPSA

5.2.1.2 ^{1}H-NMR spectroscopy of SPSA

Further structural confirmation for SPSA is made by means of ^{1}H NMR spectroscopy. As shown in Fig. 5.10, the band groups at 5.80-5.11 ppm are assigned to the protons on the carbon-carbon double bond on the structure of SPSA segments (corresponding to a, b in Fig. 5.10). The band groups at 4.51-3.00 ppm are assigned to the protons on methylene groups of the structure of SPSA segments (corresponding to d, e in Fig. 5.10).

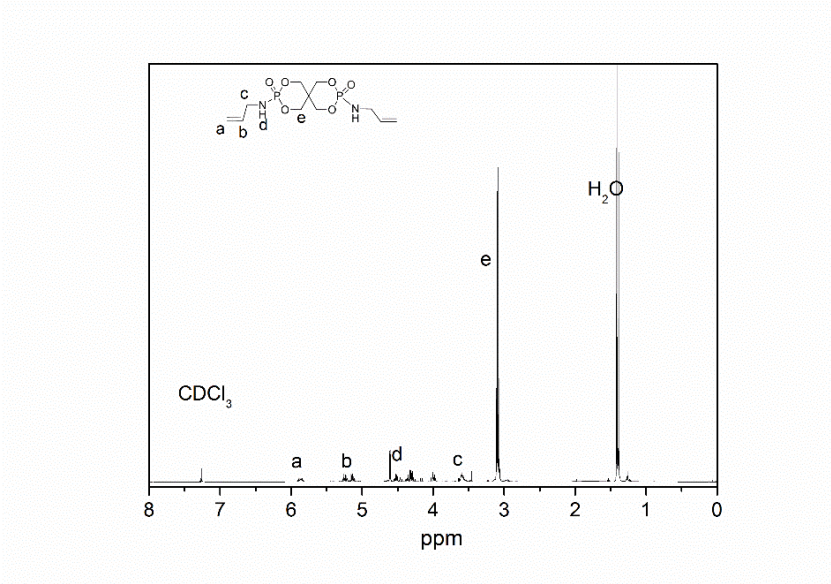

Fig. 5.10 ^{1}H NMR spectrum of SPSA

5.2.2 Fire behavior of PP/IFR2 composites

5.2.2.1 LOI and UL94

The LOI and UL94 tests are used to investigate the flammability of neat PP, PP/APP and PP/IFR2 composites. The results are shown in Table 5.5. Obviously, LOI value of neat PP is only 17.6 %, showing high flammability. At the loading of 30 wt % APP, the LOI value of PP/APP composite increases to 20.4 %, but there is no rating in the UL 94 test. In comparison, the LOI values of PP/IFR2 composites containing 20, 25 and 30 wt % IFR2 are 21.0, 22.5 and 24.0 %, respectively. PP with 30 wt % IFR2 passes UL 94 V-0, indicating that this IFR2 is more efficient than APP alone.

Table 5.5 LOI values and UL94 results of neat PP, PP/APP and PP/IFR2 composites

Sample	LOI (%)	UL94	Dripping in UL94 test
PP	17.6	N.R.	Yes
PP/30%APP	20.4	N.R.	Yes
PP/30%IFR2	24.0	V-0	NO
PP/25%IFR2	22.5	N.R.	Yes
PP/20%IFR2	21.0	N.R.	Yes

N.R.: no rating

5.2.2.2 Cone calorimeter

The HRR plots of PP, PP/APP and PP/IFR2 composites are showed Fig. 5.11. Neat PP burns fast after ignition and a sharp HRR peak appears with a peak PHRR of 842 kW /m^2. In the case of PP with 30 wt % APP, the PHRR decreases to 489 kW/m^2. However, the PHRR of PP/IFR2 containing 20, 25, and 30 wt % IFR2 are 473, 449 and 430 kW/m^2, respectively. Obviously, this IFR2 is a more efficient flame retardant to PP compared to APP.

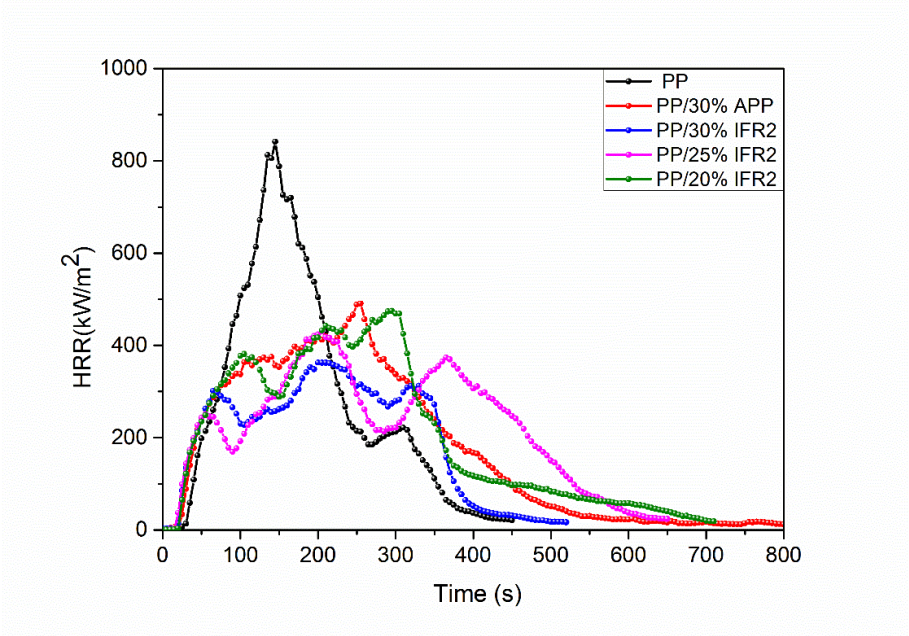

Fig. 5.11 HRR plots of neat PP, PP/APP and PP/IFR2 composites

THR values of neat PP, PP/APP and PP/IFR2 composites are presented in Fig. 5.12. In comparison to neat PP, all the flame retardant PP composites show lower THR within the first 350 s. Consequently, these flame retardant PP composites show a lower heat release during the combustion compared to that of neat PP. Further, the difference in the THR between flame retardant PP indicates that SPSA acts as an excellent flame retardant synergist to traditional APP since both composites contain 30 wt % flame retardant additives.

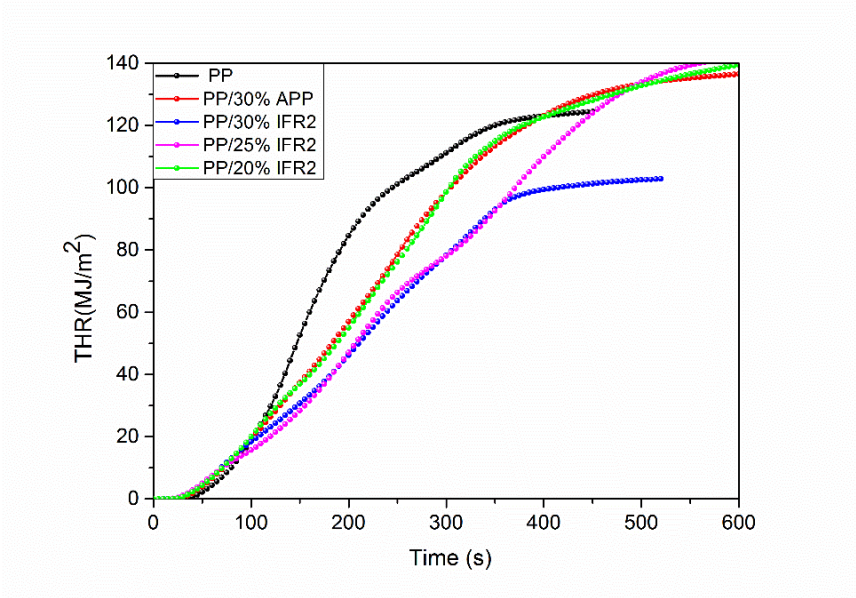

Fig. 5.12 THR plots of neat PP, PP/APP and PP/IFR2 composites

5.2.3 Morphology of burnt PP/IFR2 composites

From the digital photos (as shown in Fig. 5.13) of the specimens after cone calorimeter test, there is almost no residue for neat PP. In comparison, after adding the flame retardant to PP, more char residues remain in the sample holder. In particular, by introducing IFR2 into PP, the quantity of formed char is improved. These improved char layers will act as good barrier to prevent the transmission of fuel and oxygen.

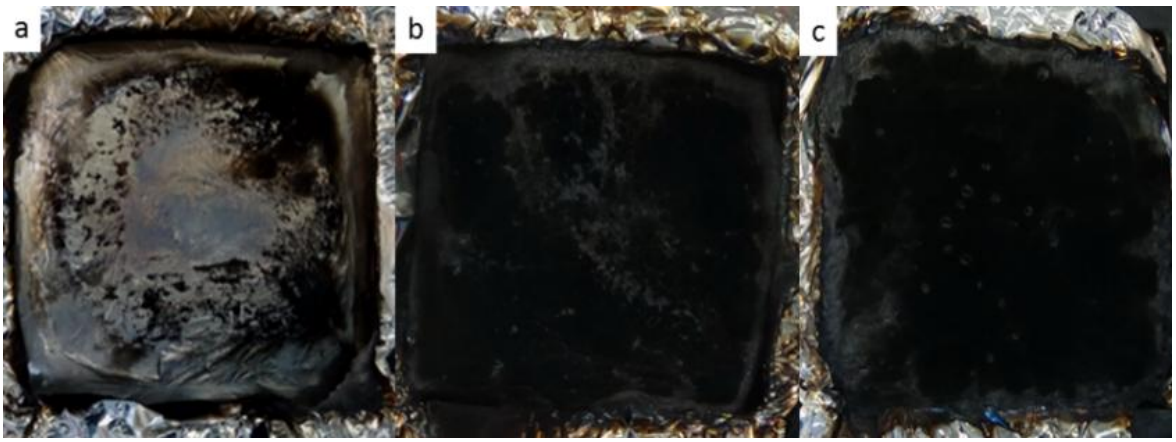

Fig. 5.13 Digital photographs of residue char for neat PP (a), PP composite with 30% APP (b), and PP composite with 30% IFR2 (c)

In order to further understand the relationship between the microstructure of intumescent chars and flame retardancy of PP composites, SEM micrographs for the char residues of the outer surface (Fig. 5.14a) and inner surface (Fig. 5.14b) of PP/30%IFR2 are imaged. It is noted

that the char morphology on the outer surface of PP/30%IFR2 showed the formation of a continuous and compact char layer, which would act as an insulating barrier to heat and it would prevent the access of oxygen during combustion. Aiming to further understand the elements distribution on the char residues, EDX is employed to characterize the residue. The results are shown in Fig. 5.14c. It is noted that in the elemental composition of the char residue of the PP/30% IFR2, the content of C, O, N, P are 34.4, 8.0, 36.8, and 20.9 %, respectively. This means that rich P and N-based compounds are formed on the surface via varied decomposition and reconstruction approaches.

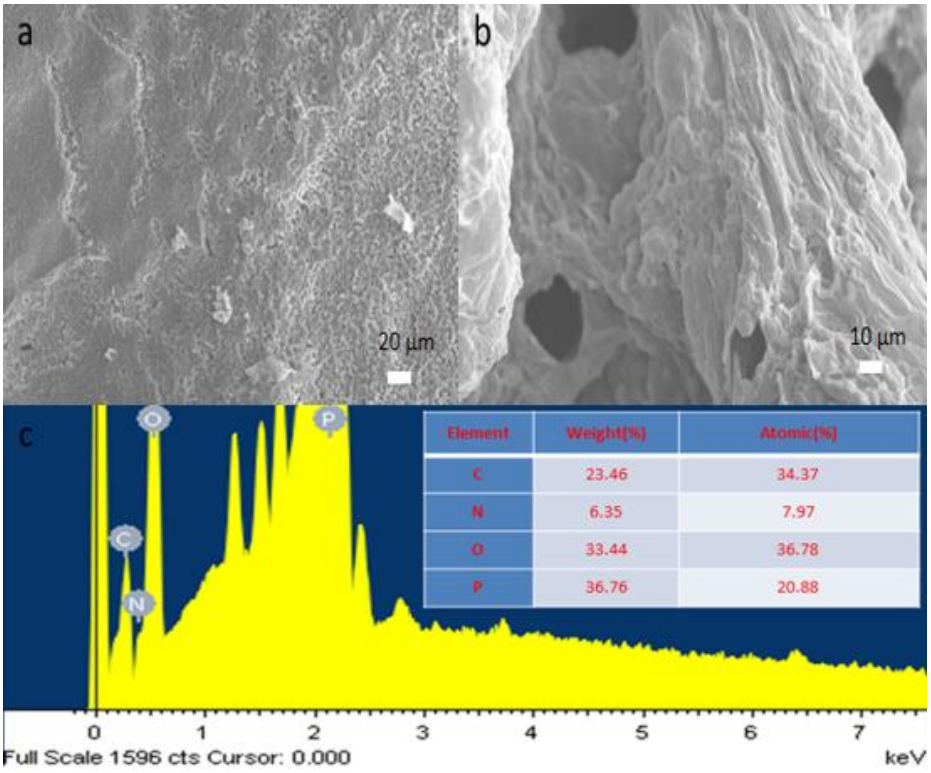

Fig. 5.14 SEM images for outer residues surface of PP/30% IFR2 (a); SEM images for the inner residues surface of PP/30% IFR2 (b); EDX spectra for the char residues of PP/30% IFR2 (c)

5.2.4 Thermal properties of PP/IFR2 composites

TGA and DTG plots of PP, PP/APP and PP/IFR2 composites are shown in Fig. 5.15. The corresponding data are given in Table 5.6. From Fig. 5.15, it is observed that all samples show only one degradation step within the experimental temperature range. It is clear from Fig. 5.15 and Table 5.6 that the addition of IFR2 had an obvious effect on the thermal stability of PP. The $T_{-5\%}$ value of neat PP is 374 ^{o}C. In the case of PP with 30 wt % of APP, the $T_{-5\%}$ decreases to 265 ^{o}C. In contrast, the $T_{-5\%}$ value of flame retardant PP composites containing 20 %, 25 %

and 30 % IFR2 are 315, 314, and 309 ºC, respectively. This indicates that the addition of IFR2 decrease the thermal stability of PP-based composites. However, as given in Table 5.6, T_{max} of PP amounts to 427 ºC, while the maximal decomposition temperature T_{max} of PP with 20 %, 25 % and 30 % IFR2 are 425 °C, 414 °C and 430 ºC. Consequently, there is only a small impact on the T_{max} of PP after adding IFR2.

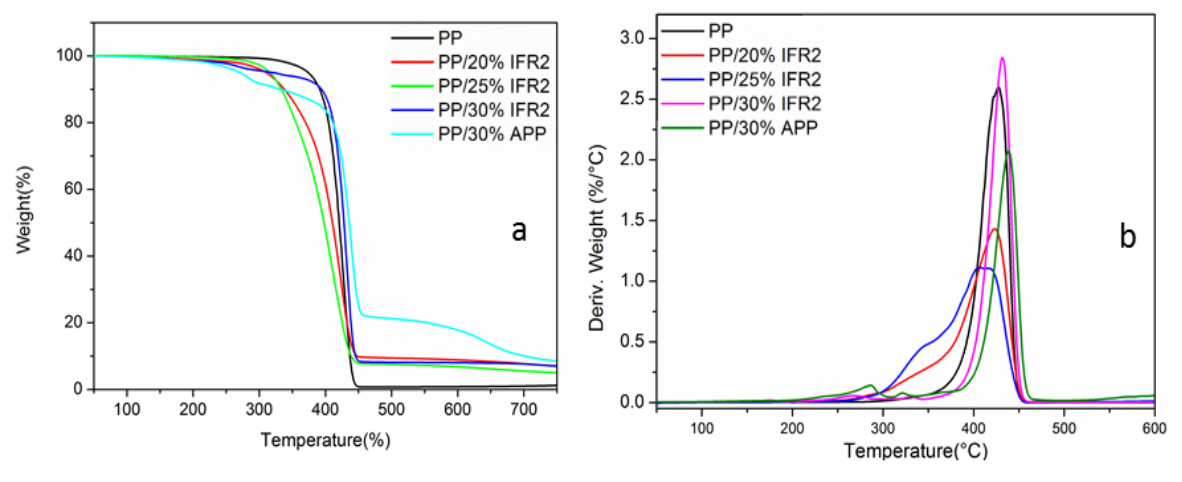

Fig. 5.15 The TGA (a) and DTG (b) plots of neat PP, PP/APP and PP/IFR2 composites

Table 5.6 Data obtained from TGA and DTG plots of neat PP, PP/APP and PP/ IFR2 composites

Sample	$T_{-5\%}$ (ºC)	T_{max} (ºC)	R_{max} (%/K)	Residue (%)	
				500 (ºC)	750 (ºC)
PP	374	427	2.5	1.1	1.0
PP/30% APP	265	439	2.0	21.2	8.6
PP/20% IFR2	315	425	1.4	6.6	6.5
PP/25% IFR2	314	414	1.1	7.3	7.2
PP/30% IFR2	309	430	2.8	7.6	7.5
EB PP/20% IFR2†	340	440	1.9	10.9	10.8
EB PP/25% IFR2†	337	438	1.8	7.3	7.2
EB PP/30% IFR2†	325	437	1.8	7.5	7.4

†The composites were irradiated with a dose of 32 kGy

Fig. 5.16 presents the TGA and DTG plots of non-irradiated and EB irradiated PP and PP/IFR2 composites and the corresponding values are listed in Table 5.6. Obviously, the thermal stability of flame retardant PP composites is remarkably improved via EB treatment. For example, $T_{-5\%}$ value of PP+20% IFR2 is increased from 315 to 340 ºC after EB treatment. Moreover, the T_{max} of flame retardant PP composites are also increased via EB treatment. Herein, a possible grafting and/or cross-linking mechanism between the novel flame retardant and PP is proposed, as shown in Fig. 5.17. Firstly, electron beam treatment results in the generation of PP macroradicals. Then, the macroradical reacts with the C=C group presented in the SPSA to generate the first grafting reaction. The same reaction can be induced by the macroradicals at the second C=C group of SPSA. Finally, a cross-linked structure is generated in the flame retardant PP composites.

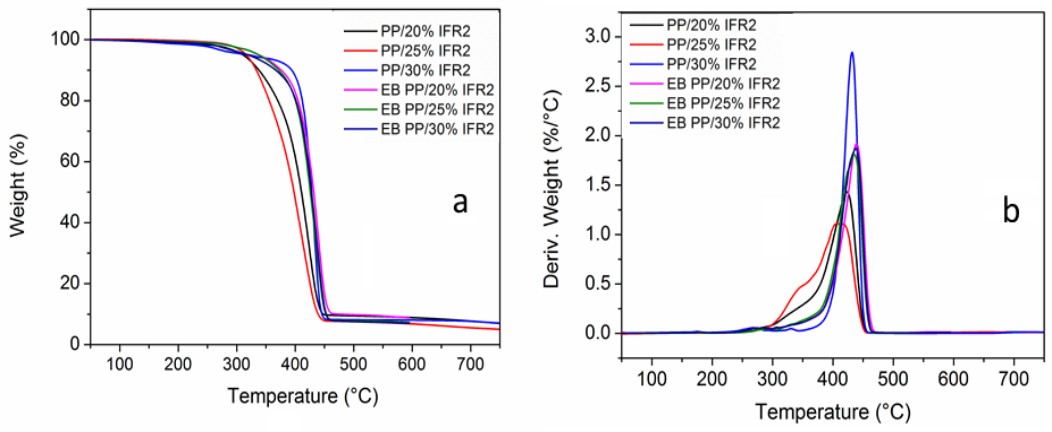

Fig. 5.16 The TGA (a) and DTG (b) plots of non-irradiated and electron beam irradiated PP/ IFR2 composites at 32 kGy

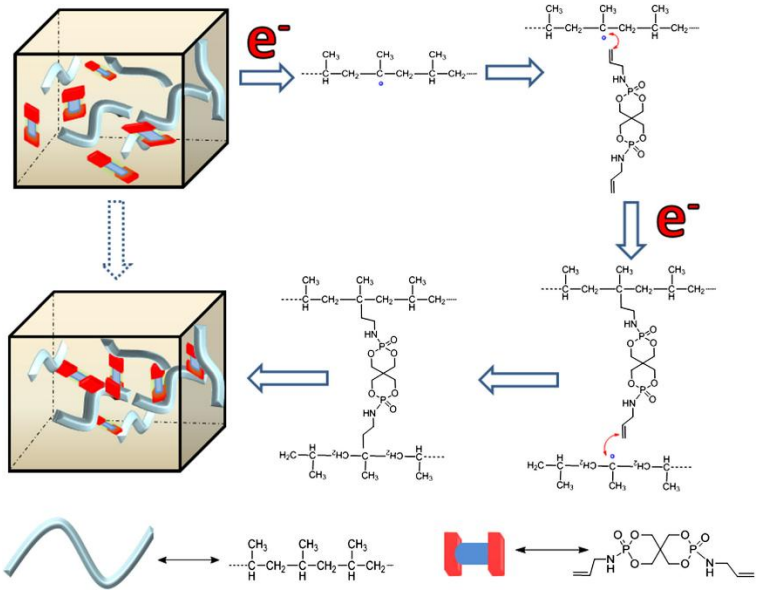

Fig. 5.17 Possible cross-linking mechanism

5.2.5 Conclusions

To develop high-performance flame retardant PP composites, a carbon source, spirocylic pentaerythritol bisphosphorate disphosphoryl-di-prop-2-en-1-amine (SPSA), containing two functional double bond (C=C) that may form crosslinked structure with PP in the EB treatment was synthesized and characterized successfully. Then, an IFR2 based on SPSA and physically combined with APP was developed and used in PP system to prepare fire retardant PP composites. LOI value of flame retardant PP composite containing 30% IFR2 was 24.0 %, while the LOI value of PP+30% APP was only 20.4 %. More importantly, PP+30% IFR2 passed UL 94 V-0, indicating that this IFR2 was more efficient than APP alone. In the case of PP/30%IFR1 composites passed the UL-94 V-0 rating and its LOI value reached 24.5 %. In the cone calorimeter test, both, PHRR and THR results of PP/IFR2 system were lower than those of PP/APP system. Moreover, EB treatment of the composites is an efficient approach to improve the thermal stability of these designed PP/IFR2 composites. In the case of PHRR of PP/30% IFR2 system is 430 kW/m^2, PHRR of PP/30 % IFR1 is 331 kW/m^2. It proved that this IFR1 is a more efficient flame retardant to PP compared to IFR2. However, the $T_{-5\%}$ value of PP/30%IFR1 and 30%IFR2 composites are 287 and 309 ℃ . That means thermal stability of PP/IFR2 composites is better than that of PP/IFR1 composites. Nevertheless, DPA and SPSA were developed from phosphorus oxychloride, which might lead to environmental risk. In addition, DPA and SPSA as carbon sources in IFR1 and IFR2 were not coupled to APP by chemical bonds. Thus, the multifunctional flame retadant would be developed in the next part.

5.3 Allylamine polyphosphate (AAPP) - a novel functional flame retardant material: Characterization and application in PP

APP is an extensively-used phosphorus-containing compound due to its low toxicity, high thermal stability, and low cost. Due to missing a carbon source, APP is not an efficient flame retardant for PP. Recently, Wang et al [15, 16] prepared modified APP by incorporation of ethanolamine and/or piperazine in APP via ion exchange reaction. This modified APP could greatly improve the stability of char layer and lead to much better flame retardancy than that of unmodified APP. However, their thermal stability is reduced due to the use of organic substances. Moreover, due to missing of any chemical bonds between these flame retardant and PP it might undergo migration. All of this greatly limits the efficiency of flame retardants and their further application. Therefore, efficient multifunctional flame retardant with a carbon source containing one double bond for stabilization by EB treatment is developed in order to increase the thermal stability in the PP matrix.

In subchapter 5.1 and subchapter 5.2 works, DPA and SPSA as carbon sources physically combined with APP were prepared to be grafted to PP by EB treatment. However, DPA and SPSA were not coupled to APP by chemical bonds. In this part, the novel multifunctional AAPP (Fig. 5.18) as an efficient flame-retardant crosslinker was synthesized by one step according to the procedure reported in 4.2.3. Then, a series of flame retarded PP composites (see Table 5.7) were prepared via twin-screw extruder. The thermal stability and fire behavior of these flame retarded PP composites were investigated by TGA, LOI, UL-94, and CC tests. Moreover, the thermal stability of non-irradiated and EB irradiated intumescent flame retarded PP composites were investigated. In addition, the relevant grafting and flame-retardant mechanism of PP/AAPP composites was also studied by TG-FTIR and SEM/EDX.

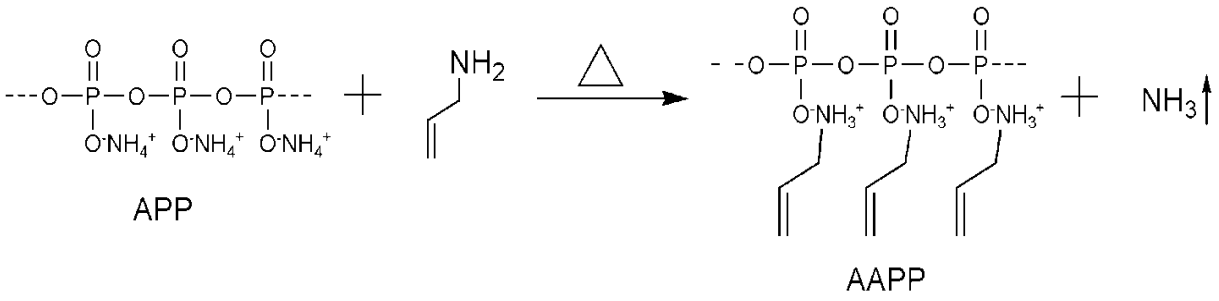

Fig. 5.18 Scheme for AAPP

5.3.1 Structural characterization of AAPP

5.3.1.1 FTIR

FTIR spectra of APP and AAPP are shown in Fig. 5.19. The regions of 3407-3000 cm^{-1} are attributed to the absorption of NH_4^+ symmetry stretching vibration. The bands at 2654 cm^{-1} and 2150 cm^{-1} correspond to the vibration of NH_3^+. Bands at 1260-1228 cm^{-1} are attributed to the P=O stretching vibration. The band at 1531 cm^{-1} is ascribed to the vibration of $–CH_2–NH_3^+$. The band at 1063 cm^{-1} is assigned to the P-O-N vibrations. After incorporating allylamine into APP, the band for the vibration of C=C appeared at 1632 cm^{-1} for AAPP.

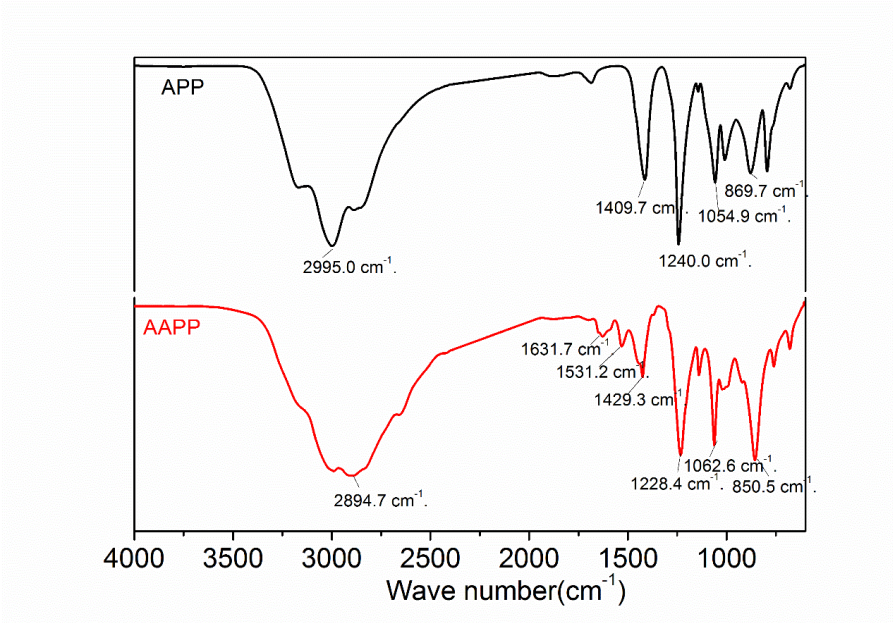

Fig. 5.19 FTIR spectra of APP and AAPP

5.3.1.2 ^{1}H-NMR and ^{31}P-NMR

The structural confirmation is made with the help of ^{1}H NMR analysis. As shown in Fig. 5.20, the peaks at 5.71 ppm and 5.25 ppm in AAPP correspond to the two protons of the carbon–carbon double bonds (corresponding to b and c in Fig. 5.20), which are related to allylamine. The peaks at 3.46 are assigned to the proton on the methylene groups (corresponding to a in Fig. 5.20) which is shifted after incorporation into AAPP compared to allylamine. For APP, there is no more ^{1}H-NMR peak other than the water peak at 4.80 ppm.

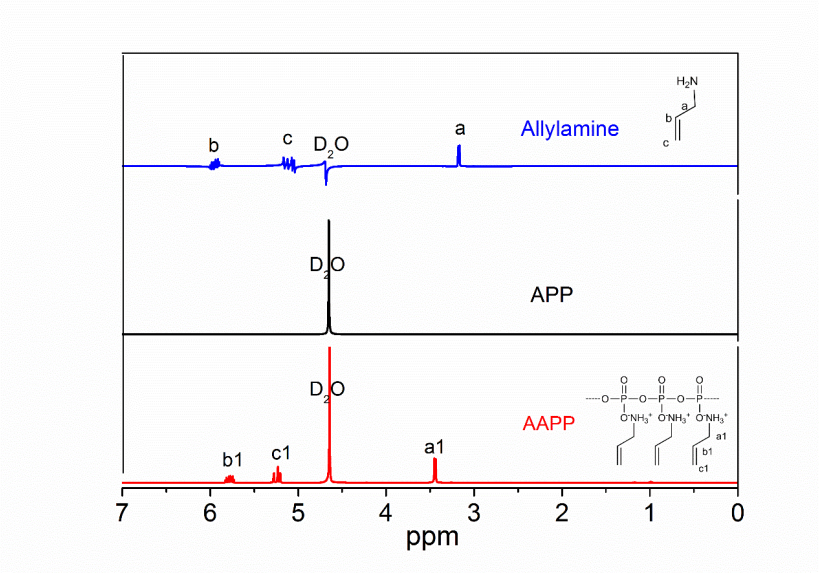

Fig. 5.20 ^{1}H NMR plots of allylamine, APP, and AAPP

The results of ^{31}P NMR are shown in Fig. 5.21. The peak at -23.4 ppm is assigned to the phosphate in APP. Since allylamine forms a strong ionic bond with APP, the corresponding peak of AAPP shifted to -24.1 ppm (Fig. 5.21). It is important to state, that in AAPP only one phosphor signal is observed which indicated that the ammonia groups of APP have been completely replaced by the allylamine groups. In summary, all these results mentioned above proved that the AAPP was successfully prepared by modification of APP.

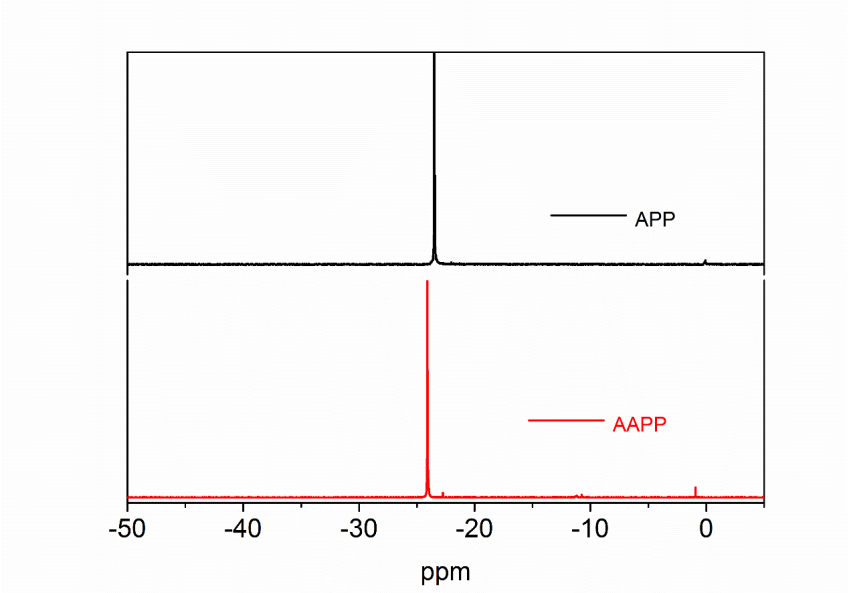

Fig. 5.21 ^{13}P NMR plots of APP and AAPP

5.3.2 Crystalline structure of AAPP

In order to investigate the effect of allylamine on the crystalline structure of APP and AAPP, XRD studies were done. The results are shown in Fig. 5.22. It is observed that APP has five typical XRD diffraction peaks (2θ = 14.8°,15.5°, 26.3°, 29.1°, 30.5°). After formation of an ionic bond between APP and allylamine, there are still peaks in the XRD spectrum of AAPP at 8.3°, 14.8°, 15.5°, 22.2°, 24.4°, 27.2°, and 29.1°. Consequently, AAPP has still a crystalline structure but, as expected, less pronounced and different compared to APP.

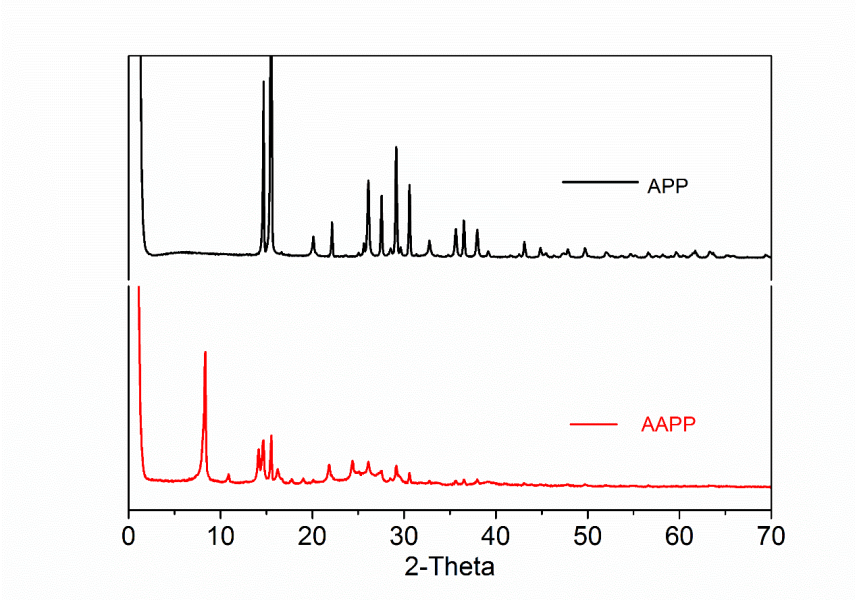

Fig. 5.22 XRD plots of APP and AAPP

5.3.3 Morphology of AAPP

The morphologies of APP and AAPP particles are shown in Fig. 5.23. The shape of APP is random and seems to be smooth in nature (Fig. 5.23a). However, the surfaces of AAPP are rougher (Fig. 5.23b) and some particles clung to each other. Obviously, the morphological surface of AAPP is rather different from those of APP, suggesting that the exchange of ammonia by allylamine occured. To further investigate the components of APP and AAPP, EDX-measurements were performed. In contrast to the EDX spectrum of APP the EDX spectrum of AAP clearly showed the presence of carbon (Fig. 5.23b).

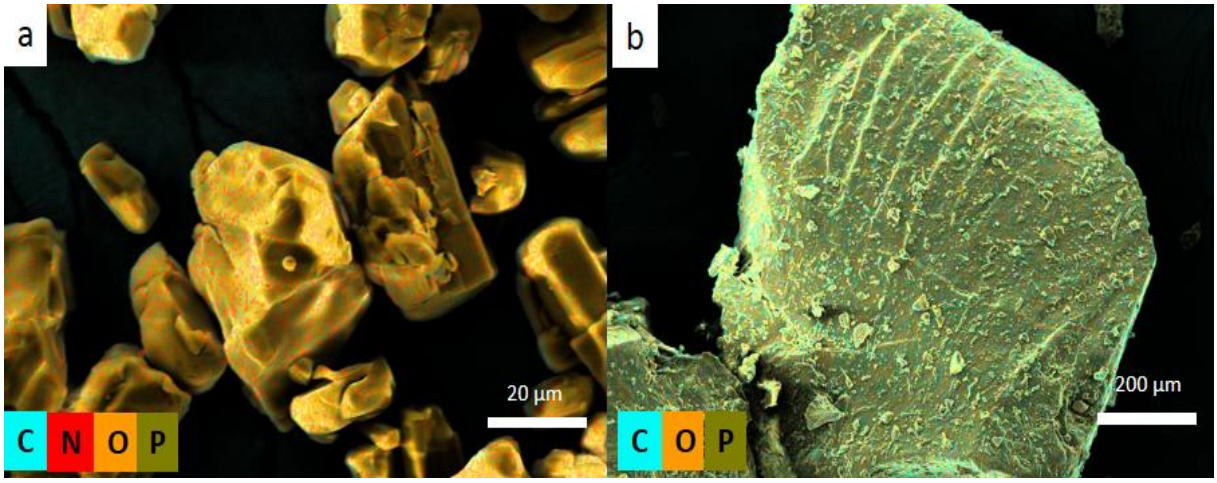

Fig. 5.23 The morphology of APP (a) and AAPP (b) as obtained by SEM and EDX via mapping of carbon (blue), nitogen (red), oxygen (bright yellow), and phosphorus (dark yellow) distribution in the sample

5.3.4 Fire behavior of functional flame retardant PP/AAPP composites

5.3.4.1 LOI and UL94

The LOI and UL-94 tests results of neat PP, PP/APP and PP/AAPP composites are shown in Table 5.7. Neat PP resin is an easily flammable polymeric material, and its LOI value is only 17.6 %. At loadings of 25, 30, and 35 wt % APP, the LOI values of the corresponding PP/APP composites increase to 19.6, 20.3, and 20.5 %, respectively. With increasing APP, the LOI value of PP/APP composite increase slightly. However, the LOI results of PP with 25, 30, and 35 wt % AAPP greatly increase to 30.5, 32.5, and 33.7 % respectively. In addition, a ceramic surface layer was observed after burning of PP/AAPP composites, which was not found for neat PP and PP/APP composites. As shown in Fig. 5.24, the PP/35%AAPP composites passed V-0 rating and had no dripping. Consequently, AAPP has a significant higher effect on the flame retardancy in PP compared to APP.

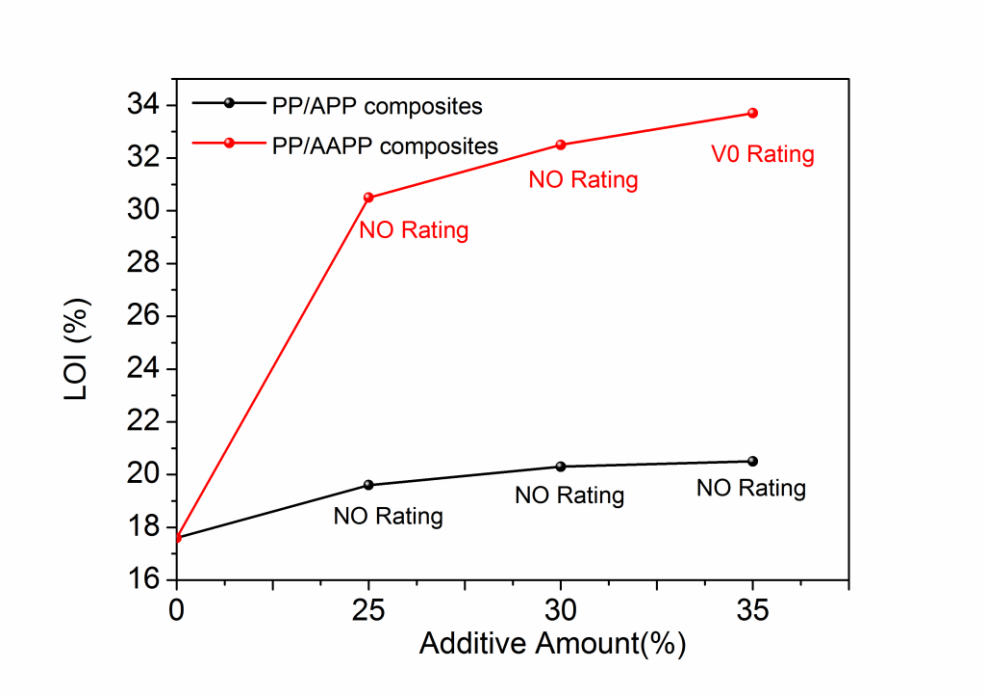

Fig. 5.24 LOI results of neat PP, PP/APP and PP/AAPP composites

Table 5.7 LOI and UL94 results of neat PP, PP/APP and PP/AAPP composites

Sample	Component (100wt %)			LOI (%)	UL94	
	PP	APP	AAPP		Dripping	Rating
PP	100	0	0	17.6	YES	N.R.
PP/25%APP	75	25	0	19.6	YES	N.R.
PP/30%APP	70	30	0	20.3	YES	N.R.
PP/35%APP	65	35	0	20.5	YES	N.R.
PP/25%AAPP	75	0	25	30.5	YES	N.R.
PP/30%AAPP	70	0	30	32.5	YES	N.R.
PP/35%AAPP	65	0	35	33.7	NO	V-0

N.R.: no rating

5.3.4.2 Cone calorimeter

In order to investigate in depth the effect of AAPP on the flame retardancy of PP, CC tests were performed. The PHRR, THR, Av-MLR, SPR, and TSP results of neat PP as well as PP/APP and PP/AAPP composites are shown in Table 5.8.

Table 5.8 Cone calorimeter results of neat PP, PP/APP and PP/AAPP composites

Sample	PHRR (kw/m^2)	THR (MJ/m^2)	Av-MLR (g/s)	TSP (m^2)	SPR (m^2/s)
PP	941±25	100±6	12±1	11±1	0.08±0.01
PP/25%APP	607±23	88±6	7±1	12±1	0.07±0.01
PP/35%APP	581±22	91±4	7±1	12±1	0.07±0.01
PP/25%AAPP	269±16	64±3	3±1	7±2	0.03±0.01
PP/35%AAPP	229±25	52±5	4±1	6±1	0.03±0.01

The HRR results of neat PP, PP/APP and PP/AAPP composites are shown in Fig. 5.25. It can be seen that neat PP burnt very rapidly after ignition and the PHRR is 941 kW/m^2. The PHRR of PP with 25 and 35 wt % APP decreases to 607 and 582 kW/m^2, respectively. However, when the loading of AAPP amounts to 25 and 35 wt %, the PHRR further are reduced to 269 and 229 kW/m^2, respectively. A few more peaks in PHRR of PP/AAPP composites are observed which are explained now in detail. The first peak is identified as the development of the ceramic surface layer protecting the sample. After the first peak, the HRR tends to a steady state. In this state, the protective ceramic surface layer suppresses the HRR. The other peak is generated by the partial break down of the protective ceramic surface layer due to further exposer of sample to the heat of CC tests [44, 54]. Thus, we can conclude that AAPP significantly reduced and delayed the heat release in the PP composite.

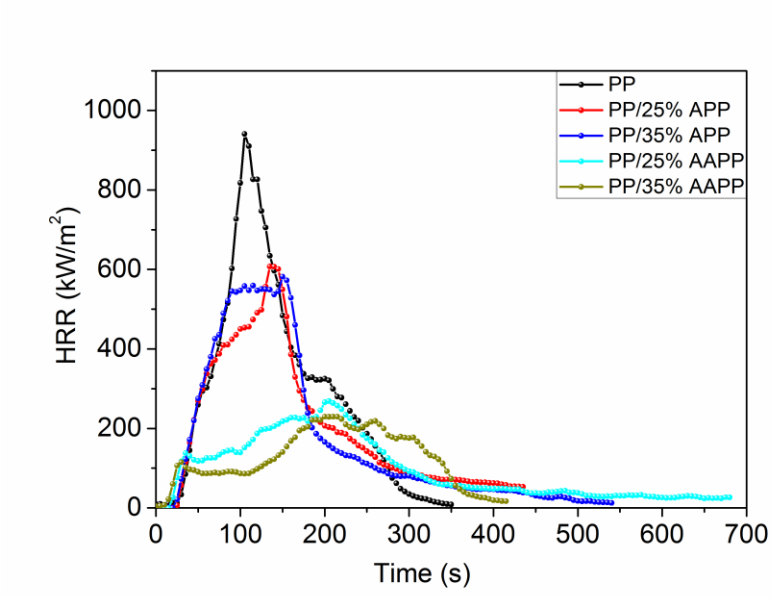

Fig. 5.25 HRR plots of neat PP, PP/APP and PP/AAPP composites

THR values of neat PP as well as PP/APP and PP/AAPP composites are shown in Fig. 5.26. At the end of burning, the neat PP released a total heat of 100 MJ/m^2, the PP/APP composites released a total heat from 84 to 90 MJ/m^2. However, THR of PP/AAPP composites with 25 and 35 wt % of AAPP showed significantly reduced total heat of 64 and 55 MJ/m^2, respectively. Thus, the flame spread rate as well as the THR of PP/35%AAPP composites have significantly decreased compared to that of PP/35%APP composites. The lower values of THR indicate that parts of the polymer are protected and not completely combusted [54, 73].

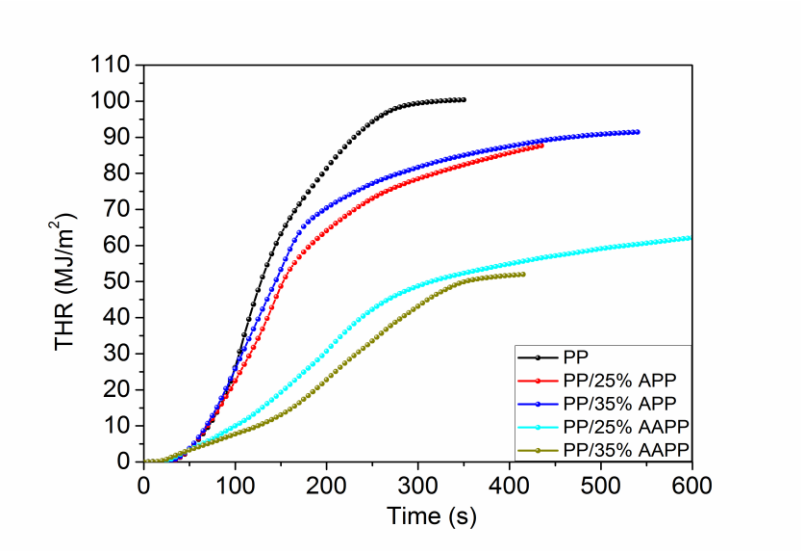

Fig. 5.26 THR plots of neat PP, PP/APP and PP/AAPP composites

The acute toxicity of fire gases is mainly responsible for over 70 % of people killed by fires [3]. The SPR (a) and TSP (b) results of neat PP as well as PP/APP and PP/AAPP composites are shown in Fig. 5.27. Compared to neat PP, the peak of SPR (about 0.08 m^2/s) is changed when APP is added. However, the SPR value of PP with 25 and 35 wt % AAPP reduces to 0.03 m^2/s. The TSP of neat PP amounts to 11.2 m^2. In the case of PP/APP composites with 25 and 35 wt % of APP, the TSP increased to 11.8 and 11.6 m^2, respectively. The decrease in smoke formation in PP/AAPP composites is probably due to the reduced amount of PP converted into organic volatiles, since the organic volatiles are the primary source of smoke particles [3, 67]. These results illustrate that AAPP can effectively suppress the smoke production.

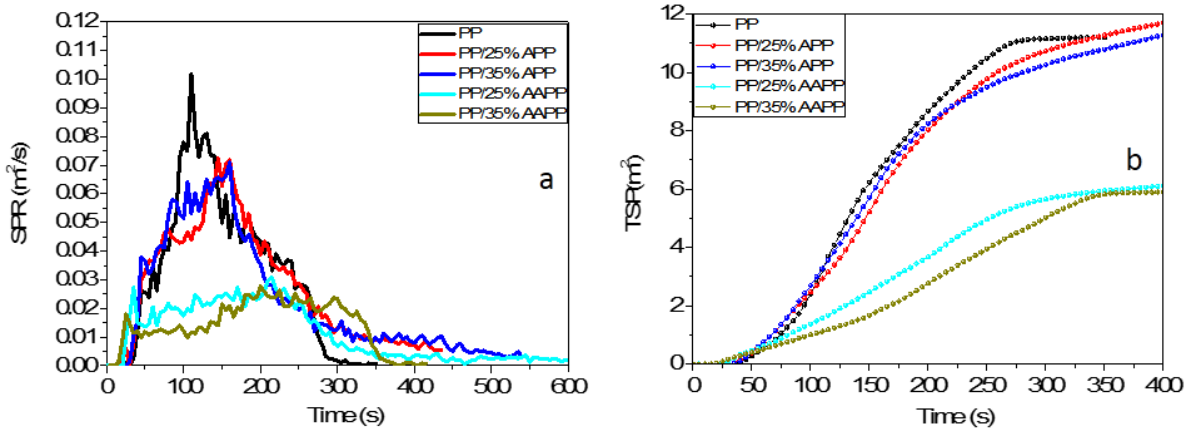

Fig. 5.27 SPR (a) and TSP (b) plots of neat PP, PP/APP and PP/AAPP composites

5.3.5 Thermal properties of PP/AAPP composites

5.3.5.1 Thermal stability of APP and AAPP

To evaluate the thermal stability of APP and AAPP, the TGA results are presented in Fig. 5.28. It can be seen that APP has nearly no mass loss for temperatures less than 300 °C. In the range from 310 to 500 °C, the mass was reduced from 97 % to 81 % due to the decomposition of APP and the release of NH_3 and H_2O. The residual of burnt APP composites amounts to 2.2 wt % at 800 °C. In the case of AAPP, the decomposition starts at about 210 °C due to its modification with organic material. In the range from 220 °C to 500 °C, the mass was reduced from 95 % to 60 %. The residual of burnt AAPP composites amounts to 7.4 wt % at 800 °C. These results showed that the carbon source in AAPP increases the residual after the combustion. However, AAPP has a lower thermal stability due higher amount of organic matter [15, 16]. Nevertheless, the residual mass at 800 °C is higher in comparison to APP due to stable char formation.

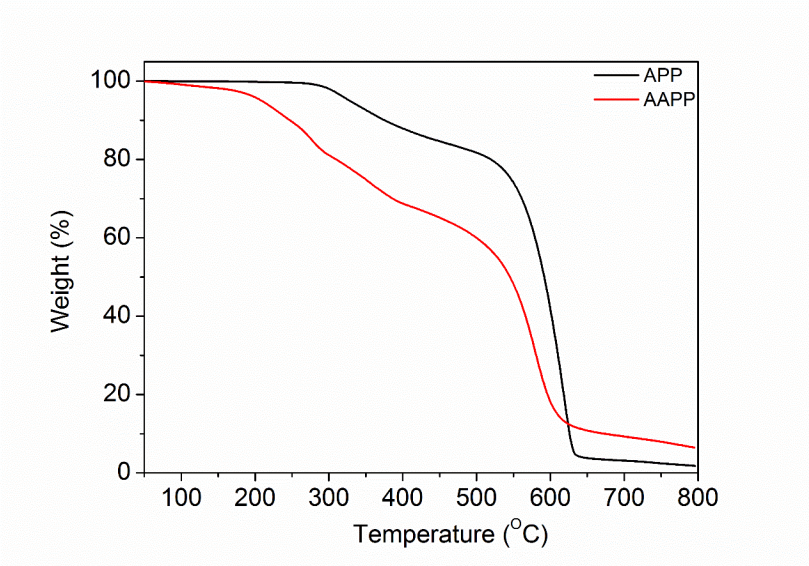

Fig. 5.28 TGA plots of APP and AAAP

5.3.5.2 Thermal stability of PP/AAPP composites

TGA and DTG plots of non-irradiated and EB irradiated PP and PP/AAPP composites are shown in Fig. 5.29. The corresponding data are listed in Table 5.9. In the case of PP/AAPP composites, the decomposition starts at temperature of about 250 °C due to the release of ammonia and water molecules. With increasing content of AAPP, the T_{max} of PP/AAPP composites decreased from 439 to 429 °C. In contrast, the rates of degradation reduced from 2.4 to 1.5 %/K.

From Fig 5.29 (b) and Table 5.9, it can be seen that the thermal degradation process of PP/AAPP composites is classified into three steps. The first step starts at 250 °C. The $T_{-5\%}$ values of PP with 25, 30, and 35 wt % AAPP amounts to 293, 266, and 265 °C, respectively. The main reason is the ammonia and vapour. The second degradation step starts at about 350 °C and ends at about 450 °C. As shown in Fig. 5.29 (b) and Table 5.9, the T_{max} of PP with 25, 30, and 35 wt % values of AAPP amounts to 439, 440, and 429 °C, respectively. It is observed that the R_{max} of PP/AAPP composites are lower in comparison to neat PP. This suggested that the addition of AAPP leads to the formation of a char layer at high temperatures. It protects the matrix from heat/oxygen transfer. The last step is located in the temperature range from 450 °C to 600 °C. The amount of char residues of PP/AAPP composites varies from 11 to 18 %. Consequently, the addition of AAPP improved the formation of char residue during the combustion.

After EB treatment of flame retardant PP composite, the $T_{-5\%}$ value of irradiated PP with 25, 30 and 35 wt % AAPP amounts to 295, 295, and 291 °C, respectively. Compared with non-irradiated PP with 35 wt % AAPP, the $T_{-5\%}$ value of EB irradiated PP/35%AAPP composites increases from 265 °C to 291 °C. T_{max} of irradiated PP with 25, 30, and 35 wt % AAPP increases to about 455 °C, respectively. Thus, EB treatment increases the values of T_{max} (see Table 5.9). Finally, R_{max} of irradiated PP/25%AAPP, PP/30%AAPP composites significantly is reduced from 2.4 and 2.0 %/K to 1.3 %/K. Thus, the thermal stability of PP/AAPP composites is remarkably improved by EB treatment. A possible graftlinking mechanism is proposed in Fig. 5.30. Firstly, EB treatment generates PP macroradicals. These the macroradicals react with carbon of the C=C of AAPP to generate the first grafting reaction. The same reaction can be induced by the macroradicals at the remaining C=C group of AAPP. Finally, a cross-linked structure can be generated in the flame retardant PP composites at high dose values.

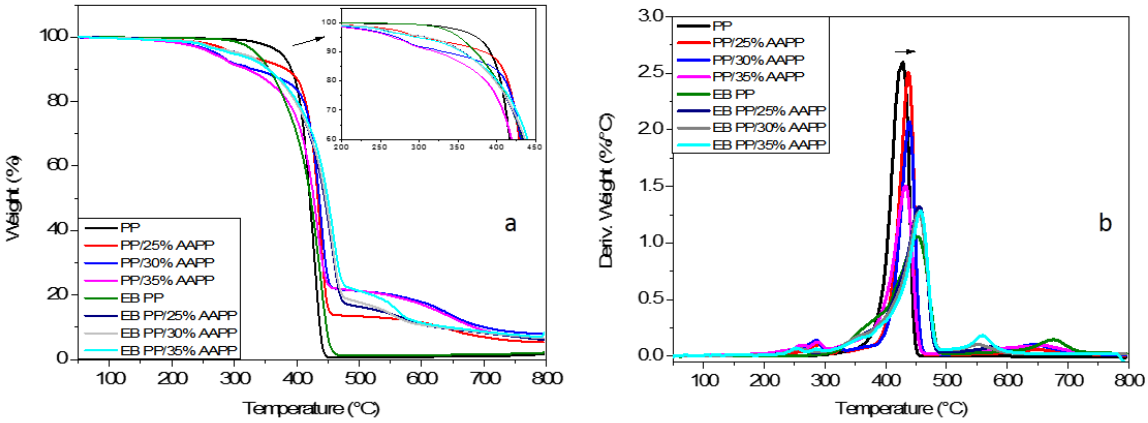

Fig. 5.29 TGA (a) and DTG (b) plots of non-irradiated and EB irradiated PP and PP/AAPP composites

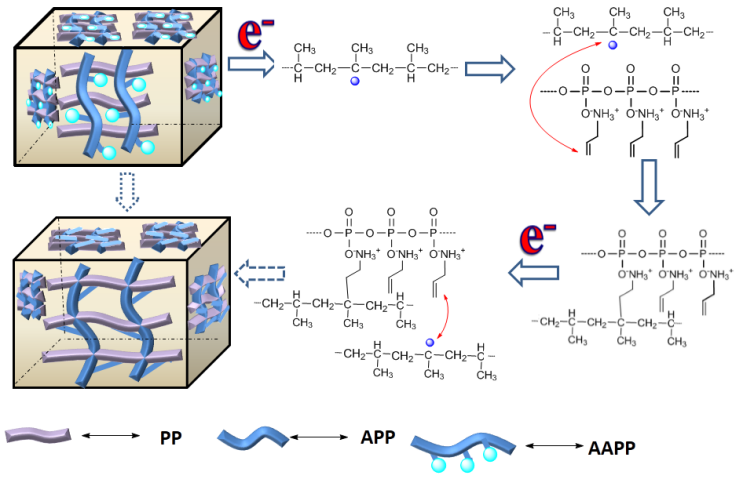

Fig. 5.30 Possible grafting mechanism of AAPP with PP upon EB treatment

Table 5.9 Data obtained from TGA and DTG plots of non-irradiated and EB irradiated PP and PP/AAPP composites

Sample	$T_{-5\%}$ (°C)	T_{max} (°C)	R_{max} (wt %/K)
PP	374	427	2.5
PP/25% AAPP	293	439	2.4
PP/30% AAPP	266	440	2.0
PP/35% AAPP	265	429	1.5
EB PP/25% AAPP*	295	455	1.3
EB PP/30%AAPP*	295	455	1.3
EB PP/35% AAPP*	291	453	1.3

$T_{-5\%}$ was the temperature of 5 % mass loss T_{max} was the temperature of maximum decomposing R_{max} was maximum mass loss rate *The composites were irradiated with a dose of 36 kGy

5.3.6 Tensile properties of PP/AAPP composites

The tensile results of the non-irradiated and EB irradiated flame retardant PP composites are presented in Table 5.10. Neat PP exhibited a tensile strength of 23.5 MPa and a Young's modulus of 984.7 MPa. After incorporating APP and AAPP into PP matrix, the tensile strength of flame retardant PP composites slightly decreases, but the Young's modulus increases. On the other hand, the tensile strength of irradiated PP with 25, 30, and 35 wt % of APP are 18.7, 18.1, and 16.9 MPa, respectively, which are greatly reduced from 19.3, 24.6, and 22.2 MPa of non-irradiated PP/APP composites. After irradiation, the Young's modulus of PP with 25, 30, and 35 wt % APP also decrease from 1464, 1581, and 1630 MPa to 1108, 1072, and 1225 MPa, respectively. However, from Table 5.10, it is seen that the tensile strength of EB irradiated PP with 25, 30, and 35 wt % AAPP are 20.6, 20.2, 18.7 MPa, respectively. The Young's modulus of the EB irradiated PP with 25, 30, and 35 wt % AAPP are enhanced from 1027, 1271, and 1384 MPa to 1042, 1537, and 1590 MPa, respectively. Compared with PP/APP system, both the tensile strength and Young modulus of PP/AAPP system are increased under EB treatment. The tensile strength of PP/AAPP composites is better than traditional PP/APP composites, since AAPP is stabilized with PP after irradiation. The Young's modulus of the composite samples is enhanced due to cross-linking of some part of AAPP with PP. However, elongation at break of EB irradiated PP with 25, 30, and 35 wt % AAPP decrease from 25.1, 16.9, and 9.2 to 13.4, 6.0,

and 5.1, respectively. The possible reasons are that the irradiation is causing chain scission (see Fig. 2.2), and AAPP is not grafted to PP chain by EB treatment due to low spacer distance of side chain of AAPP.

Table 5.10 Mechanical properties of PP, PP/APP and PP/AAPP composites

Sample	Tensile strength (MPa)	Young modulus (MPa)	Elongation at break (%)
PP	23.5±0.8	984.7±7.9	743.0±21.1
PP/25% APP	19.3±0.6	1464.3±23.9	51.4±1.8
PP/30% APP	24.6±1.8	1581.4±21.9	56.0±0.6
PP/35% APP	22.2±0.7	1630.5±27.5	46.5±3.1
PP/25% AAPP	23.5±1.4	1027.0±39.3	25.1±1.2
PP/30%AAPP	23.7±1.8	1271.0±85.2	16.9±1.7
PP/35%AAPP	21.6±0.1	1384.3±63.8	9.16±2.8
EB PP/25%APP*	18.7±0.3	1108.4±112.6	15.9±1.4
EB PP/30% APP*	18.1±0.2	1072.0±73.5	15.7±1.7
EB PP/35%APP*	16.9±0.3	1225.5±23.5	17.3±2.7
EB PP/25% AAPP*	20.6±0.2	1042.1±31.8	13.4±3.4
EB PP/30%AAPP*	20.2±0.2	1536.8±81.3	6.0±0.8
EB PP/35%AAPP*	18.7±0.2	1590.1±172.8	4.1±1.4

*The composites were irradiated with a dose of 36 kGy

5.3.7 Flame retardant mechanism

Flame retardant additives in PP may function in the condensed phase and/or in the gas phase. The flame retardant efficiency depends strongly on the structure and composition of the char after burning [134]. For detailed investigation, digital photos for the residues of PP/APP as well as PP/AAPP composites after CC test are shown in Fig. 5.31. There is no residue for PP; but a small amount of residues was generated for PP/APP composites. However, PP/35%AAPP composites (Fig. 5.31 g_1, Fig. 5.31 g_2) are covered with a continuous and intumescent residues layer. Generally, the intumescent residues layer reduceds the heat and mass transfer between gas and condensed phase as well as protects the under lying materials from further burning. Thus, the formation of intumescent residues layer is an important factor to achieve better flame retardancy of PP/AAPP than that of PP/APP at the same amount of flame retardant.

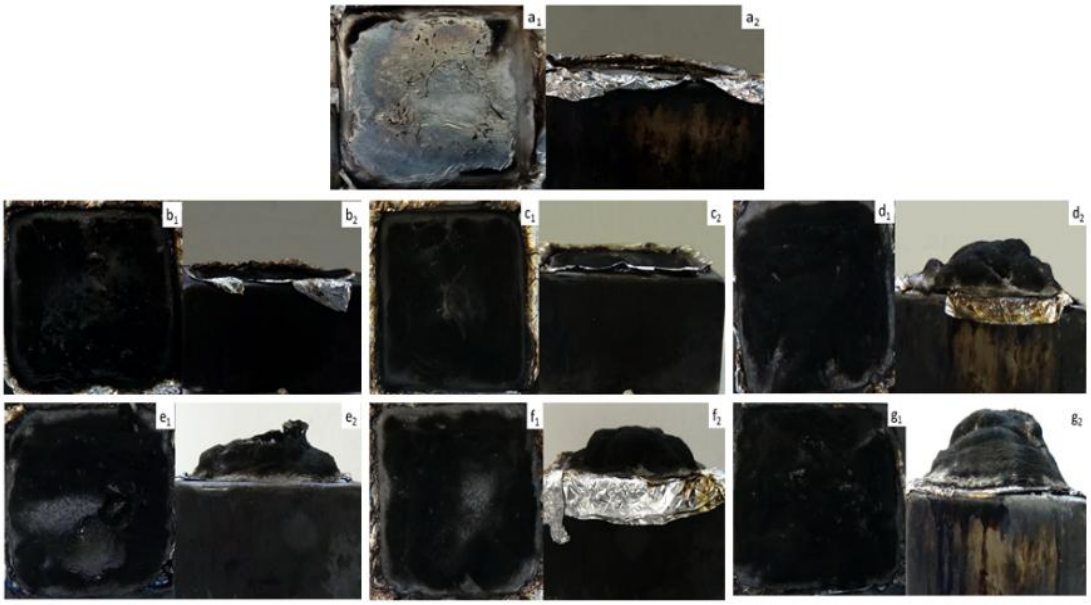

Fig. 5.31 Digital photographs for the residues of neat PP (a_1, a_2), PP/25% APP (b_1, b_2), PP/30% APP (c_1, c_2), PP/35% APP (d_1, d_2), PP/25% AAPP (e_1, e_2), PP/30% AAPP (f_1, f_2), and PP/35% AAPP (g_1, g_2) after CC test

To further explore the influence of the microstructure of char residues on the flame retardancy of PP during combustion, SEM micrographs are shown in Fig. 5.32 for the residues of PP/APP and PP/AAPP composites. There are some big bubbles and holes on the surface of PP/35%APP composites in Fig. 5.32 (a), and they are susceptible to cracking. It is seen that the inner surface of residual char of PP/35%APP (Fig. 5.32 (b)) is unexpanded due to insufficient char formation during combustion. Therefore, it cannot provide a good flame shield for the underlying material during burning. However, the residual char of the PP/35%AAPP system has a good intumescent structure. A rich charred layer is observed in the outer (Fig. 5.32 (b)) and inner surface (Fig. 5.32 (e)) of residual char. The outer surface of PP/35%AAPP composites has a continuous, compact, and thick framework. This structure of char could reduce both mass and heat transfer, which is effective in retarding the degradation of underlying materials. The inner surface of PP/35%AAPP composites exhibited a cell structure. The swollen chars are expanded which is not as thick as the outer surface. In addition, closed holes are observed in the inner surface which might result from the gases generated during the combustion. Unfortunately, we are not able to collect the residue of neat PP because no char is produced during the combustion. Aiming for further understanding, the distribution of elements on the char residues was studied by EDX. As shown in Fig. 5.32, the content of C, N, O, and P is 11.7, 10.7, 51.8, and 25.7 wt % in PP/35%APP composites, respectively (Fig. 5.32c). In the case of PP/35% AAPP, the content of C, N, O and P is 20.5, 15.2, 43.2 and 23.0 wt %, respectively

(Fig. 5.32 f). The C/P and N/P ratios of residual char of PP/35% AAPP are 0.89 and 0.65, respectively, which are much higher than that of PP/35 wt % APP (0.45 and 0.41). Consequently, a network is formed on the surface of PP/35% AAPP containing more C and N.

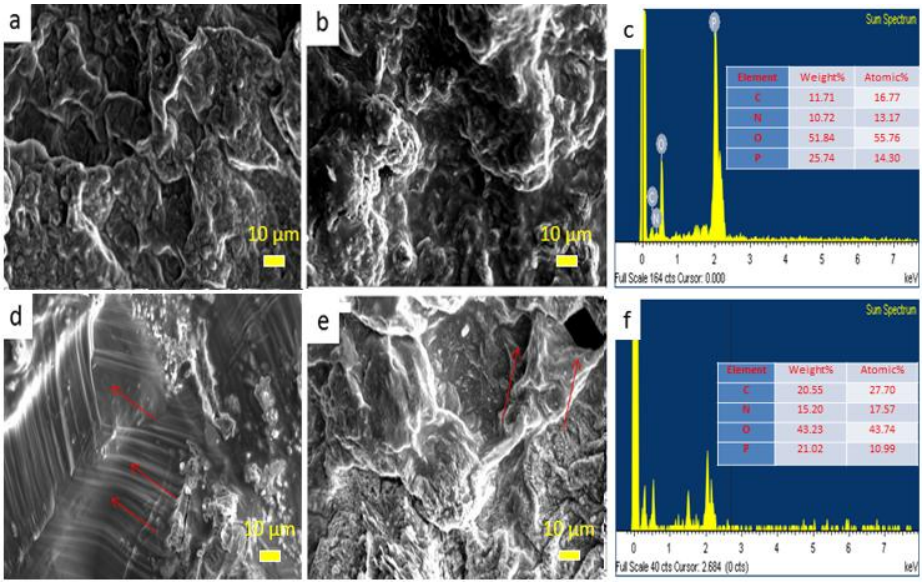

Fig. 5.32 SEM images for the outer residues surface of PP/35% APP (a) and PP/35% AAPP (d); SEM images for the inner residues surface of PP/35% APP (b) and PP/35% AAPP (e); EDX spectra for the char residues of PP/35% APP (c) and PP/35% AAPP (f)

In Fig. 5.33 the TG-FTIR results are shown for novel AAPP in PP. The release of NH_3, H_2O (3400-4000 cm^{-1}, 1650 cm^{-1}), CO_2 (2340-2370 cm^{-1}), and pyrophosphate fragments P–O–P (1075 cm^{-1}), $OP(O)(ONH_4)_2$ and some mid chain groups [–$OP(O)(ONH_4)$–] were proposed by Camino et al [136]. In addition, NH_3 and H_2O are eliminated during the thermal degradation of polyphosphate. The second step starts at about 450 °C, and the mass loss during this step is related to the release of phosphoric acid, polyphosphoric acid, and metaphosphoric acid [136]. From Fig. 5.33 (a), the structure of P–N located at around 710 cm^{-1} appeares at 416 °C for APP system [137]. For AAPP system, a plentiful of P–O–C structures exists, which is observed at 1532 cm^{-1}, as proposed in Wang's [15] and Yan's [138] report. These bands at around 1153-855 cm^{-1} are ascribed to the vibration of P–O, P=O, C–N, and C–O. The peaks of P−N−C are observed at 1086 cm^{-1} and 723 cm^{-1} [15, 16]. The band at 1636 cm^{-1} is related to C=C. Obviously, it is confirmed that additional plentiful P–N–C, P–O–C, and C=C structures are formed in the residual char of PP/AAPP composites. Generally, the P–N–C, P–O–C, and C=C structures could play a positive role in highly-efficient flame retardants [15, 16], and their cross-linked structures may further facilitate the formation of residual char by aromatization at high

temperature [139]. The possible ring closure mechanism of PP/AAPP composites residues during the combustion process is shown in Fig. 5.34.

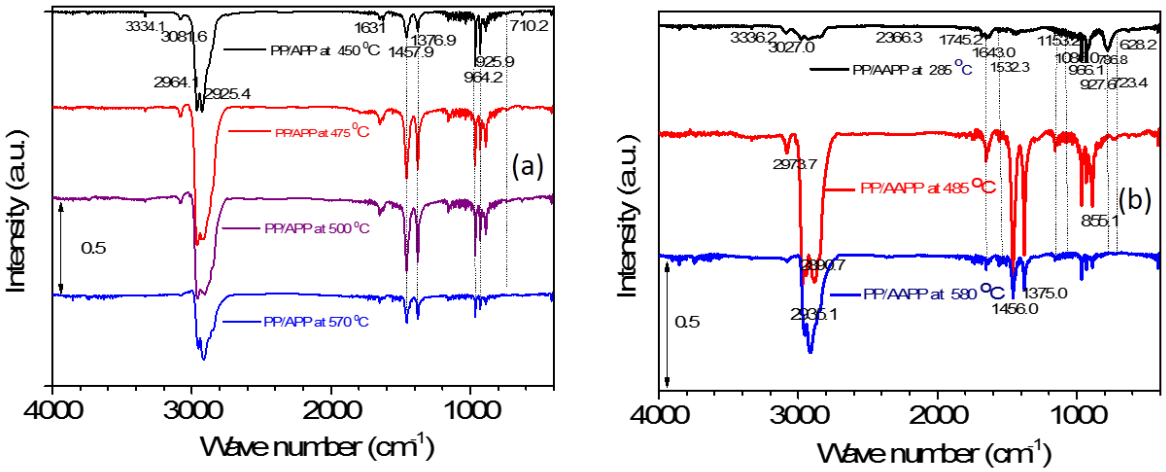

Fig. 5.33 FTIR spectra for condensed products of PP/APP (a) and PP/AAPP (b) at different temperature

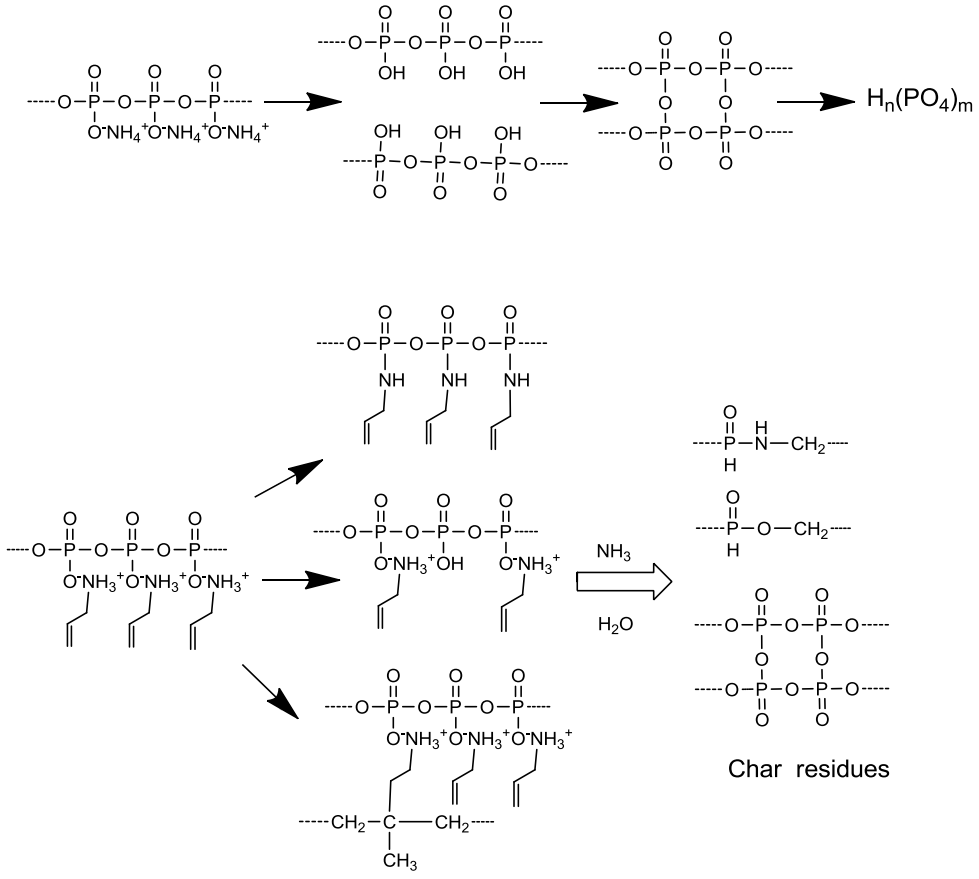

Fig. 5.34 Possible mechanisms for residues during burning processes of PP/APP and PP/AAPP composites

5.3.8 Conclusions

In this part, a multifunctional flame retardant, AAPP was successfully synthesized. AAPP exhibited remarkable flame retardancy efficiency. In comparison to the traditional PP/APP composites, the LOI value of PP/AAPP composites was enhanced to 33.7 with 35 wt % of AAPP and effective melt dripping resistance was achieved in UL-94 tests. More importantly, in the cone calorimeter test, the PHRR, THR, SPR and TSP values of PP/AAPP composites were much lower than those of PP/APP composites. In addition, the improved quality of char residue (P−N−C and P−O−C structure) acted as good barrier to prevent the transmission of fuel and oxygen. One the other hand, the thermal stability of these designed flame retarded PP composites was improved via high energy electrons. This innovative idea may be expanded to other polymer systems and opens a new possibility for the development of high performance polymer composites via environment-friendly high energy electrons.

IFR1 and IFR2 were made from two different components (APP and DPA/SPSA). In addition, DPA and SPSA were not coupled to APP by ionic bonds. Thus, APP was not stabilized in PP matrix by EB treatment. The novel multifunctional flame retardant AAPP based on APP chemically coupled with a carbon source containing one double bond. In case of PP/30 IFR1 and PP/30 IFR2 composites the PHRR of was 331 and 430 kW/m^2, respectively. When the loading of AAPP amounts to 25 wt %, the PHRR was reduced to 269 kW/m^2. Consequently, AAPP is a more efficient flame retardant to PP compared to IFR1 and IFR2. To further reduce the overall filler content and increase its properties, a nanofiller (likes MMT) as synergistic effect would be added into the polymer matrix. Thus, flame retardant nanocomposites based on AAPP and MMT will be studied in the next step.

5.4 Synergistic effect of montmorillonite (MMT) on fire behavior, thermal stability and tensile properties of PP/AAPP composites

The research and development of polymer/nanofiller always attract extensive attention [17-20]. To reduce the overall filler content and increase properties of flame retardant PP composite, MMT as asynergist is used for preparation of flame retarded polymer nanocomposites greatly decrease peak heat release rate, reduce melt dripping, and change char structure in fire tests [22-24]. The main reason is that layered MMT is based on barrier effect preventing the transition of the mass and the heat transfer during the combustion process [27, 73]. Nevertheless, the dispersion of clay within polymeric matrices is crucial for the performance of polymer/layer platelets nanocomposites.

In subchapter 5.3, a novel multifunctional macromolecule AAPP had been prepared via simple one step according to the procedure reported in 4.2.3, which had a good contribution to the flame retardancy of PP. In order to reduce the overall flame retardant filler content of PP a part of AAPP was replaced by O-MMT which was coated with bis(2-hydroxyethyl)-methyl-octadecyl-ammonium group. Under keeping the total filler loading constant (22 wt %), PP mixed with different ratios (see Table 5.11) of PP/AAPP/O-MMT nanocomposites were prepared by a twin screw extrusion. And the morphology, thermal and burning behavior of PP/AAPP/O-MMT nanocomposites were characterized by TEM, TGA, LOI, UL-94, and CC tests. Furthermore, the relevant flame-retardant mechanism of PP/AAPP/O-MMT composites was investigated by SEM and TG-FTIR.

5.4.1 Morphology of PP/AAPP/O-MMT composites

The TEM gives direct information on the state of dispersion of the MMT particles in the nanocomposite. The TEM images of PP/20%APP-2%O-MMT and PP/20%AAPP-2%O-MMT nanocomposites are shown in Fig. 5.35. From Fig. 5.35 (a), it is clearly visible that most of the MMT platelets are dispersed in the PP/APP composites, showing reunited structures. In the case of Fig. 5.35 (b), the TEM image of PP/20%AAPP-2%O-MMT nanocomposite show most of the MMT layers are exfoliated.

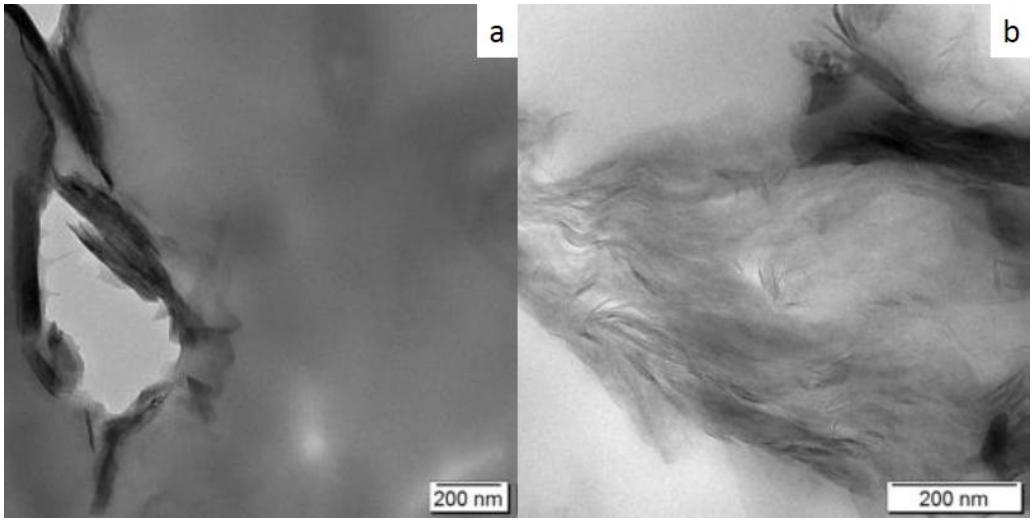

Fig. 5.35 TEM images of PP/20%APP-2%O-MMT nanocomposites (a) and PP/20%AAPP-2%O-MMT nanocomposites (b)

5.4.2 Fire behavior of PP/AAPP/O-MMT composites

5.4.2.1 LOI and UL94

To investigate the role of MMT for the flame retardancy efficiency of PP/APP and PP/AAPP composites, the results of LOI and UL-94 are listed in Table 5.11. The LOI value of PP/22% APP amounts to 20.4 %. In further composites, a part of APP is replaced by O-MMT, in order to keep the total filler loading constant (22 wt %). The LOI of PP/21%APP-1%O-MMT, PP/20%APP-2%O-MMT composites are 20.4 and 20.6%, respectively, which are not classified in UL-94 tests. As shown in Table 5.11, all PP/APP-O-MMT composites do not show any self-extinguishing feature. However, the LOI value of the PP with 22 wt % AAPP additives is up to 29.2 %. When 1 wt % and 2 wt % O-MMT are added to PP/AAPP system, LOI values are 28.4 and 29.6 %, respectively. PP with 20 wt % AAPP + 2 wt % O-MMT composites have no melt dripping during flame ignition but achieved V-0 rating in UL94 test. The experimental results clearly demonstrated that the addition of 2 wt % O-MMT leads to significant improvement in anti-melt dripping during the combustion process of PP/AAPP system.

Table 5.11 LOI and UL94 results of PP, PP/APP/O-MMT and PP/AAPP/O-MMT composites

Sample	Component (100wt %)				LOI(%)	UL94	
	PP	APP	AAPP	O-MMT		Dripping	Rating
PP	100	0	0	0	17.6	YES	N.R.
PP/22%APP	78	22	0	0	20.4	YES	N.R.
PP/21%APP-1%O-MMT	78	21	0	1	20.6	YES	N.R.
PP/20%APP-2%O-MMT	78	20	0	2	21.6	YES	N.R.
PP/22%AAPP	78	0	22	0	29.2	YES	N.R.
PP/21%AAPP-1%O-MMT	78	0	21	1	28.6	YES	N.R.
PP/20%AAPP-2%O-MMT	78	0	20	2	29.5	NO	V-0

N.R.: no rating

5.4.2.2 Cone calorimeter

In order to identify the role of the O-MMT in the formation of the PP/APP and PP/AAPP composites during the combustion process, cone calorimeter tests were performed. The PHRR, THR, Av-MLR, and SPR resultsof PP, PP/APP/O-MMT and PP/AAPP/O-MMT composites are shown in Table. 5.12.

Table 5.12 Cone calorimeter tests results of PP, PP/APP/O-MMT and PP/AAPP/O-MMT composites

Sample	PHRR (kw/m^2)	THR (MJ/m^2)	Av-MLR (g/s)	SPR (m^2/s)
PP	841±13	124±12	11±3	0.08±0.01
PP/22%APP	534±23	148±15	10±2	0.08±0.01
PP/21%APP-1%O-MMT	453±15	141±7	7±1	0.06±0.01
PP/20%APP-2%O-MMT	363±18	128±8	5±1	0.05±0.01
PP/22%AAPP	369±21	125±17	5±1	0.06±0.01
PP/21%AAPP-1%O-MMT	390±14	127±10	7±2	0.05±0.01
PP/20%AAPP-2%O-MMT	340±18	92±9	8±1	0.04±0.01

The HRR plots of PP, PP/APP/O-MMT and PP/AAPP/O-MMT composites are shown in Fig. 5.36. The PHRR values of PP with 22 wt % APP and 22 wt % AAPP are 534 and 369

kW/m^2, respectively. Obviously, the flame-retardant property of AAPP is more effective than APP in PP. As shown in Fig. 5.36, the PHRR values of PP/21%APP-1%O-MMT, PP/20%APP-2%O-MMT composites amount to 453 and 363 kW/m^2, respectively. On the contrary, the PHRR values of PP/21%AAPP-1%O-MMT, PP/20%AAPP-2%O-MMT composites reduce to 390 and 340 kW/m^2, respectively. Thus, it can be said that the flame retardant performance of AAPP-O-MMT is more effective than that of APP-O-MMT in PP matrix. However, the PHRR values of PP/20%AAPP-2%O-MMT composites are higher compared to that of PP/25%AAPP (265 kW/m^2, see table 5.8), since conventional modifed O-MMT is not flame retardant and the surfactant bis(2-hydroxyethyl)-methyl-octadecyl-ammonium group for O-MMT is flammeable. Further, in order to keep the total filler loading constant (22 wt %), with the addition of 2.0 wt % of O-MMT in PP/AAPP composites, the values of PHRR reduce from 369 to 340 kW/m^2. The experimental results demonstrated that the addition of MMT leads to improvement flame retardancy of PP/AAPP composites.

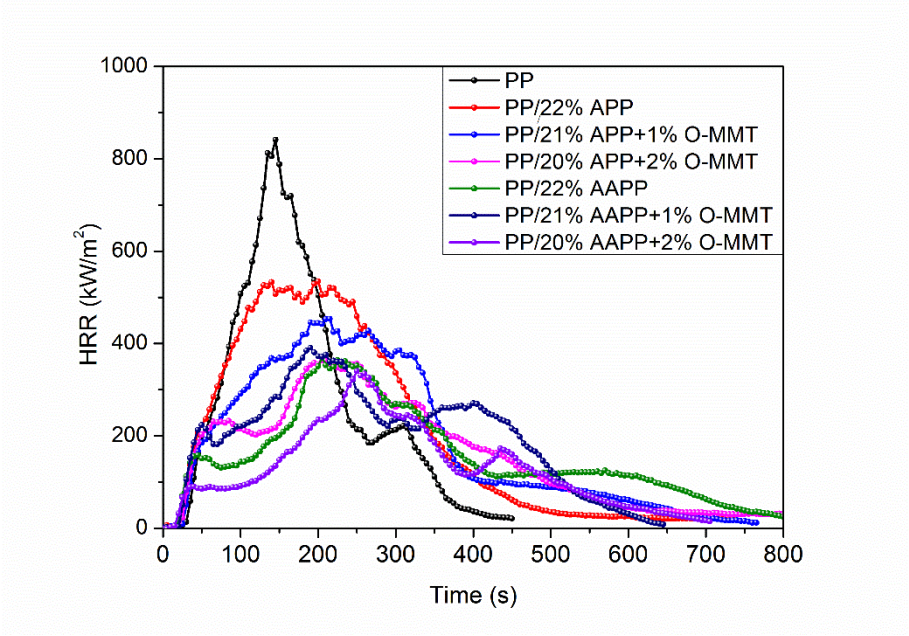

Fig. 5.36 HRR plots of neat PP, PP/APP/O-MMT and PP/AAPP/O-MMT composites

THR values of PP, PP/APP/O-MMT and PP/AAPP/O-MMT composites are shown in Fig. 5.37. At the end of burning, THR of PP with 22% AAPP amounts to 125 MJ/m^2. However, the THR value of PP/20%AAPP-2.0%O-MMT significantly decreases to 92 MJ/m^2. The lower values of THR indicate that parts of the polymer are protected and not completely combusted because of the addition of MMT in PP/AAPP composites [15].

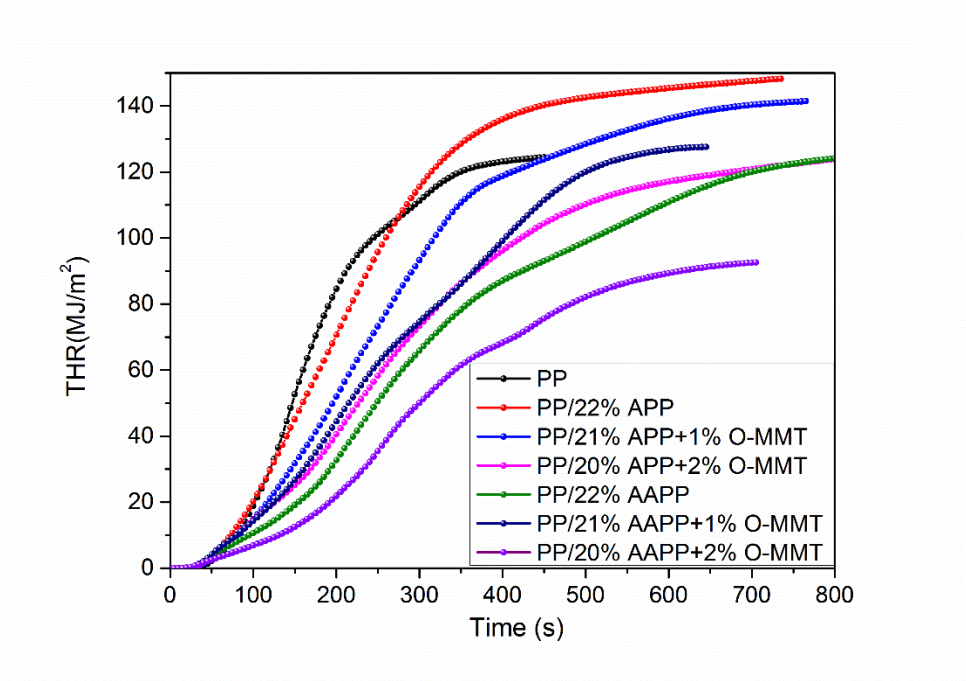

Fig. 5.37 THR plots of neat PP, PP/APP/O-MMT and PP/AAPP/O-MMT composites

The SPR (a), TSR (b), CO_2 (c) and CO (d) values of neat PP, PP/APP/O-MMT and PP/AAPP/O-MMT composites are shown in Fig.5.38. The SPR peaks of PP/22%APP, PP/21%APP-1%O-MMT, PP/20%APP-2%O-MMT, PP/22%AAPP, PP/21%AAPP-1%O-MMT, and PP/20%AAPP-2%O-MMT amount to 0.08, 0.06, 0.05, 0.06, 0.05 and 0.04 m^2/s, respectively. Consequently, SPR of PP/20%AAPP-2%O-MMT composites has significantly decreased compared to that of PP/22%APP composites. In the case of TSP, its lowest value is also observed for the PP/20%AAPP-2%O-MMT composite. Further, as shown in Fig. 5.38 (c), the peak of CO_2 for pure PP is 0.44 g/s. In the case of PP filled with 22 wt % APP, 21 wt % APP+1 wt % O-MMT, and 20 wt % APP+2 wt % O-MMT, the CO_2 production of PP/APP/O-MMT composites decreases to 0.28, 0.24 and to 0.20 g/s. However, the corresponding values of PP with 22 wt % AAPP, 21 wt % AAPP+1 wt % O-MMT, and 20 wt % AAPP+2 wt % O-MMT reduce to 0.21, 0.19 and 0.18 g/s, respectively. In the case of PP/22%AAPP composites, the CO production amounts to 0.006 g/s. The peak CO productions of PP/21%AAPP-1%O-MMT and PP/20%AAPP-2%O-MMT reduce to 0.004 and 0.003 g/s, respectively. Thus, the addition of the AAPP and the low amount (2 %) of O-MMT decrease the SPR, TSR, CO_2 and CO values of flame retarded PP composites. Again, the experimental results demonstrated the synergetic effect of O-MMT on flame retardancy of PP/AAPP composites.

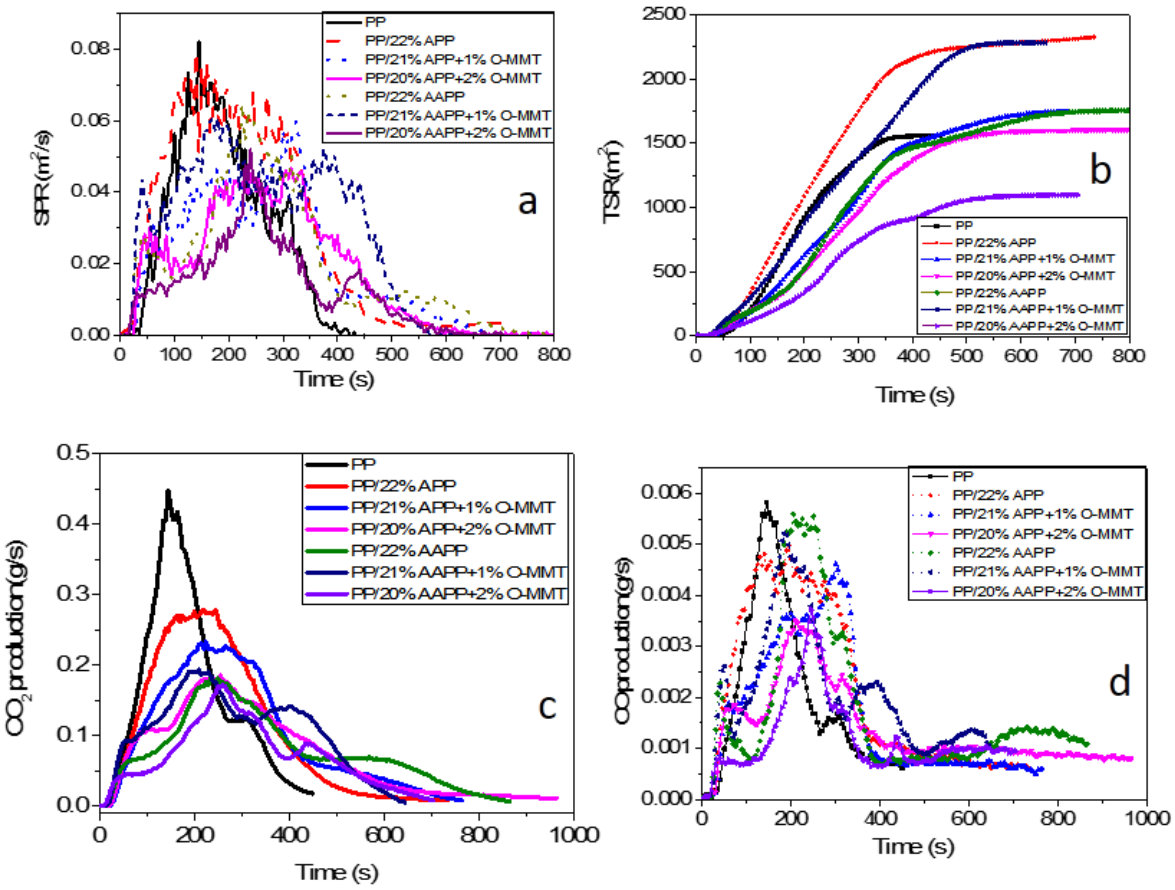

Fig. 5.38 SPR (a), TSR (b), CO_2 (c) and CO (d) plots of PP, PP/APP/O-MMT and PP/AAPP/O-MMT composites

5.4.3 Morphology of burnt PP/AAPP/O-MMT composites

Digital photos for the residues of neat PP, PP/APP/O-MMT and PP/AAPP/O-MMT composites are shown in Fig. 5.39. There are some vesicular pores and holes on the surface of burnt PP/APP/O-MMT char residue that could be less effective in reducing mass and heat transfer. However, PP/AAPP and PP/AAPP/O-MMT composites are covered with thick intumescent residues layer. In particular, the char residue of burnt PP with 20 % AAAP and 2.0 % O-MMT is more compact and strong, which may play a role in the flame retardant process, hindering the passage of combustible gases and molten PP towards the flame.

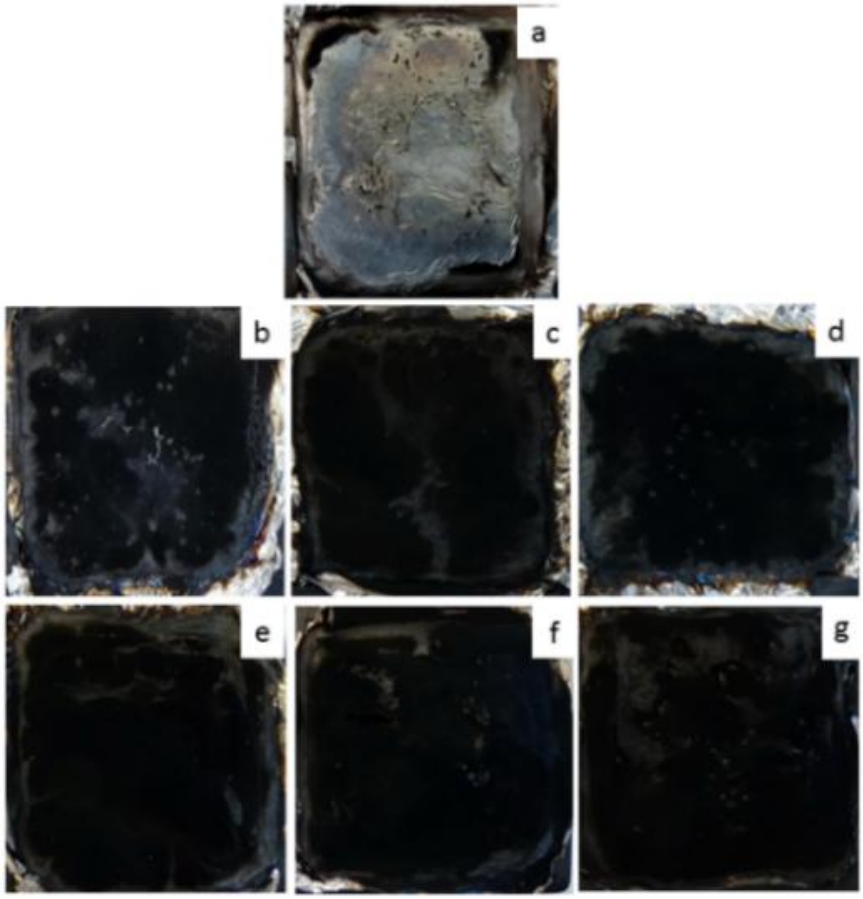

Fig. 5.39 Digital photographs for the residues of PP (a), PP/22% APP (b), PP/21%APP-1% O-MMT (c), PP/20%APP-2% O-MMT (d), PP/22% AAPP (e), PP/21%AAPP-1% O-MMT (f), and PP/20%AAPP-2% O-MMT (g) after CC test

SEM micrographs for the residues of PP/20%APP-2%O-MMT and PP/20%AAPP-2%O-MMT composites are shown in Fig. 5.40. In the case of burnt PP/20%APP-2%O-MMT system, no closed honeycomb pore intumescent charring layer is formed (Fig. 5.40 (a) and (b)). However, the charring layer of PP/20%AAPP-2%O-MMT is continuous, dense, and integrated closed honeycomb porous structure is observed in Fig. 5.40 (c) and (d), which avoids mass and heat transfer in the condensed-phase [67, 85].

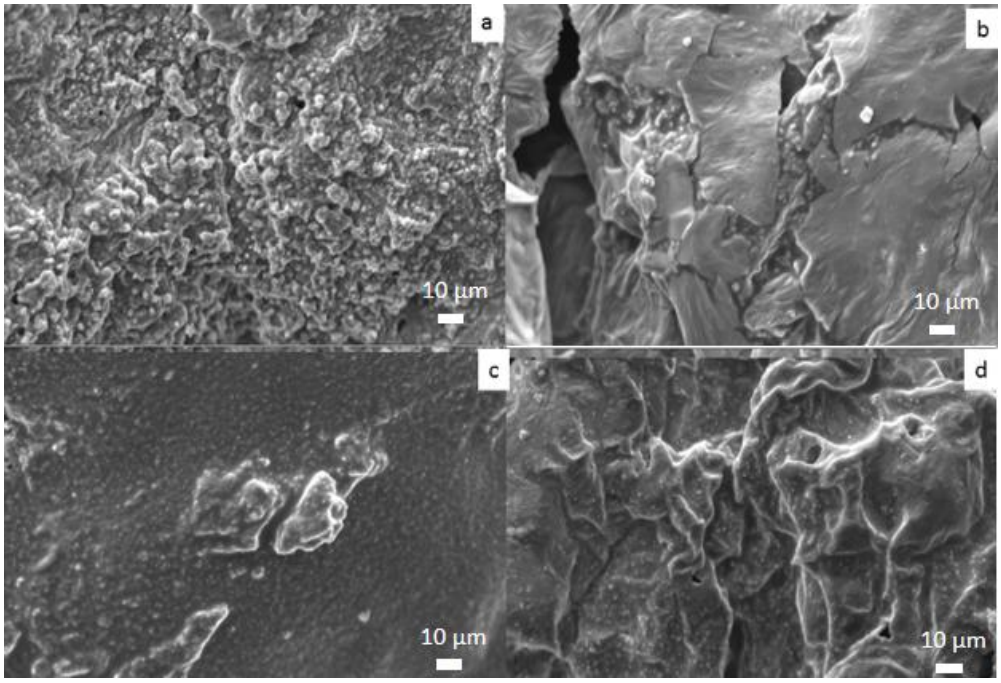

Fig. 5.40 SEM images for outer residues surface of PP/20%APP-2%O-MMT (a) and PP/20%AAPP-2%O-MMT (c); SEM images forthe inner residues surface of PP/20%APP-2%O-MMT (b) and PP/20% AAPP-2% O-MMT (d)

5.4.4 Tensile properties of PP/AAPP/O-MMT composites

Tensile properties of PP, PP/APP/O-MMT and PP/AAPP/O-MMT composites are listed in Table 5.13. After incorporating of APP and AAPP into the PP matrix, the tensile strength of PP/22%APP, PP/22%AAPP composites are 22.2 MPa, 23.4 MPa, respectively. Thus, the tensile strength of both composites is comparable within the experimental uncertainty. The same result is found for the tensile strength of PP/20%AAPP-2%O-MMT (21.7 MPa) and PP/20%APP-2%O-MMT (20.6 MPa). Finally, the Young's modulus of PP/22% APP, PP/20% APP-2% O-MMT, PP/22% AAPP, and PP/20% AAPP-2%O-MMTcomposites are 1148.6, 1150.3, 1052.0, and 1147.2, respectively.

After irradiation, the tensile strength of EB irradiated PP/22% APP, PP/20% APP-2%MMT, PP/22% AAPP, and PP/20% AAPP-2%O-MMT composites are 20.7, 19.4, 20.6, and 18.8 MPa, respectively. The elongation at break of EB irradiated PP/22%APP, PP/20% APP-2%O-MMT, PP/22% AAPP, and PP/20% AAPP-2%O-MMT composites decrease from 82.5, 74.2, 48.9 and 19.0 to 16.2, 15.4, 22.7 and 13.0, respectively.The reduction of tensile properties was expected (see Fig. 1.4), since state of the art EB treatment causes chain scission at 36 kGy (see Fig. 2.2) and the spacer length of side chain of AAPP is to short.

Table 5.13 Mechanical properties of PP, PP/APP/O-MMT and PP/AAPP/O-MMT composites

Sample	Tensile strength (MPa)	Young modulus (MPa)	Elongation at break (%)
PP/22% APP	22.2±1.1	1148.6±56.6	82.5±13.6
PP/20% APP-2% O-MMT	20.6±0.3	1150.3±49.6	74.2±6.3
PP/22%AAPP	23.4±0.5	1052.0±21.2	48.9±15.7
PP/20%AAPP-2% O-MMT	21.7±0.6	1147.2±31.0	19.0±0.3
PP/22% APP*	20.7±0.4	888.4±31.0	16.2±3.7
PP/20% APP-2% O-MMT *	19.4±0.1	934.2±37.7	15.4±0.8
PP/22%AAPP*	20.6±0.1	749.8±77.1	22.7±4.6
PP/20%AAPP-2%O-MMT*	18.8±0.7	669.1±138.4	13.0±1.5

* The composites were irradiated with a dose of 36 kGy

5.4.5 Thermal properties of PP/AAPP/O-MMT composites

TGA and DTG plots of non-irradiated and irradiated PP/AAPP and PP/AAPP/O-MMT composites are shown in Fig. 5.41 and the corresponding data are listed in Table 5.14. In comparison to PP/22%AAPP, $T_{-5\%}$ value of PP/20%AAPP-2%O-MMT composite decreases from 285 °C to 259 °C. However, the maximum mass loss rate of PP/AAPP/O-MMT composites reduces from 1.3 %/K to 0.84 %/K. In addition, it has to be mentioned that the PP/20%AAPP-2%O-MMT composite shows a lower mass loss rate than PP/22%AAPP composite. This might be an indication of a reduced heat and fuel transfer from the flame zone to the volume of polymer. After EB treatment of flame retardant PP composite, the $T_{-5\%}$ value of irradiated PP/22%AAPP and PP/20%AAPP-2%O-MMT composites increases from 285 and 258 to 288 and 277 °C, respectively. T_{max} of irradiated PP/20%AAPP-2%O-MMT enhances from 443 to 452 °C. Thus, the thermal stability of PP/AAPP/O-MMT composites is improved by EB treatment.

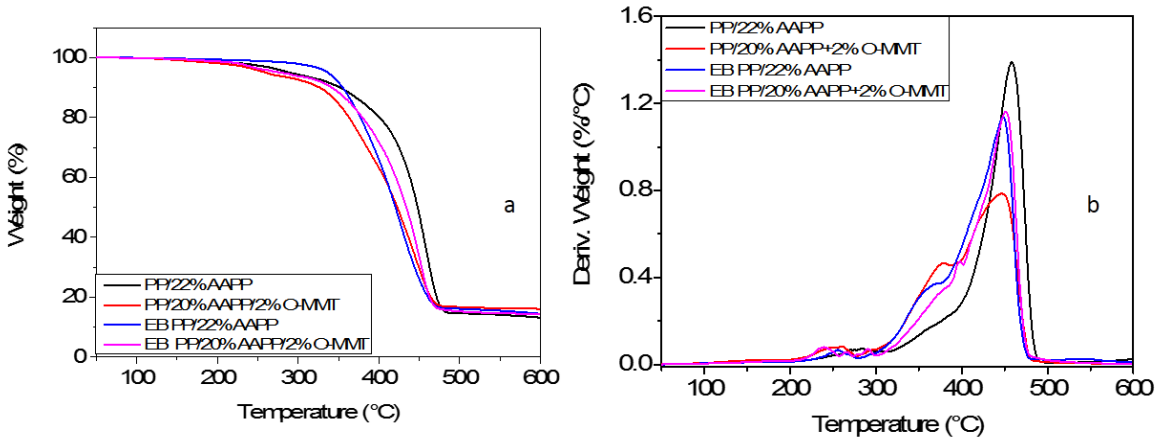

Fig. 5.41 TGA (a, b) and DTG (c, d) plots of non-irradiated and irradiated PP/APP/O-MMT MMT and PP/AAPP/O-MMT composites

Table 5.14 Data obtained from TGA and DTG plots of non-irradiated and irradiated PP/AAPP/O-MMT composites

Sample	$T_{-5\%}$ (°C)	T_{max} (°C)	R_{max} (%/K)	Residue (%)	
				500 (°C)	600 (°C)
PP/22%AAPP	285	464	1.3	16.7	13.2
PP/20%AAPP-2% O-MMT	259	443	0.84	16.8	16.7
PP/22%AAPP*	288	450	1.1	15.2	14.5
PP/20%AAPP-2% O-MMT *	277	452	1.1	15.1	14.3

* The composites were irradiated with a dose of 36 kGy

5.4.6 Possible flame retardant mechanism

In the case of PP/AAPP/O-MMT composites, there are two flame retardant mechanisms. The TG-FTIR results are shown in Fig. 5.42 for AAPP part. The band at 1532 cm^{-1} confirms the formation of plentiful P–O–C structure [75, 76]. Further, the bandsat 1153 and 855 cm^{-1} are ascribed to the vibration of P–O, P=O, C–N, and C–O. Moreover, the bands of P−N−C are observed at 1086 cm^{-1} and 723 cm^{-1} [15, 16]. Finally, we can conclude that the P–N–C, P–O–C, and C=C structures could be the most important reason for the increased flame retardation of AAPP compared to APP.

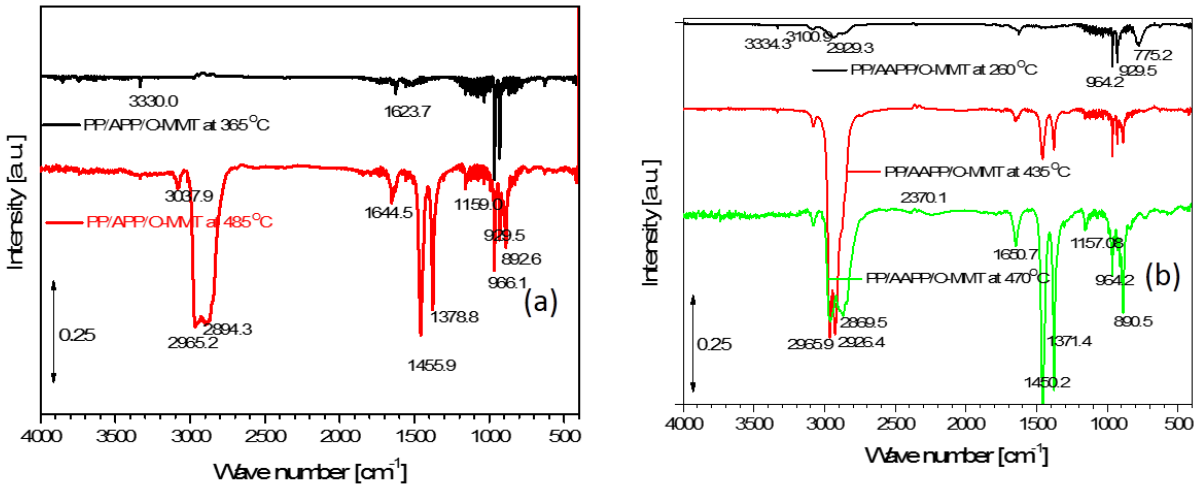

Fig. 5.42 TG-FTIR plots of PP/22%APP-2% O-MMT composites (a) and PP/22%AAPP-2% O-MMT composites (b)

The second flame retardant mechanism is related to O-MMT in PP/AAPP matrix, leading to a ceramic-like structure during the combustion process. PP/AAPP composites combined with MMT act as a physical barrier to prevent the transmission of fuel and heat. The layer of O-MMT could retard flame spread and reduce the heat release rate. Moreover, both the mass of intumescent carbonaceous chars and silicon layer are rich on the surface of burning nanocomposites, which provides self-extinguishing and anti-dripping promoters. In particular, PP/AAPP/O-MMT composites show a better flame retardant property due to the exfoliated nature of the O-MMT layers. The possible combustion mechanism is shown in Fig. 5.43.

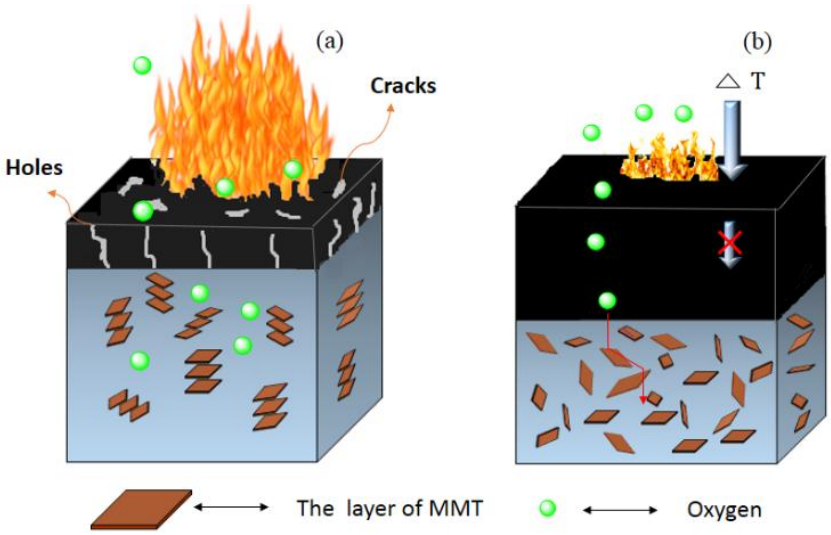

Fig. 5.43 Possible mechanisms of PP/APP/O-MMT composites (a) and PP/AAPP/O-MMT composites (b) during the combustion process

5.4.7 Conclusions

To further reduce the overall multifunctional AAPP content and increase properties of flame retardant PP composite, a part of AAPP is replaced by O-MMT, in order to keep the total filler loading constant (22 wt %). The TGA results showed that the maximum-decomposition-rate temperatures of these PP/AAPP/O-MMT nanocomposites were higher than that of pure PP. The LOI value of the PP/20%AAPP-2%O-MMT composites increased to 29.5, and passed V-0 rating in UL-94 tests. The results of CC tests showed that PP/20%AAPP-2%O-MMT had increased flame retardant properties than PP/20%APP-2%O-MMT and PP/22%AAPP. The fire retardant mechanism from the analysis of char residues proved that this PP/AAPP/O-MMT nanocomposite provided relatively good quality of char residue in the combustion that acted as good barrier to prevent the transmission of fuel and oxygen. It was confirmed that the P-N-C and P-O-C structure appear during the thermal decomposition, which could play a positive role in the highly-efficient flame retardancy of AAPP-O-MMT system. Moreover, PP/AAPP/O-MMT composites showed a better flame retardant property owing to the exfoliation of MMT layers. All results indicate that MMT has a synergistic effect on the flame retardancy of PP/AAPP. However, the thermal stability of modifiers for O-MMT is low and MMT alone is not flame retardant. Thus, temperature stable functional (flame retardant) surfactant for MMT have to be developed, which can be used for the preparation of multifunctional high-performance FR polymer/AAPP-FO-MMT nanocomposites.

5.5 Functionalized organo montmorillonite (FO-MMT) with high thermal stability: Preparation, characterization and application in PP/AAPP composites via EB irradiation

In subchapter 5.4, flame retardant PP nanocomposites based on PP with AAPP and O-MMT was prepared, however, the low thermal stability of modified MMT by alkylammonium salts leads to restacking of silicate layers. In addition, most of these surfactants are flammable. Thus, the triphenyl(undec-10-enyl)phosphonium bromide (TPB), consisting cation for ion exchange, carbon-carbon double bonds for grafting during EB treatment, phosphorus for flame retardancy, and long carbon chain for increasing the layer of MMT, was synthesized. It has been a great challenge to develop an efficient and in-situ method for improvement the flame-retardant properties of molded polymer nanocomposites. However, up to now, there is few reported how to improve flame-retardant properties of these molded nanocomposites.

Herein, the novel surfactant TPB was developed according to the procedure reported in Fig. 4.2.4, FO-MMT was prepared according to the procedure reported in 4.2.5 and multifunctional macromolecule AAPP was prepared according to the procedure reported in 4.2.3. Then PP/AAPP/FO-MMT nanocomposites based on PP with 20 % AAPP and 2 % FO-MMT were prepared by using a twin-screw extruder at a temperature of ~180 °C and a rotor speed of 80 rpm. Subsequently, specimens were prepared by injection molding at ~ 210 °C to obtain the standard samples. Finally, all samples were modified by state of the art EB treatment at 30 kGy in nitrogen atmosphere and at room temperature. The electron energy and electron current amounted to 1.5 MeV and 4 mA, respectively. The preparation procedures are shown as described in Fig. 5.44.

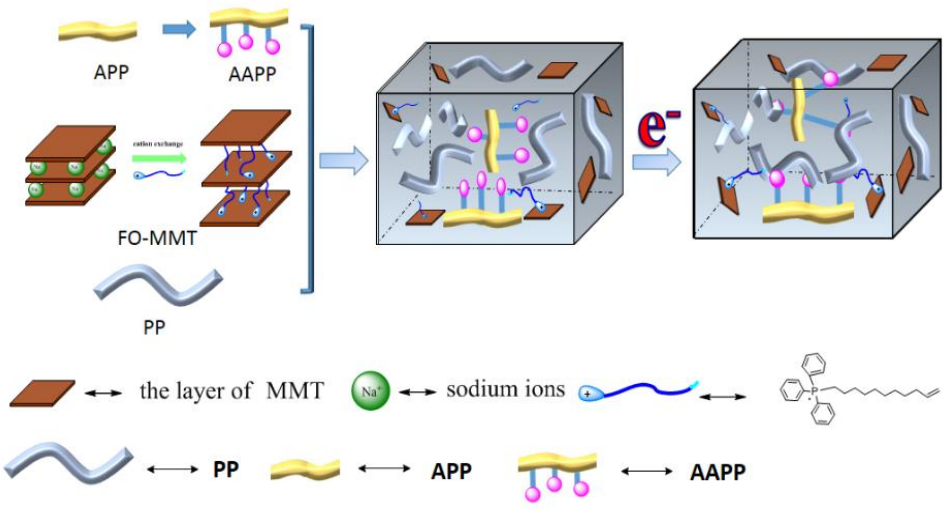

Fig. 5.44 Preparation procedures of PP/AAPP/FO-MMT nanocomposites with variable doses

5.5.1 Structural characterization of TPB

5.5.1.1 FTIR of TPB

TPB was prepared according to the procedure reported in Fig. 4.4. Its FTIR spectrum TPB is shown in Fig. 5.45. The characteristic absorption peaks at 1473, 1430, 738, and 689 cm^{-1} are attributed to the benzene ring stretching of TPB. The characteristic absorption peaks at 2921, 1307, and 1182 cm^{-1} can be attributed to the vibration of methane in the long carbon chain structure of TPB. In the spectrum of TPB, the characteristic absorption peak for carbon-carbon double bonds (1585 cm^{-1}) was clearly observed.

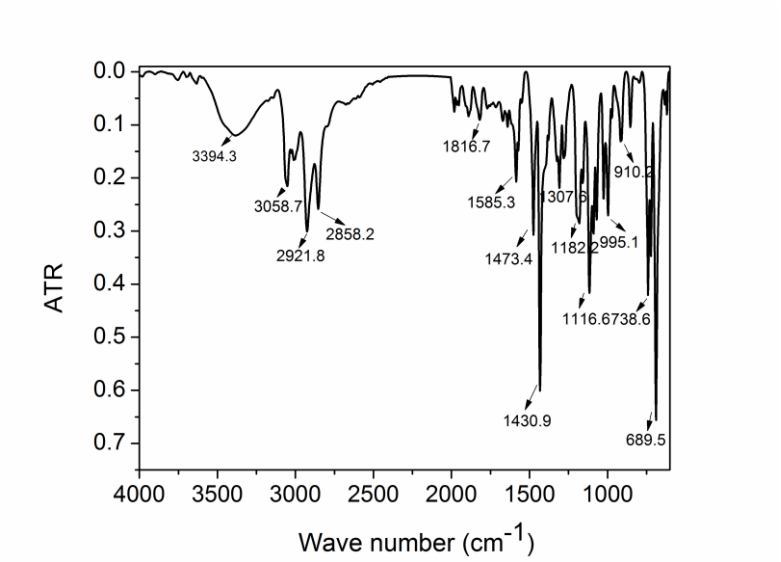

Fig. 5.45 FTIR spectra of TPB

5.5.1.2 ^{1}H NMR of TPB

The structure of TPB is further confirmed by ^{1}H NMR. As shown in Fig. 5.46, the peaks in the range from 8.00 to 7.25 ppm are assigned to the protons of hydrogen on the benzene rings of TPB (a, b, c in Fig. 5.46). Intensities in the range from 5.87 to 5.80 ppm correspond to the protons of the methylene group (d in Fig. 5.46) which is connected to the phosphorus of TPB. The peaks in the range from 4.98 to 4.11 ppm are assigned to the protons on the carbon-carbon double bonds (f and g in Fig. 5.46) of TPB. The peaks from 1.56 ppm to 1.08 ppm belong to the methylene groups (e in Fig. 5.46) in the long carbon chain of TPB. All these characteristic NMR peaks match the expect structure of TPB.

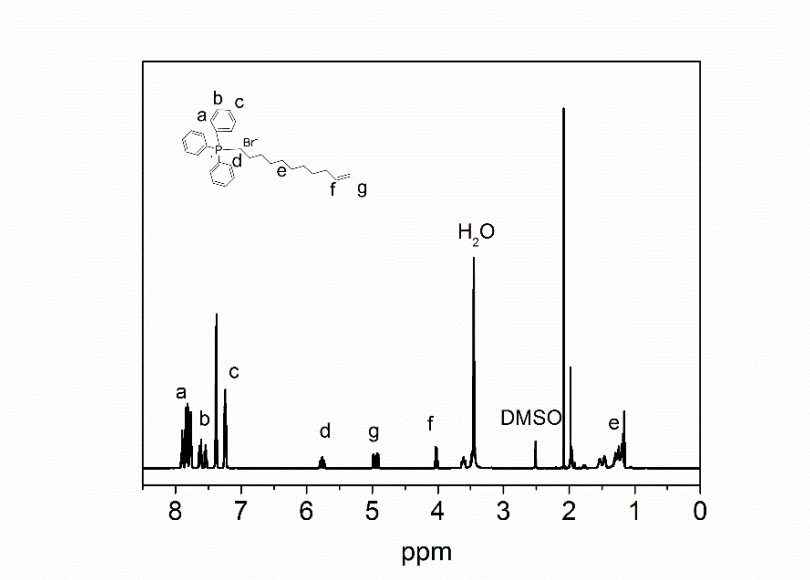

Fig. 5.46 ^{1}H NMR spectra of TPB

5.5.1.3 Wide-angle X-ray scattering (WAXS) of FO-MMT

The WAXS patterns for FO-MMT are shown in Fig. 5.47. Usually, the patterns show the characteristic reflections of MMT materials with a series of (001) reflections at a low angle, corresponding to the basal spacing and higher order reflections. In the case of FO-MMT, the first reflection peak is shifted to 4.76°. Thus, the interlayer distance is 1.85 nm according to the Bragg equation. In comparison, the unmodified MMT shows an interlayer distance of 0.98 nm. Consequently, the use of synthesized functional surfactant leads to an about twofold interlayer distance.

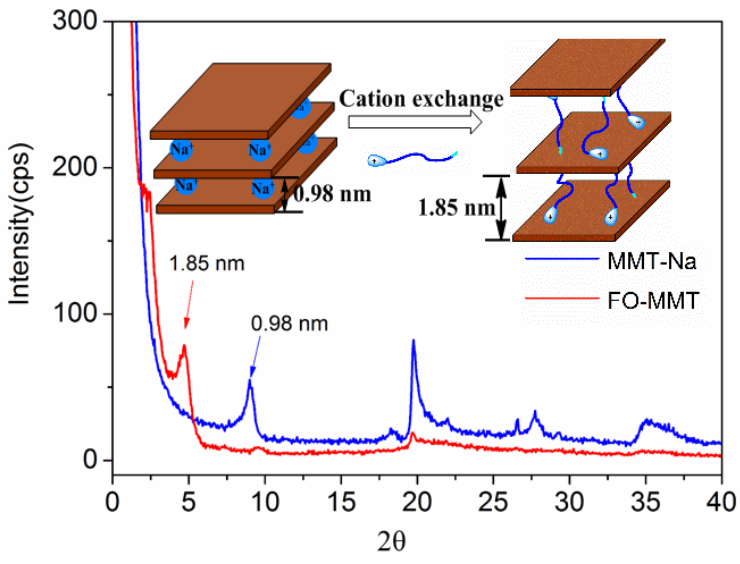

Fig. 5.47 WAXS analysis of MMT-Na and FO-MMT

5.5.1.4 Thermal stability of FO-MMT

TGA and DTG plots of MMT-Na, TPB and FO-MMT are shown in Fig. 5.48. In addition, normal temperatures and rate maximum mass loss (R_{max}) are summarized in Table 5.15 to enable a detailed quantitative evaluation of thermal stability for MMT-Na, TPB and FO-MMT. The temperatures $T_{-1\%}$, $T_{-3\%}$, $T_{-5\%}$ and T_{max} characterize the temperature at which a mass loss of 1 wt %, 3 wt % and 5 wt % as well as maximum mass loss rate were observed, respectively. The TGA curve of MMT-Na is very simple. There is a small loss of mass in the range from 50 to 100 °C due to the loss of interlayer water molecules of MMT. In the case of TPB, $T_{-1\%}$, $T_{-3\%}$ and $T_{-5\%}$ were 255, 267 and 270 °C, respectively. Thus, TPB shows a higher thermal stability than the onset temperature of traditional alkylammonium salts between 165 and 200 °C [27]. TGA curve of FO-MMT shows two steps of mass loss. The first step is observed in the temperature range from 250 to 360 °C and corresponds to the loss of long alkyl chains of TPB. The second step is observed in the temperature range from 360 to 450 °C. In comparison to TPB, $T_{-5\%}$ value of FO-MMT is slightly increased from 270 °C to 275 °C.

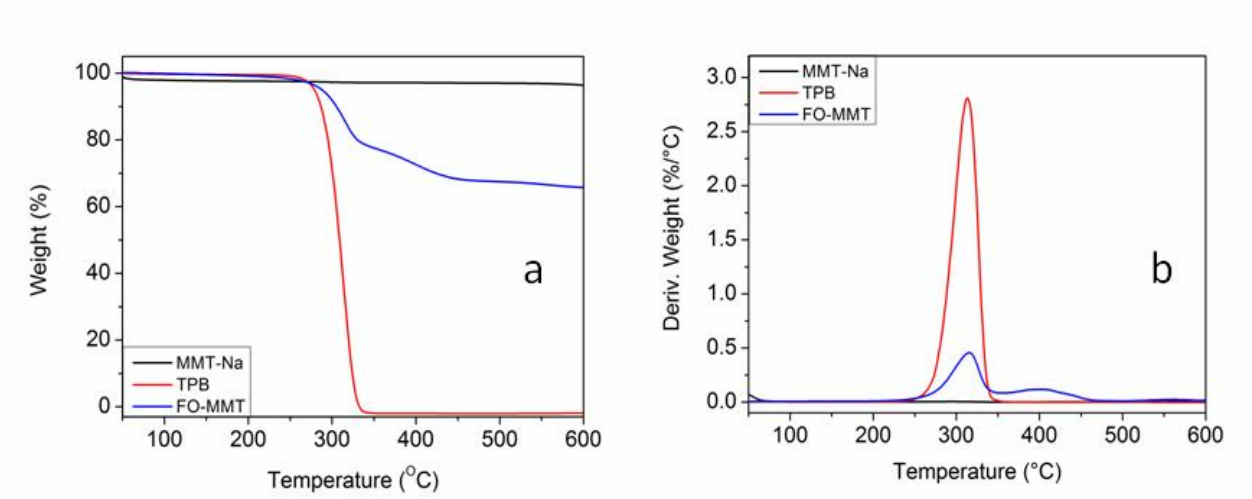

Fig. 5.48 TGA (a) and DTG (b) analysis of MMT-Na, TPB and FO-MMT

Table 5.15 Data obtained from TGA and DTG plots for MMT-Na, TPB and FO-MMT

Sample	$T_{-1\%}$ (°C)	$T_{-3\%}$ (°C)	$T_{-5\%}$ (°C)	T_{max} (°C)	R_{max} (wt %/K)
MMT-Na	50	530	-	-	-
TPB	255	267	270	314	2.8
FO-MMT	223	263	275	316	0.4

†The composites were irradiated with a dose of 32 kGy

5.5.2 Thermal properties of PP/AAPP/FO-MMT nanocomposites with variable doses

TGA and DTG plots of irradiated PP/20%AAPP/2%FO-MMT composites at 0, 15, 30 and 60 kGy in N_2 atmosphere at room temperature are depicted in Fig. 5.49. The related data are listed in Table 5.16. In comparison to non-irradiated flame retardant PP, $T_{-5\%}$ value of PP/AAPP/FO-MMT nanocomposites at 15, 30 and 60 kGy slightly reduce from 346 °C to 345, 336, 341 °C, respectively. However, it is noted that the T_{max} of irradiated flame retardant PP composites at 0, 15, 30 and 60 kGy are 427, 446, 439 and 458 °C, respectively. The possible reasons (see Fig. 5.49) are that flame retardant AAPP and/or functional surfactant of are grafted to backbone of PP.

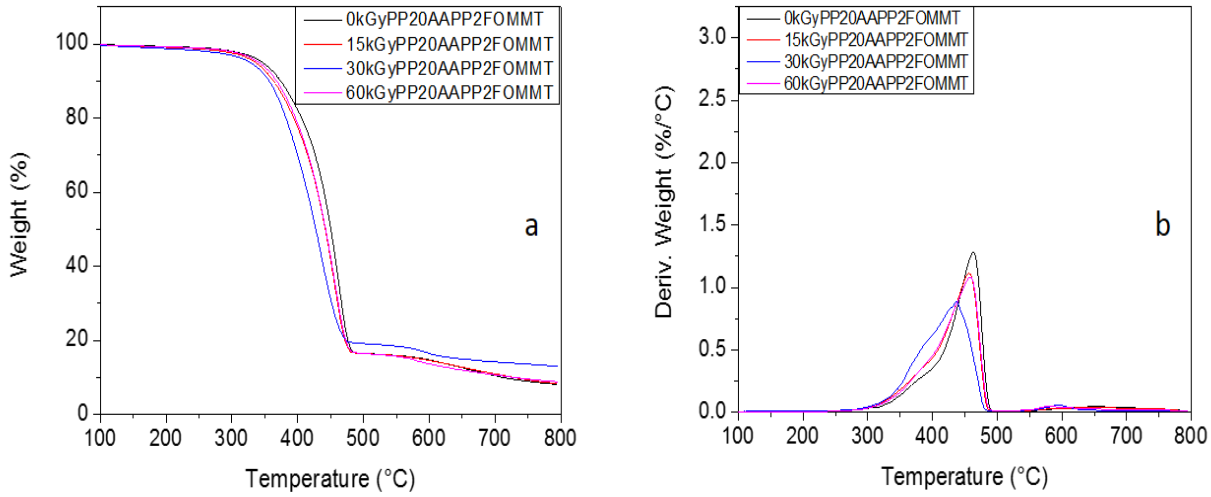

Fig. 5.49 TGA (a) and DTG (b) plots of PP/20%APP/2% FO-MMT composites irradiated at 0, 15, 30 and 60 kGy in N_2 atmosphere at room temperature

Table 5.16 Data obtained from TGA and DTG plots of PP/20%APP/2% FO-MMT composites irradiated at 0, 15, 30 and 60 kGy

Sample	$T_{-5\%}$ (°C)	T_{max} (°C)	R_{max} (%/K)	Residue (%)	
				500 (°C)	600 (°C)
0kGyPP20AAPP2FOMMT	346	464	1.3	16.5	14.7
15kGyPP20AAPP2FOMMT	345	459	1.1	16.5	14.8
30kGyPP20AAPP2FOMMT	336	441	0.9	19.1	16.3
60kGyPP20AAPP2FOMMT	341	459	1.1	16.4	13.8

5.5.3 Fire behavior of PP/AAPP/FO-MMT nanocomposites with variable doses

5.5.3.1 LOI and UL94

The LOI and UL-94 results of PP/20%AAPP/2%FO-MMT composites irradiated at 0, 15, 30 and 60 kGy are listed in Table 5.17. The LOI value of non-irradiated PP/20%AAPP/2%FO-MMT is 28.7 %. The LOI values of irradiated PP/AAPP/FO-MMT nanocomposites with 15, 30 and 60 kGy slightly increase to 29.1, 29.2 and 29.2 %, respectively. In addition, all PP/20%AAPP/2%FO-MMT passed UL94 V-0 rating. Therefore, no negative influence of electron treatment on LOI and UL94 of PP/AAPP/FO-MMT nanocomposites was found.

Table 5.17 LOI and UL94 results of PP/20%AAPP/2%FO-MMT composites irradiated at 0, 15, 30 and 60 kGy

Sample	LOI (%)	Rating	Dripping in UL94test
0kGyPP20AAPP2FOMMT	28.7	V-0	NO
15kGyPP20AAPP2FOMMT	29.1	V-0	NO
30kGyPP20AAPP2FOMMT	29.2	V-0	NO
60kGyPP20AAPP2FOMMT	29.2	V-0	NO

5.5.3.2 Cone calorimeter

The HRR of PP/20%AAPP/2%FO-MMT composites at 0 and 30 kGy are shown in Fig. 5.50. It is seen that the PHRR of non-irradiated flame retarded PP amounts to 586 kW/m^2. When PP/20%AAPP/2%FO-MMT composites are treated by EB with a dose of 30 kGy, the PHRR of EB modified PP/20%AAPP/2%FO-MMT significantly reduces to 327 kW/m^2. Nevertheless, it is still higher in comparison to PP/35%AAPP and PP/25%AAPP composites, but less than for non-irradiated PP/20%AAPP/2%FO-MMT. This corresponds to a reduction of 44 %, which illustrates that the HRR of PP/AAPP/FO-MMT composites is greatly reduced and delayed via EB irradiation.

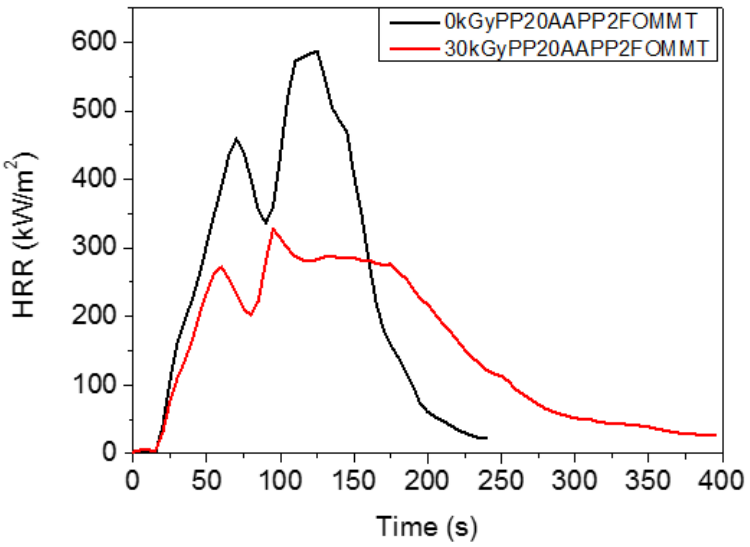

Fig. 5.50 HRR plots of PP/20%AAPP/2% FO-MMT composites irradiated at 0 and 30 kGy

The THR values of PP/20%AAPP/2%FO-MMT composites at 0 and 30 kGy are shown in Fig. 5.51. At the end of burning, both the THR of non-irradiated and EB irradiated PP/20%AAPP/2%FO-MMT composites are 61.5, and 59.8 MJ/m^2, respectively. It can be seen that the total heat release is slightly decreased by EB treatment.

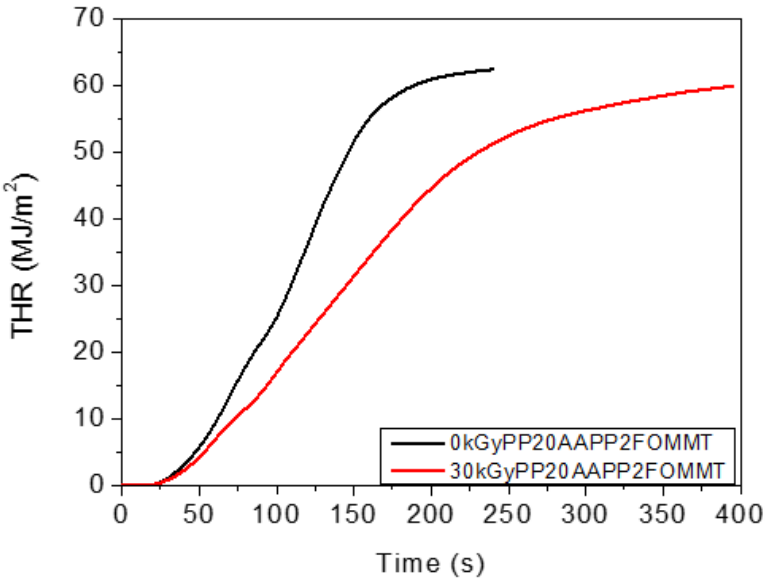

Fig. 5.51 THR plots of PP/20%AAPP/2% FO-MMT composites irradiated at 0 and 30 kGy

Smoke has been identified as the most significant hazard to people during fire. Thus smoke and the toxic gases are the primary cause of fatalities in fires, which can also impair visibility

and prevent escape from threatened areas [3]. The experimental values of SPR (a), TSP (b), CO_2 (c) and CO (d) for PP/20%AAPP/2%FO-MMT composites at 0 and 30 kGy are shown in Fig. 5.52. The SPR of non-irradiated PP/20%AAPP/2%FO-MMT composites is 0.07 m^2/s. However, when PP/20%AAPP/2%FO-MMT composite is treated by EB irradiation at 30 kGy, the SPR further significantly is reduced to 0.04 m^2/s. With regard to the TSP, the non-irradiated and irradiated PP/20%AAPP/2%FO-MMT composites are almost unchanged. As shown in Fig. 5.52 (c) and (d), the CO_2 and CO productions of non-irradiated PP/20%AAPP/2%FO-MMT composites are 0.35 and 0.008 g/s respectively. After EB irradiation, the CO_2 and CO production of EB irradiated PP/20%AAPP/2%FO-MMT composites are 0.17 and 0.005 g/s, respectively. These results illustrated that EB irradiation could effectively suppress the rate of smoke production.

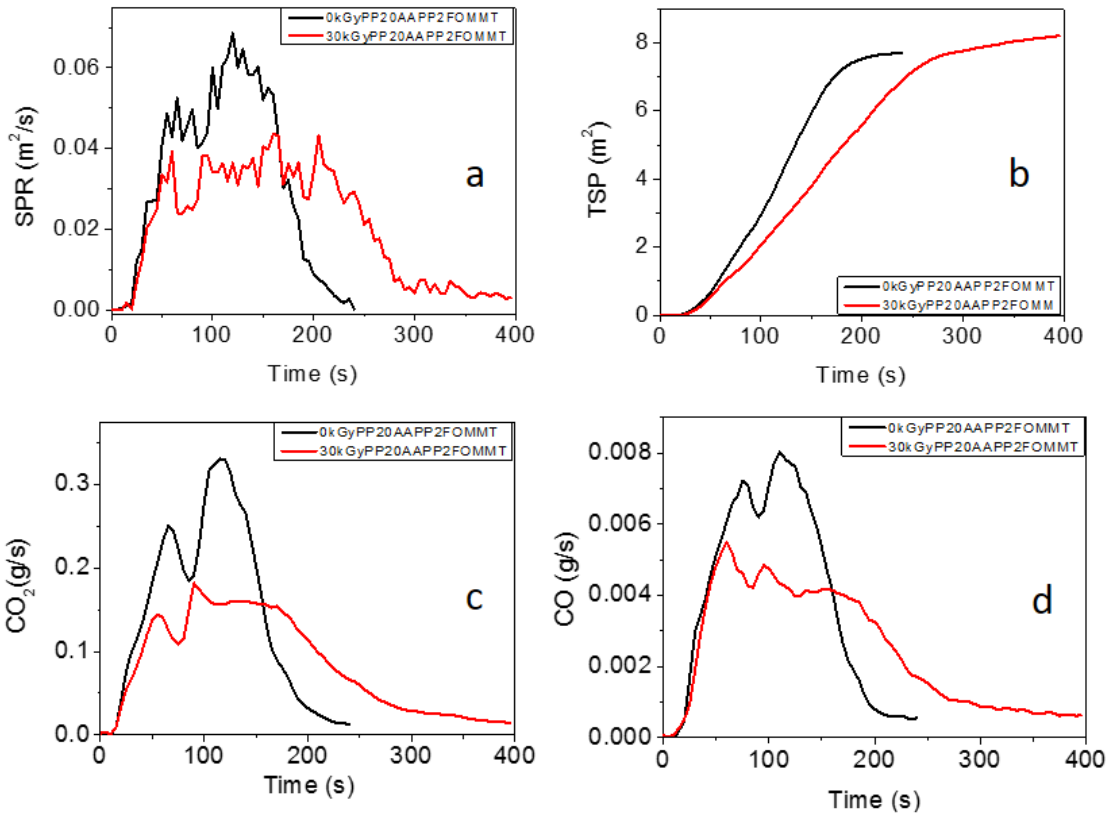

Fig. 5.52 SPR (a), TSP (b), CO_2 (c) and CO (d) plots of PP/20%AAPP/2% FO-MMT composites irradiated at 0 and 30 kGy

The mass loss (ML) plots of PP/20%AAPP/2%FO-MMT composites at 0 and 30 kGy are shown in Fig. 5.53. The residual mass of the non-irradiated and EB irradiated PP/20%AAPP/2%FO-MMT composites amounts to 25 %. The ML rate of irradiated

PP/20%AAPP/2%FO-MMT composites is lower compared to irradiated PP/20%AAPP/2%FO-MMT composites.

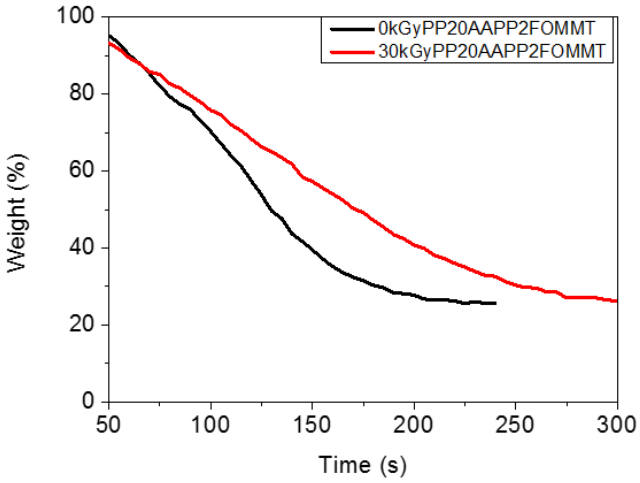

Fig. 5.53 ML plots of PP/20%AAPP/2% FO-MMT composites irradiated at 0 and 30 kGy

5.5.4 Morphology of burnt PP/AAPP/FO-MMT nanocomposites

To investigate the residues, digital photos for non-irradiated and irradiated PP/20%AAPP/2%FO-MMT are shown in Fig. 5.54. It is seen that irradiated burnt PP/20%AAPP/2%FO-MMT composites are more stable than non-irradiated PP/20%AAPP/2%FO-MMT. A possible reason is that the designed flame retardant nanocomposites are modified by EB and can form more stable residues layer.

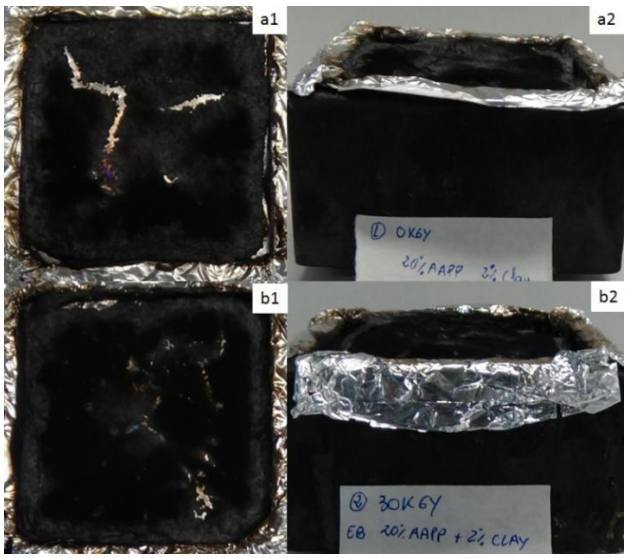

Fig. 5.54 Digital photographs for the residues of PP/20%AAPP/2% FO-MMT composites irradiated at 0 (a1, a2) and 30 kGy (b1, b2) after CC test

5.5.5 Mechanical properties of PP/AAPP/FO-MMT nanocomposites at various doses

Mechanical properties of PP/20%AAPP/2% FO-MMT composites irradiated at 0, 15, 30 and 60 kGy are shown in Fig. 5.55. In Fig. 5.55(a), tensile strength of non-irradiated PP/20%AAPP/2% FO-MMT composites is 28 MPa. Tensile strength of irradiated flame retardant PP at 15, 30 and 60 kGy are 28, 28, and 29 MPa, respectively. It meant that the tensile strength of irradiated flame retardant PP composites is not changed by EB treatment. In addition, the Young's modulus of non-irradiated PP/20%AAPP/2%MMT composites is 2038 MPa in Fig. 5.55(b). The Young's modulus of irradiated flame retardant PP at 15, 30 and 60 kGy amounts to 2230, 2299, and 2566 MPa, respectively. Thus, the Young's modulus of irradiated flame retardant PP increases via state of the art EB treatment. From Fig. 5.55(c), the elongation at break (%) of non-irradiated PP/20%AAPP/2%FO-MMT composites amounts to 12.8 %. It can be noted that the elongation at break of irradiated flame retardant PP at 15, 30 and 60 kGy reduced to 10.1, 7.0 and 4.2 %, respectively. Thus, the elongation at break of PP/20%AAPP/2% FO-MMT composites decreases at high dose values. Finally, the impact strength of non-irradiated PP/20%AAPP/2% FO-MMT composites is 3.0 K J/m^2. However, the impact strength of irradiated flame retardant PP at 15, 30 and 60 kGy reduced to 2.5, 2.1, and 1.9 kJ/m^2, respectively. In comparison to the elongation at break of PP containing 60 wt % of $Mg(OH)_2$ is 0.8 % (see Fig. 1.4), the lower loading of fillers (PP with AAPP and FO-MMT system) increase mechanical properties of nanocomposites. Maximum dose to be applied in EB treatment about 15 kGy. This is in agreement with Krause et al. [140].

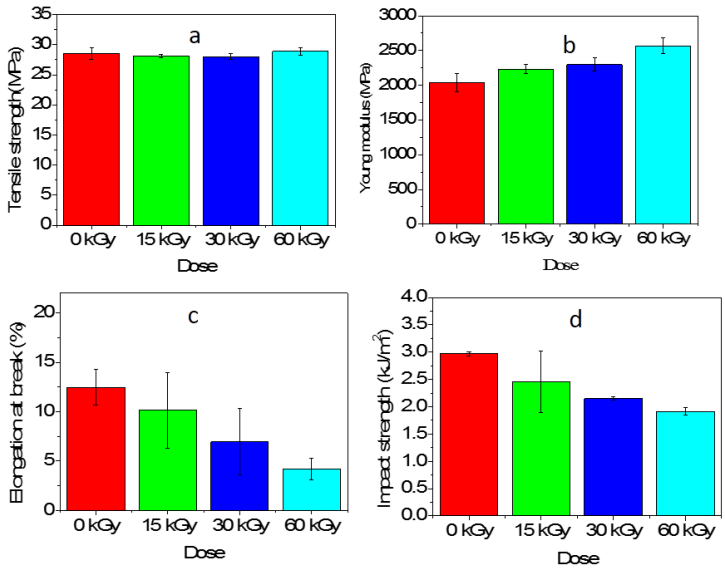

Fig. 5.55 Tensile strength (a), Young's modulus (b), elongationat break (c) and impact strength(d) plots of PP/20%APP/2% FO-MMT composites irradiated at 0, 15, 30 and 60 kGy

5.5.6 Conclusions

A novel functional surfactant for the modification of MMT was designed, synthesized and analyzed. In comparison to traditional alkylammonium, the novel modifier triphenyl(undec-10-enyl)phosphonium bromide (TPB) showed significantly increased thermal stability. Consequently, it was used to prepare a novel functional organo-modified nanoclay (FO-MMT) with high thermal stability. To study the effect of EB treatment on the thermal stability, flame retardance, and tensile properties of high performance fire retardant polymer nanocomposites, flame retardant polypropylene nanocomposites based on multifunctional AAPP and FO-MMT were prepared. LOI values of flame retardant PP nanocomposites are almost the same even using EB treatment. T_{max} of irradiated flame retardant PP composites is improved under EB treatment. In the cone calorimeter test, the total heat release, total smoke production, and total mass loss of these fire retardant polymer nanocomposites are not influenced by EB treatment. More importantly, it was found that EB treatment of these designed flame retardant PP nanocomposites is an efficient approach to further reduce peak heat release rate, smoke production rate, and mass loss rate. In addition, the analysis of char residues proved that irradiated flame retardant composites provided relatively better quality of char residue in the combustion that acted as better barrier to prevent the transmission of fuel and oxygen. This innovative idea may be expanded to other polymer systems to develop high performance polymer nanocomposites to significantly reduce the heat release rate, smoke production, and mass loss rate and increase mechanical properties of nanocomposites via environment-friendly high energy electrons.

In subchapter 5.5, these flame retardant polymer nanocomposites were molded and then modified by EB treatment at stationary condition at ambient temperature in the solid state. Howevet, in Fig. 5.55, the elongationat break of PP/20%AAPP/2% FO-MMT composites was decreased by EB treatment due to chain scission of PP. To develop the state of the art technology, a new reactive processing technology electron induced reactive processing (EIReP) simultaneously combines the polymer modification and melt mixing at conventional dynamic condition via high energy electrons, which might bring about desired physical and chemical reaction in the flame retardant nanocomposites melts via high energy electrons. Thus, PP/20%AAPP/2%FO-MMT nanocomposites modification with accelerated electrons offers the EIReP in the next step.

5.6 Flame retardant PP nanocomposites via EIReP

Electon beam (EB) processing is widely used in the production of flame retardant insulated wires and cables because of fast, controllable and economical [34, 35]. Nevertheless, all these EB processing pathway is almost the same. Firstly, the polymer(s) and flame retardants additive(s) are mixed by melt compounding. And then, the flame retardant composites are thermoformed by shaping or molding. After that, final product is irradiated by EB treatment at atambient temperature in the solid state (Fig. 5.56). According to previous studies [41, 42, 43], elongation at break of non-irradiated and irradiated PP/60 wt % $Mg(OH)_2$ composites were 1 % and 0.8 %. Also, in previous subchapters 5.5, the elongationat break of PP/20%AAPP/2% FO-MMT composites was decreased by EB treatment due to chain scission of PP. Therefore, state of the art EB treatment is not able to increase the tensile properties.

Recently, electron induced reactive processing (EIReP) is developed using an electron accelerator directly coupled with an internal mixe, which omits the thermoforming before irradiation. Both physical and chemical reactions of flame retardant nanocomposites are held by high energy electrons during melt mixing (Fig. 5.56). As shown in Fig 1.4, elongation at break of modified PP/60 wt % $Mg(OH)_2$ composites by EIReP was increased to 5 %. indicates an improved interfacial adhesion between $Mg(OH)_2$ and PP. In this study, PP with low lording fillers AAPP and FO-MMT nanocomposites were prepared by melt compounding and EIReP. The FR contains double bonds in order to graft these AAPP and modifier by high-energy electrons to PP. The amount of AAPP and MMT depends strongly on the requirements of flame retardancy. Thus, the absorbed dose has to be determined in such a way, that the numbers of PP radicals are equal to the number molecules of FR in order to graft each FR to PP chain. According to previous studies [41, 42, 43] and the procedure reported in 4.3.3, the doses at 9, 18 and 27 kGy are choosen for PP/AAPP/FO-MMT nanocomposites.

In previous subchapters 5.3, 5.4 and 5.5 multifunctional macromolecule AAPP had been synthesized by a simple one step procedure, which had a good contribution to the flame retardancy of PP composites. Moreover, FO-MMT had been prepared and provided an excellent synergistic effect on the flame retardancy of PP/AAPP composite. AAPP and FO-MMT were prepared according to the procedure reported in 4.2.3, 4.2.4 and 4.2.5, respectively. The flame-retardant properties of the PP/AAPP/FO-MMT nanocomposites with variable doses were characterized in detail by LOI, UL94, and CC tests. Finally, the morphology of burnt PP/AAPP/FO-MMT nanocomposites was studied by SEM in order to explain the effect of EIReP on their flame-retardant properties.

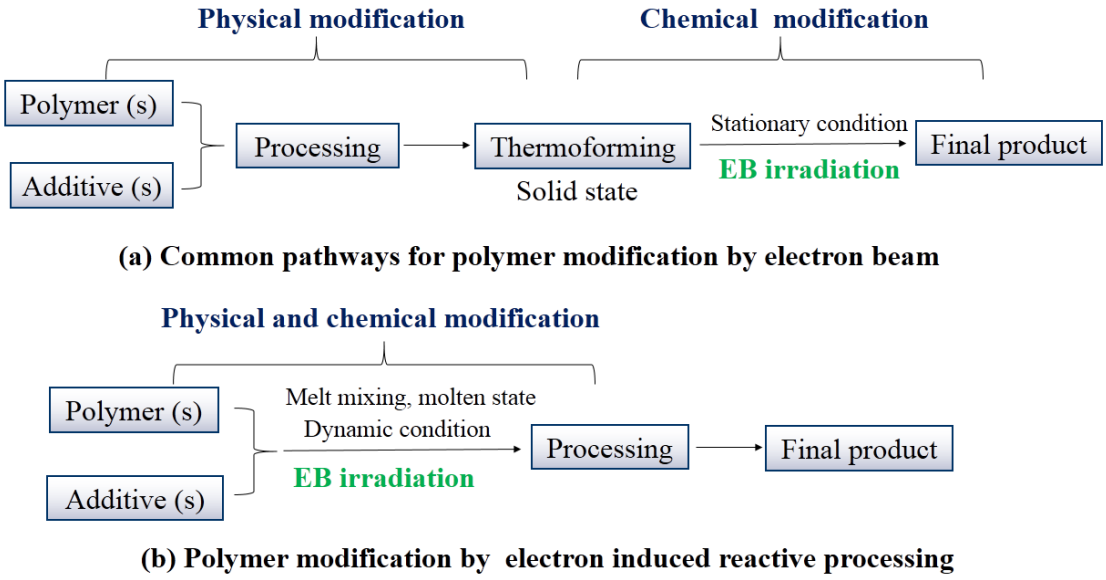

Fig. 5.56 Polymer modification via electron beam (EB) (a) and electron induced reactive processing (EIReP) (b)

5.6.1 Fire behavior of EIReP modified PP/AAPP/FO-MMT nanocomposites

LOI and UL94

The results of LOI and UL-94 tests are shown in Table 5.18. The LOI value of melt compounded PP with 20 wt % AAPP and 2 wt % FO-MMT is 28.9 %. The LOI values of EIReP modified PP/AAPP/FO-MMT nanocomposites irradiated with 9, 18 and 27 kGy slightly increase to 29.3, 29.5, and 29.6 %, respectively. All prepared PP/AAPP/FO-MMT nanocomposites passed the UL94 V-0 rating.

Table 5.18 LOI and UL94 results of PP/AAPP/FO-MMT nanocomposites irradiated with 0, 9, 18 and 27 kGy by EIReP

Sample	LOI (%)	UL94test	
		Dripping	Rating
0kGy-EIReP-PP20AAPP2FOMMT	28.9	NO	V-0
9kGy-EIReP- PP20AAPP2FOMMT	29.3	NO	V-0
18kGy-EIReP- PP20AAPP2FOMMT	29.5	NO	V-0
27kGy-EIReP- PP20AAPP2FOMMT	29.6	NO	V-0

Heat release

The HRR results of PP/AAPP/FO-MMT nanocomposites irradiated at 0, 9, 18 and 27 kGy are shown in Fig. 5.57. The PHRR of melt compounded PP/AAPP/FO-MMT nanocomposites amounts to 466 kW/m^2. However, when PP/AAPP/FO-MMT nanocomposites are prepared by EIReP with a dose of 9, 18 and 27 kGy, the PHRR of EIReP modified flame-retardant PP nanocomposites significantly reduces to 294, 258, and 224 kW/m^2, respectively. These are the lowest values of PHRR achieved in this work. The PHRR of EIReP modified PP/AAPP/FO-MMT nanocomposites at 9, 18 and 27 kGy were reduced by 37 %, 44 % and 52 %, respectively compared to melt compounded sample. Consequently, the heat release of flame-retardant PP/AAPP/FO-MMT nanocomposites is reduced and delayed by EIReP.

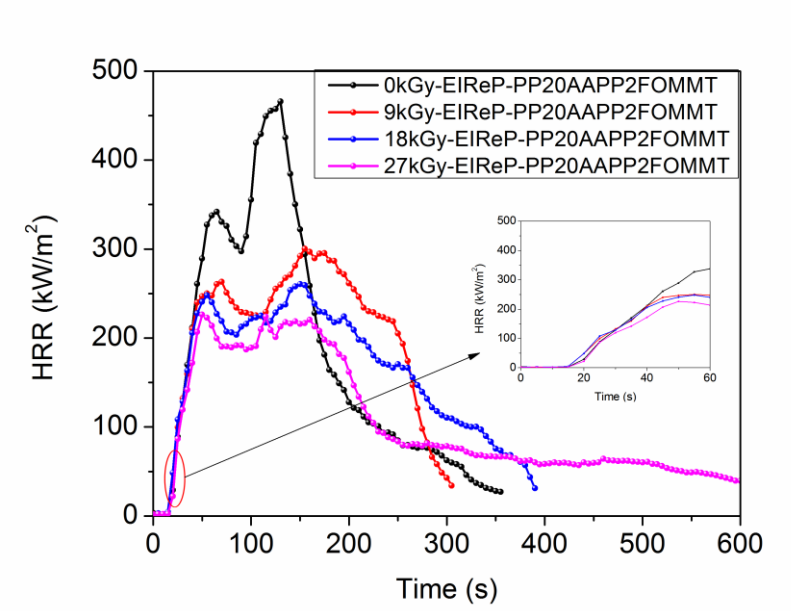

Fig. 5.57 HRR curves of PP/AAPP/FO-MMT nanocomposites at 0, 9, 18 and 27 kGy by EIReP

The THR values of PP/AAPP/FO-MMT nanocomposites at 0, 9, 18 and 27 kGy are shown in Fig. 5.58. At the end of burning, the THR of PP/AAPP/FO-MMT nanocomposites at 0, 9, 18 and 27 kGy amounts to 63, 61, 61 and 61 MJ/m^2, respectively. Thus, the total heat release of EIReP modified PP/AAPP/FO-MMT nanocomposites is not reduced by EIReP within the experimental uncertainty.

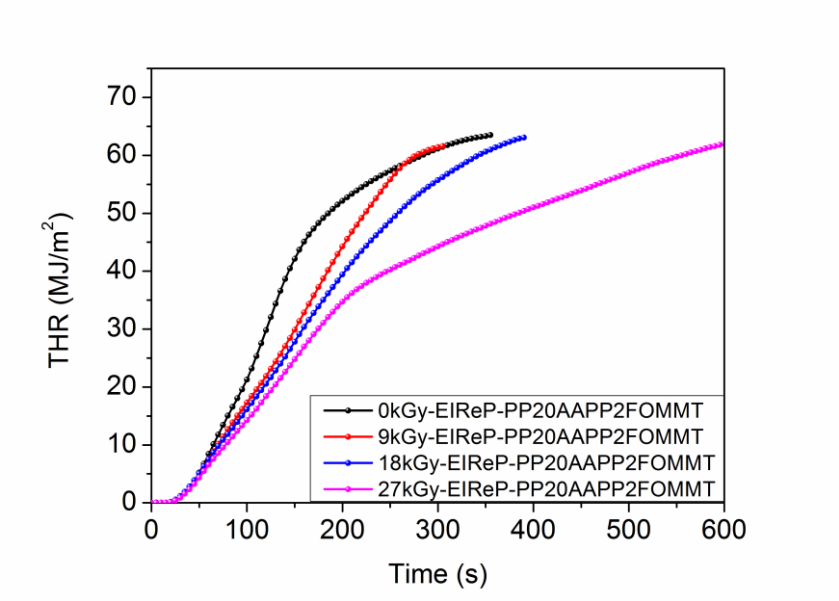

Fig. 5.58 THR curves of irradiated PP/AAPP/FO-MMT nanocomposites at 0, 9, 18 and 27 kGy by EIReP

Smoke release

The SPR (a), TSP (b), CO (c) and CO_2 (d) plots of PP/AAPP/FO-MMT nanocomposites at 0, 9, 18 and 27 kGy are shown in Fig. 5.59. The SPR of melt compounded PP/AAPP/FO-MMT nanocomposites amounts to 0.058 m^2/s. When PP/AAPP/FO-MMT nanocomposites are prepared by EIReP using dose values of 9, 18 and 27 kGy, the PHRR of EIReP modified flame-retardant PP nanocomposites reduces to 0.046, 0.04 and 0.037 m^2/s, respectively. In the case of TSP, there is no influence of EIReP. As shown in Fig. 5.59 (c), the CO production of PP/AAPP/FO-MMT nanocomposites at 0, 9, 18 and 27 kGy amounts to 0.004, 0.004, 0.003 and 0.003 g/s, respectively. In comparison to melt compounded PP/AAPP/FO-MMT nanocomposites, the CO_2 production of EIReP modified PP/AAPP/FO-MMT nanocomposites at 9, 18 and 27 kGy reduces from 0.25 to 0.16, 0.14 and 0.11 g/s, respectively. Consequently, EIReP could effectively suppress the production of smoke and toxic gases during burning of flame retardant polymer nanocomposites.

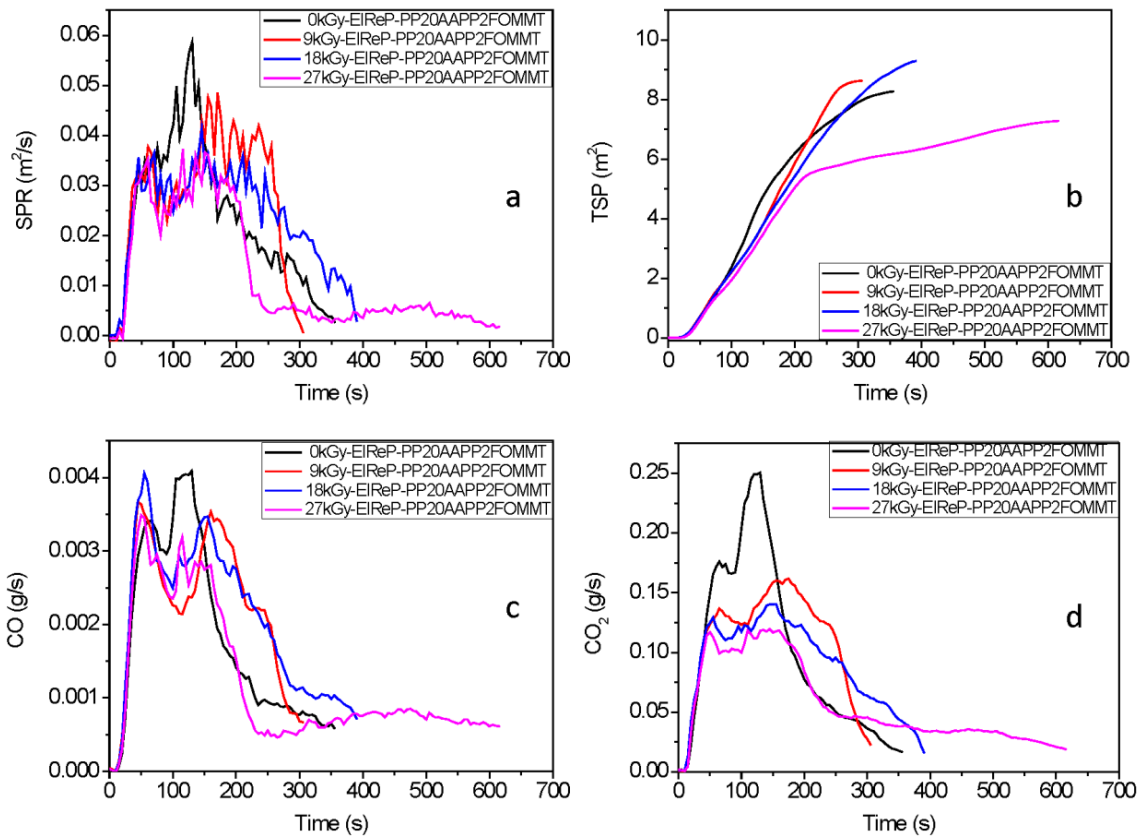

Fig. 5.59 SPR (a), TSP (b), CO (c) and CO_2 (d) plots of irradiated PP/AAPP/FO-MMT nanocomposites at 0, 9, 18 and 27 kGy by EIReP

5.6.2 Mechanical properties of EIReP modified PP/AAPP/FO-MMT nanocomposites

Mechanical properties of EIReP modified PP/AAPP/FO-MMT nanocomposites at 0, 9, 18 and 27 kGy are shown in Fig. 5.60. Tensile strength of EIReP modified PP/AAPP/FO-MMT nanocomposites at 9, 18 and 27 kGy are 30, 28, and 28 MPa, respectively. Thus, the tensile strength of EIReP modified PP/AAPP/FO-MMT nanocomposites is slightly reduced within increasing dose since PP tends to degradation using EIReP at 185 °C [43]. The Young's modulus of EIReP modified PP/AAPP/FO-MMT nanocomposites at 9, 18 and 27 kGy are 1993, 1975, and 2066 MPa, respectively. Thus, the Young's modulus of irradiated flame retardant PP slightly increases via EIReP. It can be noted that the elongation at break of irradiated flame retardant PP at 9, 18 and 27 kGy reduced to 11.8, 9.9 and 6.7 %, respectively. Thus, the elongationat break of PP/20%AAPP/2% FO-MMT composites is reduced by EIReP due to degradation of PP during EIReP [140]. Finally, the impact strength of EIReP modified flame retardant PP at 9, 18 and 27 kGy reduced to 2.9, 2.6, and 2.3 kJ/m^2, respectively. There are two possible reasons for these experimental results. Firstly, AAPP is not grafted to PP chain by EIReP due to low spacer distance of side chain of AAPP. Secondly, PP tends to degradation

during EB treatment in molten state [140]. Consequently, toughened crosslinkable PP has to be used in order to prepare flame retardant PP/AAPP/FO-MMT nanocomposites with enhanced mechanical properties [121].

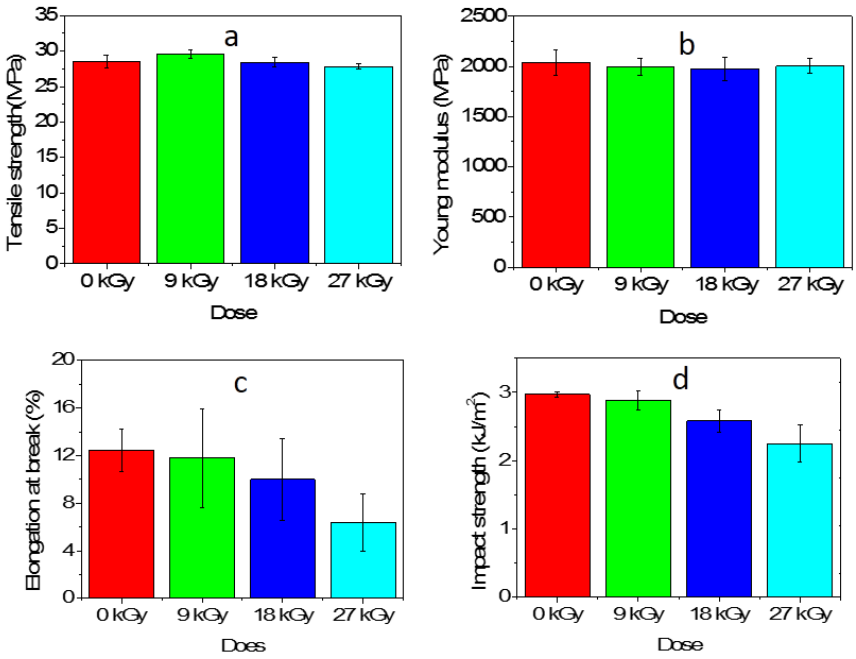

Fig. 5.60 Tensile strength (a), Young's modulus (b), elongationat break (c) and impact strength (d) plots of EIReP modified PP/AAPP/FO-MMT nanocomposites at 0, 9, 18 and 27 kGy

5.6.3 Possible flame retardant mechanism

Flame retardant additives in PP may function in the condensed phase and/or in the gas phase. The flame retardant efficiency depends strongly on the structure and composition of the char generated during burning [15, 16, 44]. To further explore how the microstructure of char residues influences the flame retardancy of PP during combustion, SEM micrographs are shown for residues of PP/AAPP/FO-MMT nanocomposites at 0 kGy and 27 kGy in Fig. 5.61. The surface of residual char of melt compounded PP/AAPP/FO-MMT nanocomposites (Fig. 5.61 (a)) is unexpanded due to insufficient char formation during the combustion. A rich charred layer surface of EIReP modified PP/AAPP/FO-MMT nanocomposites at 27 kGy (Fig. 5.61 (b)) has a continuous, compact, and thick structure. Consequently, it could reduce both mass and heat transfer, which is effective in retarding the degradation of underlying polymer.

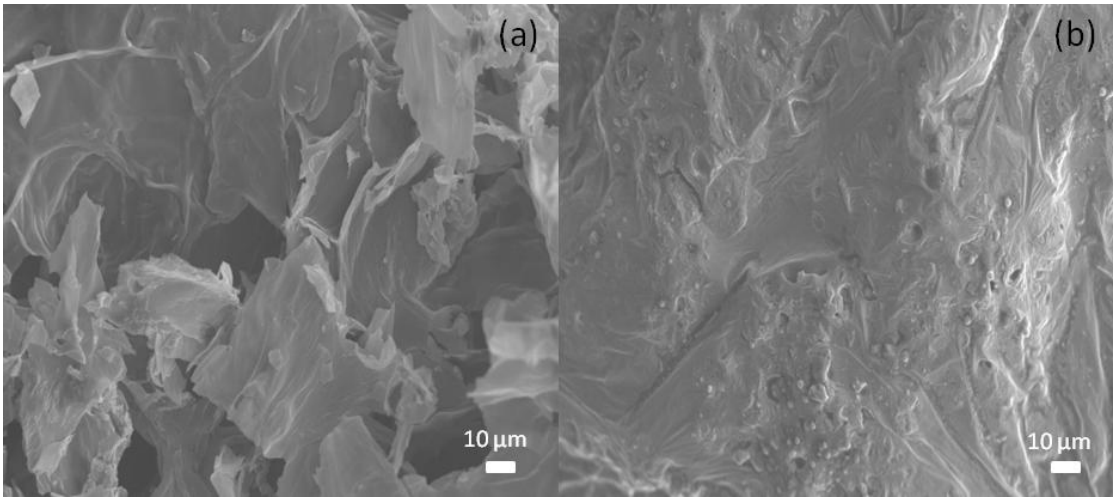

Fig. 5.61 SEM images for residues surface of melt compounded PP/AAPP/FO-MMT nanocomposites (a) and EIReP modified PP/AAPP/FO-MMT nanocomposites at 27 kGy (b)

Based on the results of CC tests, EIReP modified PP/AAPP/FO-MMT nanocomposites showed a significantly lower heat release and smoke compared to that of melt compounded sample. As shown in Fig. 5.57, the PHRR of EIReP modified PP/AAPP/FO-MMT nanocomposites at 27 kGy is reduced by 52% compared to melt compounded nanocomposites. In addition, the SEM analysis of char residues proved that irradiated PP/AAPP/FO-MMT nanocomposites by EIReP provided relatively better quality of char residue in the combustion that acted as good barrier to prevent the transmission of fuel and oxygen. Based on these experimental data, a possible mechanism between PP and AAPP by EIReP is proposed in Fig. 5.62. During EIReP, PP macro-radicals are generated reacting with the C=C bond of AAPP to generate a grafting reaction. The same reaction can be induced by the PP macro-radicals at the other C=C bonds of AAPP. Finally, a cross-linked structure is generated in the flame retardant PP composites.

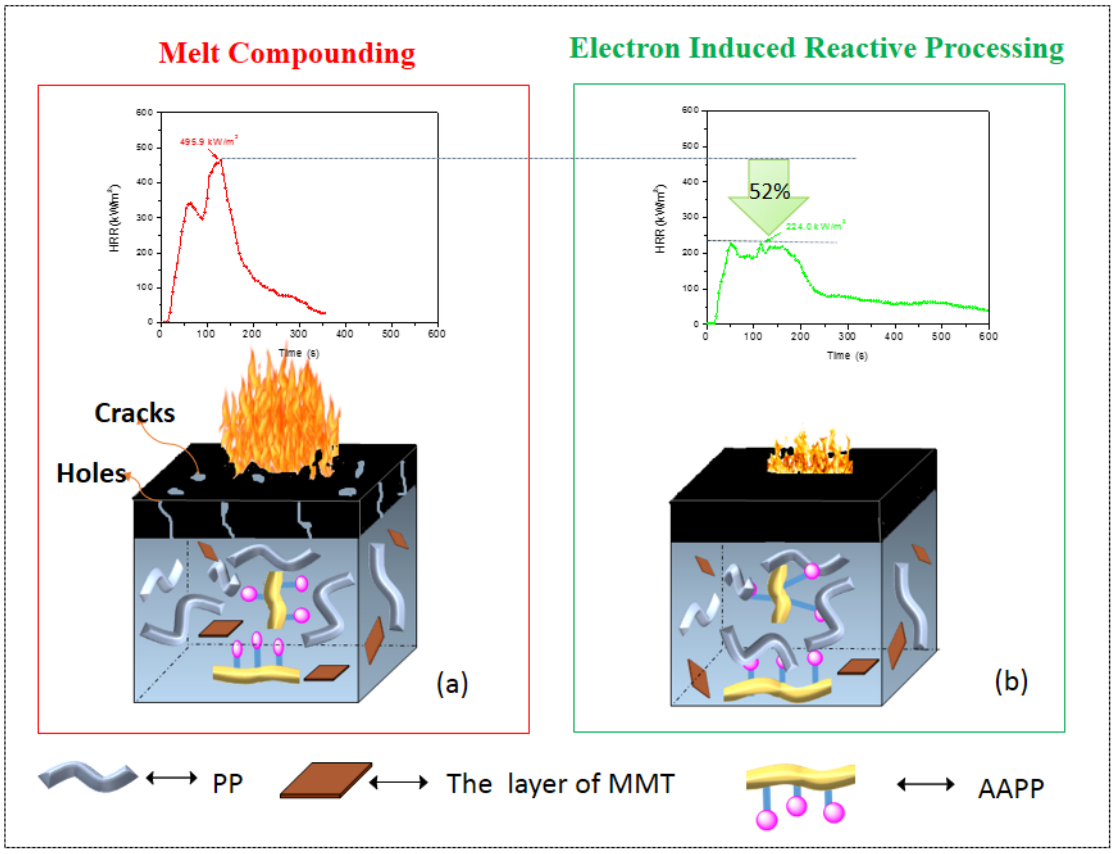

Fig. 5.62 Schematic illustration of barrier effect of the flame-retardant polypropylene nanocomposites by normal processing (a) and electron induced reactive processing (b)

5.6.4 Conclusions

Flame retardant PP nanocomposites were prepared by melt compounding and EIReP. The flame-retardant properties of PP/AAPP/FO-MMT nanocomposites with different dose values were studied in detail. The results suggest that EIReP is a novel, fast and environment-friendly technology to reduce the heat and smoke toxicity release of flame retardant PP nanocomposites without any use of additional additives. Based on these results following conclusions can be drawn:

a) EIReP could effectively suppress the heat release rate as well as the production rate of smoke and toxic gases of PP/AAPP/FO-MMT nanocomposites.

b) The LOI values of PP/APP/FO-MMT nanocomposites increase slightly by EIReP with increasing dose.

c) EIReP has no influence on total heat release of PP/APP/FO-MMT nanocomposites.

d) EIREP modified PP/APP/FO-MMT nanocomposites provided a better quality of char residue acting as good barrier to prevent the transmission of fuel and oxygen.

e) EIReP of PP/APP/FO-MMT nanocomposites led to slightly reduced mechanical properties in comparison to non-modified PP/APP/FO-MMT nanocomposites due to degradation of PP.

Normally, polyfunctional monomers with long carbon chain (at least 10 carbons) are used for their grafting to polymers by EB treatment. Amine with long carbon chain (spacer distant) is very expensive. Consequently, AAPP with short carbon chain were synthesized in this work. Other different multifunctional flame retardant with long carbon chain could be developed for EB technology. Further investigations are required in order to explain the raw material-process-structure-property relationship of flame retardant PP nanocomposites.

Chapter 6

Conclusions and outlooks

6.1 Conclusions

In order to develop high-performance fire safe PP composites, efficient flame retardants and nanomaterial were synthesized. In addition, the modifiers and flame retardants in the PP matrix were partially immobilized by high energy electrons to increase the thermal, flame retardant and mechanical properties of fire safe PP composites. There are two main tasks in this work.

- A new flame retardant (FR) based on ammonium polyphosphate (APP) was developed by modification of APP with carbon source in order to get highly efficient intumescent flame retardant (IFR) which can be coupled by electron beam (EB) to polymer matrix.

The subchapter 5.1 and subchapter 5.2 contain synthesis and characterization of functional charring agents acting together with APP as novel IFR. We explored novel flame retardant, N^1-(5,-dimethyl-1,3,2-dioxaphosphinyl-2-yl)-acrylamide (DPA) and spirocylic pentaerythritol bisphosphorate disphosphoryl-di-prop-2-en-1-amine (SPSA), containing one or two functional double bond which can form a grafted/crosslinked structure with PP after EB treatment. DPA and SPSA were physically combined with APP (mass ratio of DPA or SPSA and APP were 1:2) to prepared IFR1 and IFR2, respectively. As shown in Table 6, PP+30% IFR1 and PP+30% IFR2 passed UL 94 V-0 rating, indicating that these PP+30% IFR1 and PP+30% IFR2 were more efficient than APP alone. In the cone calorimeter test, both, peak heat release rate (PHRR) and total heat release (THR) results of PP+30% IFR1 and PP+30% IFR2 systems were lower than those of PP/APP system. It proved that these IFR1 and IFR2 were a more efficient flame retardant to PP compared to APP. Moreover, EB treatment of the composites is an efficient approach to improve the thermal stability of these designed PP/IFR1 and PP/IFR2 composites.

To develop a more effective flame retardant, in the subchapter 5.3 a multifunctional allylamine polyphosphate (AAPP) has been designed and synthesized via a simple one-step method in order to be used as flame retardant crosslinker with the host polymer under the EB treatment. In comparison to the traditional PP/APP composites, limiting oxygen index (LOI) value of PP/AAPP composites was enhanced to 33.7 % with 35 wt % of AAPP and effective melt drip resistance was achieved in UL-94 test. More importantly, in the cone calorimeter test,

the PHRR, THR, SPR (smoke production rate) and TSP (total smoke production) results of PP/AAPP composites were much lower than those of PP/APP composites. In addition, the analysis of char residues proved that this AAPP provided relatively good quality of char residue (P−N−C and P−O−C structure) in the combustion and acted as good barrier to prevent the transmission of fuel and oxygen. Moreover, EB was an efficient approach to improve the thermal stability of these designed flame retardant PP composites. However, the tensile properties of these flame retardant PP composites were not increased. The possible reasons are that the irradiation of PP is causing chain scission and producing lower molecular substance at 36 kGy, and some part of AAPP can not be completely crosslinked with long chain of PP by EB treatment due to carbon chain of AAPP is short.

- Development of temperature stable functional (flame retardant) surfactant for montmorillonite (MMT) to be used for the modification of MMT as well as to be coupled to the polymer matrix by accelerated electrons.

To reduce the overall multifunctional AAPP content and increase properties of flame retardant PP composite, in subchapter 5.4, we explored the synergistic mechanisms of AAPP with MMT as a nanofiller. For nanofiller filled composites, the LOI value of PP with 20.0 wt % AAPP and 2.0 wt % of O-MMT can be increased to 29.5 %, and reached V-0 rating in UL94 tests. In particular, TEM results demonstrated that MMT could be better dispersed in PP/AAPP system compared with traditional PP/APP system. In comparison to PP/AAPP (22 wt %) composites, PP/AAPP (20 wt %) + O-MMT (2 wt %) composites showed improved flame retardancy. In details, it passed the UL-94 V-0 rating, showed reduced values of HRR, THR, SPR and TSP. Moreover, high quality char residue was formed, which acted as a barrier during combustion process and prevented the transfer of fuel and oxygen to the volume of flame retardant PP composites. Furthermore for MMT, a novel functional surfactant was synthesized and analyzed. In comparison to traditional alkylammonium, the novel modifier triphenyl(undec-10-enyl)phosphonium bromide (TPB) showed significantly increased thermal stability. Consequently, it was used to prepare novel functional organo-modified nanoclay (FO-MMT) with high thermal stability.

Within the scope of this research work, we tried to understand the fire retardant PP nanocomposites treated by EB technology in different conditions. The dose (ca. 15 kGy) was seletected in order to reach a good balance between crosslinking/grafting of AAPP and TPB and degradation of PP. The thermal stability of flame retardant PP nanocomposites is almost the same after EB treatment. LOI values of flame retardant PP nanocomposites were slightly

increased by high energy electrons. In the cone calorimeter test, it was shown that the total heat release, total smoke production, and total mass loss of these fire retardant polymer nanocomposites are not negative influenced by EB treatment. For the first time, it was found that EB treatment of these designed flame retardant PP nanocomposites is an efficient approach for reduction of peak heat release rate, smoke production rate, and mass loss rate. In addition, the analysis of char residues proved that irradiated flame retardant PP composites provided better quality of char residue in the combustion.

Nevertheless, the use of this state of the art technology is mostly limited to form parts (after molding) in solid state and at room temperature (stationary conditions). Thus, a novel procedure of polymer modification with accelerated electrons offers the electron induced reactive processing (EIReP), which modify AAPP, FO-MMT and PP during their melt mixing by high energy electrons in order to precisely control the desired chemical reactions. These flame retardant PP nanocomposites were prepared by melt compounding and EIReP. The flame-retardant properties of PP/AAPP/FO-MMT nanocomposites with different dose values were studied in detail. The results suggest that EIReP is a novel, fast and environment-friendly technology to reduce the heat and smoke toxicity release of flame retardant PP nanocomposites without any use of additional additives. This innovative idea may be expanded to other polymer systems to develop high-performance polymer nanocomposites to greatly reduce the rate of heat release, smoke production, and mass loss and increase mechanical properties of nanocomposites by environment-friendly EIReP.

As shown in Table 6, at the loading of 30 wt % APP, the LOI value of PP/APP composite increases to 20.4 %, but there is no rating in the UL 94 test. PP/30%IFR1 and PP/30%IFR2 composites pass the UL-94 V-0 rating and their LOI values reached 24.5 % and 24.0 %, respectively. IFR1 and IFR2 based on a physical mixure of APP and new char agent (DPA or SPSA) have a higher flame retardancy to PP compared to APP. However, their LOI values are low in comparison to PP/60% $Mg(OH)_2$ composites (27.5%). Thus, multifunctional flame retardant AAPP with a carbon source containing one double bond is synthesized by one step. The LOI results of PP with 35 wt % AAPP greatly increase to 33.7 %. Consequently, AAPP has a higher efficiency on the flame retardance of PP compared to $Mg(OH)_2$, APP, IFR1 and IFR2 in PP. Furthermore, a part of AAPP is replaced by O-MMT, in order to reduce the total filler loading. The LOI values of PP with 20 wt % AAPP + 2 wt % O-MMT composites is 29.5 % and the samples have no melt dripping during flame ignition and achieved V-0 rating in UL94 test. Finally, EB and and EIReP modified nanocomposites showed slightly increase of LOI.

The cone calorimeter is regarded as one of most important bench-scale fire facilities. The experimental setup defines a specific fire scenario. Consequently the mass flow (C-factor), thickness and thermal feedback influence the peak of heat release rate of sample [141]. In the case of PP/IFR1 and PP/IFR2, the PHRR are 331 and 430 kW/m^2. However, when the loading of AAPP amounts to 35 wt %, the PHRR reduces 229 kW/m^2. The PHRR of EIReP modified PP/AAPP/FO-MMT nanocomposites at 27 kGy is reduced by 52 % compared to melt compounded nanocomposites.

Table 6 LOI and UL94 results of PP/AAP + DPA (chapter 5.1), PP/APP + SPSA (chapter 5.2), PP/APP + allylamine (chapter 5.3), PP/AAPP + O-MMT (chapter 5.4), PP/AAPP + FO-MMT (chapter 5.5), EB PP/AAPP + FO-MMT (chapter 5.5) and EIReP PP/AAPP + FO-MMT (5.6) composites

Sample	FR loading (wt %)	LOI (%)	UL 94 test	
			Rating	Dripping
PP	0	17.6	N.R.	Yes
PP/60%Mg(OH)$_2$[#]	60	27.5	V-0	NO
PP/30%APP	30	20.3	N.R.	Yes
PP/30% (AAP + phys. DPA) (IFR1) (5.1)	30	24.5	V-0	NO
PP/30% (APP + phys. SPSA) (IFR2) (5.2)	30	24.0	V-0	NO
PP/35% (APP + chem Allylamine) (AAPP) (5.3)	35	33.7	V-0	NO
PP/20%AAPP + 2%O-MMT (5.4)	22	29.5	V-0	NO
PP/20%AAPP + 2%FO-MMT (5.5)	22	28.7	V-0	NO
EB PP/20%AAPP + 2%FO-MMT* (5.5)	22	29.2	V-0	NO
EIReP PP/20%AAPP + 2%FO-MMT[§] (5.6)	22	29.6	V-0	NO

N.R.: no rating [#] Reference [43] * EB PP/20%AAPP + 2%FO-MMT composites was irradiated at 25 °C with a dose of 30 kGy [§] EIReP PP/20%AAPP + 2%FO-MMT composites was irradiated at 170 °C with a dose of 27 kGy

In comparison to PP containing 60 wt % of Mg(OH)$_2$, the lower loading of fillers (PP with AAPP and FO-MMT system) leads to enhanced elongation at break of nanocomposites. However, the mechanical properties of EIReP modified PP/AAPP/FO-MMT nanocomposites are still reduced. Firstly, PP chain and AAPP can not be fully grafted by high energy electrons because of low spacer distance of side chain of AAPP. Secondly, PP tends to degradation during EB treatment in molten state. Consequently, toughened crosslinkable PP and multifunctional

flame retardant with long carbon chain have to be used in order to prepare flame retardant nanocomposites with enhanced mechanical properties.

Table 7 Mechanical properties results of PP/AAPP (chapter 5.3), PP/AAPP + O-MMT (chapter 5.4), PP/AAPP + FO-MMT (chapter 5.5), EB PP/AAPP + FO-MMT (5.6) and EIReP PP/AAPP + FO-MMT (5.6) composites

Sample	Tensile strength (MPa)	Young modulus (MPa)	Elongation at break (%)
PP[&]	23.5±0.8	984.7±7.9	743.0±21.1
PP/35%AAPP[&]	21.6±0.1	1384.3±63.8	9.2±2.8
PP/20%AAPP-2%O-MMT[&]	21.7±0.6	1147.2±31.0	19.0±0.3
PP/60%$Mg(OH)_2$[#Δ]	27.4±1.0	5070.0±425.2	1.0±0.2
PP/20%AAPP+2%FO-MMT[Δ]	28.5±0.9	2037.9±139.7	12.8±1.8
EB PP/20%AAPP+2%FO-MMT*[Δ]	28.0±0.5	2299.6±92.5	7.0±3.3
EIReP PP/20%AAPP+2%FO-MMT[§Δ]	28.0±0.4	2001.0±74.5	6.7±2.4

[#] Reference [43] * EB PP/20%AAPP + 2%FO-MMT composites was irradiated at 25 °C with a dose of 30 kGy [§] EIReP PP/20%AAPP + 2%FO-MMT composites was irradiated at 170 °C with a dose of 27 kGy [&] Flame retardant composites was processed by extrusion and tested using ISO 527/1BA/10 at IMDEA. [Δ] Flame retardant composites was processed by mixing chamber and tested using DIN EN ISO 527-2/1BA/50 at IPF.

6.2 Outlooks

Despite the progress made within the scope of this research work, there are still some issues related to these topics to be studied further.

- Due to amine with long carbon chain is expensive, in this work, AAPP with short carbon chain were synthesized. Other different multifunctional flame retardant with long carbon chain could be developed for EB technology in the future.
- Toughened crosslinkable PP should be used in order to prepare flame retardant PP/AAPP/FO-MMT nanocomposites with enhanced mechanical properties
- Different functional carbon chain surfactants from renewable resource could be prepared for EB technology. It could be interesting to find the effect of carbon chain surfactants on the development of functional organic MMT.

- The multifunctional flame retardant grafting agent could be developed. Other different functional flame retardants with a carbon source containing one double bond and silicone coupled agent could be explored to gain better insight into the development of flame retardant polymer nanocomposites.
- Several other properties like water resistance; electrical condctivity etc. could also be envisaged.
- Different electron energy are influencing the dispersion of MMT in PP. If possible, the structural properties relationship between electron energy and dispersion of FO-MMT in polymer could be explored for EIReP.
- Thermoplastic vulcanizates are a commercially high valued group of polymer blend. Multifunctional flame retardant and functional organic nanofillers could be used in thermoplastic vulcanizates by electron induced reactive processing.
- PP fibers have been widely used in car industry, floor coverings, automotives textiles, etc. Crosslinkable multifunctional flame retardant PP fibre nanocomposites could be developed using EIReP.

In a nutshell, high-performance fire retardant polypropylene nanocomposites have been developed via high energy electrons (Fig. 6.1), which is an interesting topic for fire retardant and EB technology. However, a long term vision and further interest are necessary to draw a comprehensive picture about the relevant topic.

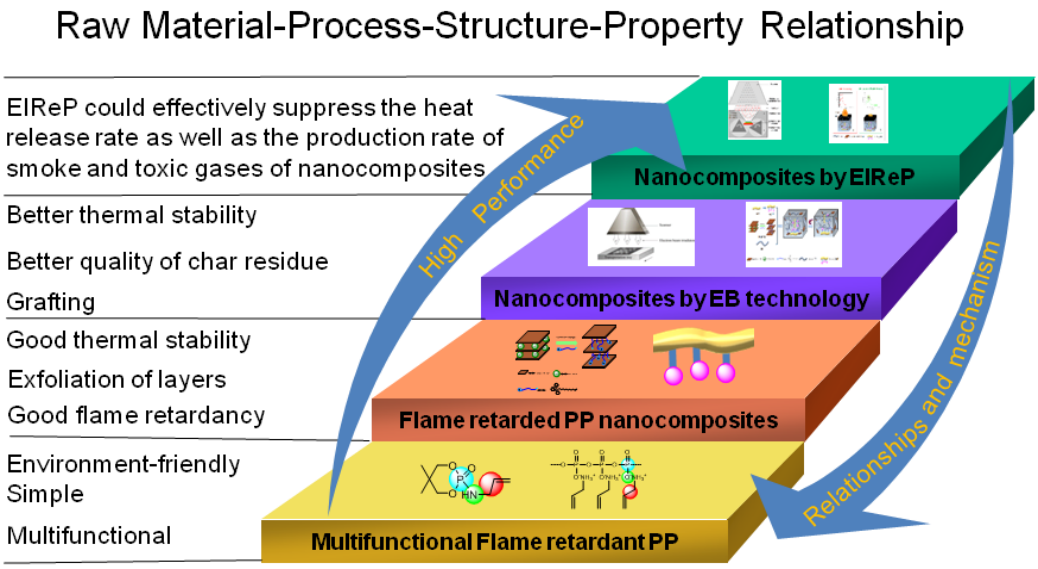

Fig. 6.1 The raw material-process-structure-property relationship of fire retardant polymer nanocomposites

References

[1] A.B. Morgan, C.A. Wilkie. The non-halogenated flame retardant handbook. Wiley, 2014. ISBN: 9781118686249.

[2] M. Rakotomalala, S. Wagner, M. Döring. Recent developments in halogen free flame retardants for epoxy resins for electrical and electronic applications. Materials, 2010, 3, 4300-4327.

[3] A.A. Stec, T.R. Hul. Fire toxicity. Woodhead Publishing, 2016. ISBN: 9781845698072.

[4] S.Y. Lu, I. Hamerton. Recent developments in the chemistry of halogen-free flame retardant polymers. Progress in Polymer Science, 2002, 27, 1661-1712.

[5] M. Alaee, P. Arias, A. Sjödin, Å. Bergman. An overview of commercially used brominated flame retardants, their applications, their use patterns in different countries/regions and possible modes of release. Environment International, 2003, 29, 683-689.

[6] F. Rahman, K.H. Langford, M.D. Scrimshaw, J.N. Lester. Polybrominated diphenyl ether (PBDE) flame retardants. Science of TheTotal Environment, 2001, 275, 1-17.

[7] The Restriction of the Use of Certain Hazardous Substances (RoHS) in Electrical and Electronic Equipment (EEE) Directive. 2011/65/ EU.

[8] The Waste Electrical and Electronic Equipment Directive (WEEE Directive) is the European Community directive. 2012/19/EU.

[9] The Registration, Evaluation, Authorisation and Restriction of Chemicals (REACH), European Registration. 2006/1907.

[10] K.S. Lim, S.T. Bee, L.T. Sin, T.T. Tee, C.T. Ratnam, D. Hui. Review of application of ammonium polyphosphate as intumescent flame retardant in thermoplastic composites. Composites Part B: Engineering, 2016, 84, 155-174.

[11] Y.H. Guan, J.Q. Huang, J.C. Yang, Z.B. Shao, Y.Z. Wang. An effective way to flame-retard biocomposite with ethanolamine modified ammonium polyphosphate and its flame retardant mechanisms. Industrial & Engineering Chemistry Research, 2015, 54, 3524-3531.

[12] B. Rimez, H. Rahier, M. Biesemans, S. Bourbigot, B. Van Mele. Flame retardancy and degradation mechanism of poly(vinyl acetate) in combination with intumescent flame retardants: I. Ammonium poly(phosphate). Polymer Degradation and Stability, 2015, 121, 321-330.

[13] B. Wang, X. Qian, Y. Shi, B. Yu, N. Hong, L. Song, Y. Hu. Cyclodextrin microencapsulated ammonium polyphosphate: Preparation and its performance on the thermal, flame retardancy and mechanical properties of ethylene vinyl acetate copolymer. Composites Part B: Engineering, 2015, 69, 22-30.

[14] L. Boccarusso, L. Carrino, M. Durante, A. Formisano, A. Langella, F. Memola, C. Minutolo. Hemp fabric/epoxy composites manufactured by infusion process: Improvement of fire properties promoted by ammonium polyphosphate. Composites Part B: Engineering, 2016, 89, 117-126.

[15] Z.B. Shao, C. Deng, Y. Tan, M.J. Chen, L. Chen, Y.Z. Wang. An efficient mono-component polymeric intumescent flame retardant for polypropylene: preparation and application. ACS Applied Materials & Interfaces, 2014, 6, 7363-7370.

[16] Z.B. Shao, C. Deng, Y. Tan, L. Yu, M.J. Chen, L. Chen, Y.Z. Wang. Ammonium polyphosphate chemically-modified with ethanolamine as an efficient intumescent flame retardant for polypropylene. Journal of Materials Chemistry A, 2014, 2, 13955-13965.

[17] S.S. Ray, M. Okamoto. Polymer/layered silicate nanocomposites: a review from preparation to processing. Progress in Polymer Science, 2003, 28, 1539-1641.

[18] T. Lan, T.J. Pinnavaia. Clay-reinforced epoxy nanocomposites. Chemistry of Materials, 1994, 6, 2216-2219.

[19] Y. Kojima, A. Usuki, M. Kawasumi, A. Okada, T. Kurauchi, O. Kamigaito. Synthesis of nylon 6–clay hybrid by montmorillonite intercalated with ϵ-caprolactam. Journal of Polymer Science Part A: Polymer Chemistry, 1993, 31, 983-986.

[20] M.S. Wang, T.J. Pinnavaia. Clay-polymer nanocomposites formed from acidic derivatives of montmorillonite and an epoxy resin. Chemistry of Materials, 1994, 6, 468-474.

[21] J.H. Chang, Y.U. An. Nanocomposites of polyurethane with various organoclays: thermomechanical properties, morphology, and gas permeability. Journal of Polymer Science: Part B: Polymer Physics, 2002, 40, 670-677.

[22] M. Zammarano, M. Franceschi, S. Bellayer, J.W. Gilman, S. Meriani. Preparation and flame resistance properties of revolutionary self-extinguishing epoxy nanocomposites based on layered double hydroxides. Polymer, 2005, 46, 9314-9328.

[23] E. Manias, A. Touny, L. Wu, K. Strawhecker, B. Lu, T.C. Chung. Polypropylene/montmorillonite nanocomposites. Review of the synthetic routes and materials properties. Chemistry of Materials, 2001, 13, 3516-3523.

[24] M. Zanetti, G. Camino, D. Canavese, A.B. Morgan, F.J. Lamelas, C.A. Wilkie. Fire retardant halogen-antimony-clay synergism in polypropylene layered silicate nanocomposites. Chemistry of Materials, 2002, 14, 189-193.

[25] T.D. Fornes, D.L. Hunter, D.R. Paul. Nylon-6 nanocomposites from alkylammonium-modified clay: The role of alkyl tails on exfoliation. Macromolecules, 2004, 37, 1793-1798.

[26] H. Zou, W. Xu, Q. Zhang, Q. Fu. Effect of alkylammonium salt on the dispersion and properties of poly(p-phenylene sulfide)/clay nanocomposites via melt intercalation. Journal of Applied Polymer Science, 2006, 99, 1724-1731.

[27] A. Leszczyńska, J. Njuguna, K. Pielichowski, J.R. Banerjee. Polymer/montmorillonite nanocomposites with improved thermal properties: Part I. factors influencing thermal stability and mechanisms of thermal stability improvement. Thermochimica Acta, 2007, 453, 75-96.

[28] H.A. Patel, R.S. Somani, H.C. Bajaj, R.V. Jasra. Preparation and characterization of phosphonium montmorillonite with enhanced thermal stability. Applied Clay Science, 2007, 35, 194-200.

[29] J.W. Gilman, W.H. Awad, R.D. Davis, J. Shields, R.H. Harris Jr., C. Davis, A.B. Morgan, T.E. Sutto, J. Callahan, P.C. Trulove, H.C. DeLong. Polymer/layered silicate nanocomposites from thermally stable trialkylimidazolium-treated montmorillonite. Chemistry of Materials, 2002, 14, 3776-3785.

[30] J. Golebiewski, A. Galeski. Thermal stability of nanoclay polypropylene composites by simultaneous DSC and TGA. Composites Science and Technology, 2007, 67, 3442-3447.

[31] V. Thakur, U. Gohs, U. Wagenknecht, G. Heinrich. In situ modification of unmodified montmorillonite in polypropylene by electron-induced reactive processing. Macromolecular Chemistry and Physics, 2012, 213, 729-737.

[32] A. Bhattacharya. Radiation and industrial polymers. Progress in Polymer Science, 2000, 25, 371-401.

[33] J.S. Sefadi, A.S. Luyt, J. Pionteck, F. Piana, U. Gohs. Effect of surfactant and electron treatment on the electrical and thermal conductivity as well as thermal and mechanical properties of ethylene vinyl acetate/expanded graphite composites. Journal of Applied Polymer Science, 2015, 132, 42396.

[34] M.R. Cleland. Industrial Applications of Electron Accelerators. 2005. Netherlands.

[35] B.G. Ershov. Radiation Technologies: Their possibilities, state, and prospects of application. Herald of the Russian Academy of Sciences, 2013, 83, 437-447.

[36] R. Rajeshbabu, U. Gohs, K. Naskar, M. Mondal, U. Wagenknecht, G. Heinrich. Electron-induced reactive processing of poly(propylene)/ethylene-octene copolymer blends: a novel route to prepare thermoplastic vulcanizates. Macromolecular Materials and Engineering, 2012, 297, 659-669.

[37] R. Rajeshbabu, U. Gohs, K. Naskar, V. Thakur, U. Wagenknecht, G. Heinrich. Preparation of polypropylene (PP)/ethylene octene copolymer (EOC) thermoplastic vulcanizates (TPVs) by high energy electron reactive processing. Radiation Physics and Chemistry, 2011, 80, 1398-1405.

[38] K. Naskar, U. Gohs, U. Wagenknecht, G. Heinrich. PP-EPDM thermoplastic vulcanisates (TPVs) by electron induced reactive processing. XPRESS Polymer Letters, 2009, 3, 677-683.

[39] S. Rooj, V. Thakur, U. Gohs, U. Wagenknecht, A.K. Bhowmick, G. Heinrich. In situ reactive compatibilization of polypropylene/epoxidized natural rubber blends by electron

induced reactive processing: novel in-line mixing technology. Polymers for Advanced Technologies, 2011, 22, 2257-2263.

[40] M. Mondal, U. Gohs, U. Wagenknecht, G. Heinrich. Polypropylene/natural rubber thermoplastic vulcanizates by eco-friendly and sustainable electron induced reactive processing. Radiation Physics and Chemistry, 2013, 88, 74-81.

[41] U. Wagenknecht, U. Gohs, A. Leuteritz, S. Volke, S. Wiessner, G. Heinrich. Modification of particle filled polymers with high energy electrons under in-stationary conditions of melt mixing. Macromolecular Symposia, 2011, 301, 146-150.

[42] U. Gohs, A. Leuteritz, K. Naskar, S. Volke, S. Wiessner, G. Heinrich. Reactive EB processing of polymer compounds. Macromolecular Symposia, 2010, 296, 589-595.

[43] C. Zschech. Flammgehemmte polyolefin compounds mittels elektronen induzierter reaktiver aufbereitung, Master thesis, 2015.

[44] A.R. Horrocks, D. Price, D. Price. Fire retardant materials. Woodhead, 2001, ISBN: 9781855737464.

[45] A.B. Morgan, C.A. Wilkie. Flame retardant polymer nanocomposites. Wiley, 2008, ISBN: 9780471734260.

[46] M.L. Bras, S. Bourbigot. Intumescent fire retardant polypropylene formulations. Polymer Science and Technology Series, 1999, 2, 357-365.

[47] R. Bernstein, S.M. Thornberg, A.N. Irwin, J.M. H. D.K. Derzon, S.B. Klamo, R.L. Clough. Radiation-oxidation mechanisms: Volatile organic degradation products from polypropylene having selective C-13 labeling studied by GC/MS. Polymer Degradation and Stability, 2008, 93, 854-870.

[48] J. Green. Mechanisms for flame retardancy and smoke suppression- a review. Journal of Fire Sciences, 1996, 14, 426-442.

[49] V. Babushok, W. Tsang, G.T. Linteris, D. Reinelt. Chemical limits to flame inhibition. Combustion and Flame, 1998, 115, 551-560.

[50] M. Sain, S.H. Park, F. Suhara, S. Law. Flame retardant and mechanical properties of natural fibre-PP composites containing magnesium hydroxide. Polymer Degradation and Stability, 2004, 83, 363-367.

[51] Z.Z. Wang, B.J. Qu, W.C. Fan, P. Huang. Combustion characteristics of halogen-free flame-retarded polyethylene containing magnesium hydroxide and some synergists. Journal of Applied Polymer Science, 2001, 81, 206-214.

[52] X. Chen, J. Yu, M. He, S. Guo, Z. Luo, S. Lu. Effects of zinc borate and microcapsulated red phosphorus on mechanical properties and flame retardancy of polypropylene/magnesium hydroxide composites. Journal of Polymer Research, 2009, 16, 357-362.

[53] U. Braun, B. Schartel. Flame retardant mechanisms of red phosphorus and magnesium hydroxide in high impact polystyrene. Macromolecular Chemistry and Physics, 2004, 205, 2185-2196.

[54] J. Alongi, Z. Han, S. Bourbigot. Intumescence: tradition versus novelty. a comprehensive review. Progress in Polymer Science, 2015, 51, 28-73.

[55] I. Ravadits, A. Tóthb, G. Marosi, A. Márton, A. Szép. Organosilicon surface layer on polyolefins to achieve improved flame retardancy through an oxygen barrier effect. Polymer Degradation and Stability, 2001, 74, 419-422.

[56] B. Li, M. Xu. Effect of a novel charring-foaming agent on flame retardancy and thermal degradation of intumescent flame retardant polypropylene. Polymer Degradation and Stability, 2006, 91, 1380-1386.

[57] J.W. Gu, G.C. Zhang, S.L. Dong, Q.Y. Zhang, J. Kong. Study on preparation and fire-retardant mechanism analysis of intumescent flame-retardant coatings. Surface and Coatings Technology, 2007, 201, 7835-7841.

[58] M. Modesti, A. Lorenzetti, F. Simioni, G. Camino. Expandable graphite as an intumescent flame retardant in polyisocyanurate–polyurethane foams. Polymer Degradation and Stability, 2002, 77, 195-202.

[59] F. Laoutid, L. Bonnaud, M. Alexandre, J.M. Lopez-Cuesta, Ph. Dubois. New prospects in flame retardant polymer materials: From fundamentals to nanocomposites. Materials Science and Engineering: R: Reports, 2009, 63, 100-125.

[60] B.K. Kandola, D. Price, G.J. Milnes, A.D. Silva. Development of a novel experimental technique for quantitative study of melt dripping of themoplastic polymers. Polymer Degradation and Stability, 2013, 98, 52-63.

[61] Source: Townsend Solutions Estimate. The flame retardants market. 2011. http://www.flameretardants-online.com

[62] M.J.L. Guardia, R.C. Hale, E. Harvey, T.M. Mainor, S. Ciparis. In situ accumulation of HBCD, PBDEs, and several alternative flame-retardants in the bivalve (Corbicula fluminea) and Gastropod (Elimia proxima). Environmental Science & Technology, 2012, 46, 5798-5805.

[63] N. Pecoul, S. Bourbigot, B. Revel. C-13, Mg-25 and B-11 solid-state NMR study of a fire retarded ethylene-vinyl acetate copolymer. Macromolecular Symposia, 1997, 119, 309-315

[64] P. Intharapat, C. Nakason, A. Kongnoo. Preparation of boric acid supported natural rubber as a reactive flame retardant and its properties. Polymer Degradation and Stability, 2016, 128, 217-227

[65] X. Qian, L. Song, B. Yuan, Y. Shi, Y. Hu, R.K. Yuen. Organic/inorganic flame retardants containing phosphorus, nitrogen and silicon: Preparation and their performance on the flame retardancy of epoxy resins as a novel intumescent flame retardant system. Materials Chemistry and Physics, 2014, 143, 1243-1252.

[66] F. Liao, L. Zhou, Y. Ju, Y. Yang, X. Wang. Synthesis of a novel phosphorus-nitrogen-silicon polymeric flame retardant and its application in poly(lactic acid). Industrial & Engineering Chemistry Research, 2014, 53, 10015-10023.

[67] Y. Liu, J.S. Wang, C.L. Deng, D.Y. Wang, Y.P. Song, Y.Z. Wang. The synergistic flame-retardant effect of O-MMT on the intumescent flame-retardant PP/CA/APP systems. Polymers for Advanced Technologies, 2010, 21, 789-796.

[68] H. Qin, S. Zhang, C. Zhao, G. Hu, M. Yang. Flame retardant mechanism of polymer/clay nanocomposites based on polypropylene. Polymer, 2005, 46, 8386-8395.

[69] D.Y. Wang, Y.Z. Wang, J.S. Wang, D.Q. Chen, Q. Zhou, B. Yang, W.Y. Li. Thermal oxidative degradation behaviours of flame-retardant copolyesters containing phosphorous linked pendent group/montmorillonite nanocomposites. Polymer Degradation and Stability, 2005, 87, 171-176.

[70] E.N. Kalali, X. Wang, D.Y. Wang. Functionalized layered double hydroxide-based epoxy nanocomposites with improved flame retardancy and mechanical properties. Journal of Materials Chemistry A, 2015, 3, 6819-6826.

[71] G. Beyer. Short cmmunication: carbon nanotubes as flame retardants for polymers. Fire Mater, 2002, 26, 291-293.

[72] S. Bourbigot, T. Turf, S. Bellayer, S. Duquesne. Polyhedral oligomeric silsesquioxane as flame retardant for thermoplastic polyurethane. Polymer Degradation and Stability, 2009, 94, 1230-1237.

[73] Y. Hu, X. Qian, L. Song, H. Lu. Polymer/layered compound nanocomposites: a way to improve fire safety of polymeric materials. Fire Safety Science, 2014, 11, 66-82.

[74] E.D. Weil. Fire-protective and flame-retardant coatings-a state-of-the-art review. Journal of Fire Sciences, 2011, 29, 259-296.

[75] M.L. Bras, S. Bourbigot, G. Camino, R. Delobel. Fire retardancy of polymers: the use of intumescence. Elsevier Science & Technology, 1998, ISBN: 978185573-8041

[76] G. Camino, L. Costa. Mechanism of intumescence in fire retardant polymers. Reviews in Inorganic Chemistry, 1986, 6, 69-100.

[77] G. Camino. Flame retardants: intumescent systems. Plastics Additives Volume 1 of the series Polymer Science and Technology, 1998, 297-306.

[78] C.M. Tai, R.Y. Li. Mechanical properties of flame retardant filled polypropylene composites. Journal of Applied Polymer Science, 2001, 80, 2718-2728.

[79] P. Song, Y. Shen, B. Du, M. Peng, L. Shen, Z. Fang. Effects of reactive compatibilization on the morphological, thermal, mechanical, and rheological properties of intumescent flame-retardant polypropylene. ACS Applied Materials & Interfaces, 2009, 1, 452-459.

[80] C.H. Ke, J. Li, K.Y. Fang, Q.L. Zhu, J. Zhu, Q. Yan, Y.Z. Wang. Synergistic effect between a novel hyperbranched charring agent and ammonium polyphosphate on the flame retardant and anti-dripping properties of polylactide. Polymer Degradation and Stability, 2010, 95, 763-770.

[81] Q. Zhang, Y. Chen. Synergistic effects of ammonium polyphosphate/melamine intumescent system with macromolecular char former in flame-retarding polyoxymethylene. Journal of Polymer Research, 2011, 18, 293-303.

[82] W.K.P. Lim, M. Mariatti, W.S. Chow, K.T. Mar. Effect of intumescent ammonium polyphosphate (APP) and melamine cyanurate (MC) on the properties of epoxy/glass fiber composites. Composites Part B: Engineering, 2012, 43, 124-128.

[83] Y. Liu, Q. Wang. Catalytic action of phospho-tungstic acid in the synthesis of melamine salts of pentaerythritol phosphate and their synergistic effects in flame retarded polypropylene. Polymer Degradation and Stability, 2006, 91, 2513-2519.

[84] S. Bourbigot, M.L. Bras, S. Duquesne, M. Rochery. Recent advances for intumescent polymers. Macromolecular Materials and Engineering, 2004, 289, 499-511.

[85] Y. Liu, D.Y. Wang, J.S. Wang, Y.P. Song, Y.Z. Wang. A novel intumescent flame-retardant LDPE system and its thermo-oxidative degradation and flame-retardant mechanisms. Polymers for Advanced Technologies, 2008, 19, 1566-1575.

[86] C.H. Ke, J. Li, K.Y. Fang, Q.L. Zhu, J. Zhu, Q. Yan, Y.Z. Wang. Synergistic effect between a novel hyperbranched charring agent and ammonium polyphosphate on the flame retardant and anti-dripping properties of polylactide. Polymer Degradation and Stability, 2010, 95, 763-770.

[87] H. Ma, L. Tong, Z. Xu, Z. Fang, Y. Jin, F. Lu. A novel intumescent flame retardant: Synthesis and application in ABS copolymer. Polymer Degradation and Stability, 2007, 92, 720-726.

[88] D.Q. Chen, Y.Z. Wang, X.P. Hu, D.Y.Wang, M.H. Qu, B. Yang. Flame-retardant and anti-dripping effects of a novel char-forming flame retardant for the treatment of poly(ethylene terephthalate) fabrics. Polymer Degradation and Stability, 2005, 88, 349-356.

[89] X.P. Hu, Y.L. Li, Y.Z. Wang. Synergistic effect of the charring agent on the thermal and flame retardant properties of polyethylene. Macromolecular Materials and Engineering, 2004, 289, 208-212.

[90] C.H. Ke, J. Li, K.Y. Fang, Q.L. Zhu, J. Zhu, Q. Yan, Y.Z. Wang. Synergistic effect between a novel hyperbranched charring agent and ammonium polyphosphate on the flame retardant and anti-dripping properties of polylactide. Polymer Degradation and Stability, 2010, 95, 763-770.

[91] S.S. Mahapatra, N. Karak. s-Triazine containing flame retardant hyperbranched polyamines: Synthesis, characterization and properties evaluation. Polymer Degradation and Stability, 2007, 92, 947-955.

[92] J. Dai, B. Li. Synthesis, thermal degradation, and flame retardance of novel triazine ring-containing macromolecules for intumescent flame retardant polypropylene. Journal of Applied Polymer Science, 2010, 116, 2157-2165.

[93] C. Feng, Y. Zhang, S. Liu, Z. Chi, J. Xu. Synthesis of novel triazine charring agent and its effect in intumescent flame-retardant polypropylene. Journal of Applied Polymer Science, 2012, 123, 3208-3216.

[94] S. Nie, Y. Hu, L. Song, Q. He, D. Yang, H. Chen. Synergistic effect between a char forming agent (CFA) and microencapsulated ammonium polyphosphate on the thermal and flame retardant properties of polypropylene. Polymers for Advanced Technologies, 2008, 19, 1077-1083.

[95] B. Wang, X. Wang, G. Tang, Y. Shi, W. Hu, H. Lu, L. Song,Y. Hu. Preparation of silane precursor microencapsulated intumescent flame retardant and its enhancement on the properties of ethylene-vinyl acetate copolymer cable. Composites Science and Technology, 2012, 72, 1042-1048.

[96] Q. Tang, B. Wang, Y. Shi, L. Song, Y. Hu. Microencapsulated ammonium polyphosphate with glycidyl methacrylate shell: application to flame retardant epoxy resin. Industrial & Engineering Chemistry Research, 2013, 52, 5640-5647.

[97] G.B. Quistad, N. Zhang, S.E. Sparks, J.E. Casida. Phosphoacetylcholinesterase: toxicity of phosphorus oxychloride to mammals and insects that can be attributed to selective phosphorylation of acetylcholinesterase by phosphorodichloridic acid. Chemical Research in Toxicology, 2000, 13, 652-657.

[98] G. Matheis. Phosphorylation of food proteins with phosphorus oxychloride-Improvement of functional and nutritional properties: A review. Food Chemistry, 1991, 39, 13-26.

[99] F. M. Veronese, R. Largajolli, E. Boccú, C.A. Benassi, O. Schiavon. Surface modification of proteins activation of monomethoxy-polyethylene glycols by phenylchloroformates and modification of ribonuclease and superoxide dismutase. Applied Biochemistry and Biotechnology, 1985, 11, 141-152.

[100] L. Zhang, X.Q. Liu, Y. Li, H. Yuan. Risk analysis of environmental pollution by secondary hydrogen chloride from leakage of phosphorus trichloride. Applied Mechanics and Materials, 2014, 675, 213-216.

[101] B. Puschner, R.H. Poppenga, L. Lowenstine, M. S. Filigenzi, P. A. Pesavento. Assessment of melamine and cyanuric acid toxicity in cats. Journal of Veterinary Diagnostic Investigation, 2007, 19, 616-624.

[102] S. Pavlidou, C.D. Papaspyrides. A review on polymer-layered silicate nanocomposites. Progress in Polymer Science, 2008, 33, 1119-1198.

[103] P. Kiliaris, C.D. Papaspyrides. Polymer/layered silicate (clay) nanocomposites: An overview of flame retardancy. Progress in Polymer Science, 2010, 35, 902-958.

[104] A.B. Morgan. Flame retarded polymer layered silicate nanocomposites: a review of commercial and open literature systems. Polymer, 2006, 17, 206-217.

[105] Y. Tang, Y. Hu, B. Li, L. Liu, Z. Wang, Z. Chen, W. Fan. Polypropylene/montmorillonite nanocomposites and intumescent, flame-retardant montmorillonite synergism in polypropylene nanocomposites. Journal of Polymer Science Part A: Polymer Chemistry, 2004, 42, 6163-6173.

[106] H. Qin, S. Zhang, C. Zhao, G. Hu, M. Yang. Flame retardant mechanism of polymer/clay nanocomposites based on polypropylene. Polymer, 2005, 46, 8386-8395.

[107] L. Haurie, A.I. Fernández, J.I. Velasco, J.M. Chimenos, J.L.Cuesta, F. Espiell. Thermal stability and flame retardancy of LDPE/EVA blends filled with synthetic hydromagnesite/aluminium hydroxide/montmorillonite and magnesium hydroxide/aluminium hydroxide/montmorillonite mixtures. Polymer Degradation and Stability, 2007, 92, 1082-1087.

[108] Reportlinker global polyolefins (PO) market - Segmented by type, application and geography - trends and forecasts (2015-2020) - Reportlinker Review. 2015, http://www.reportlinker.com

[109] K.D. Gagnon, R.W. Lenz, R.J. Farris, R.C. Fuller. Chemical modification of bacterial elastomers: 1. Peroxide crosslinking. Polymer, 1994, 5, 4358-4367.

[110] C. Decker. The use of UV irradiation in polymerization. Polymer International, 1998, 45, 133-141.

[111] S. Camara, B.C. Gilbert, R.J. Meier, M. Duin, A.C. Whitwood. EPR studies of peroxide decomposition, radical formation and reactions relevant to cross-linking and grafting in polyolefins. Polymer, 2006, 47, 4683-4693.

[112] R. Anbarasan, O. Babot, B. Maillard. Crosslinking of high density polyethylene in the presence of organic peroxides. Journal of Applied Polymer Science, 2004, 93, 75-81.

[113] D. Vaillant. Ultraviolet radiation stabilized polyolefins, Nr. US 7259198 B2

[114] F. Truica-Marasescu, M.R. Wertheimer. Vacuum ultraviolet–induced photochemical nitriding of polyolefin surfaces. Journal of Applied Polymer Science, 2004, 91, 3886-3898.

[115] R.L. Clough. High-energy radiation and polymers: A review of commercial processes and emerging applications. Nuclear Instruments and Methods in Physics Research Section B: Beam Interactions with Materials and Atoms, 2001, 185, 8-33.

[116] M. Mondal, U. Gohs, U. Wagenknecht, G. Heinrich. High-performance, natural rubber thermoplastic elastomers using accelerated electrons. Society of Plastics Engineers, 2013, 1-3

[117] D.Y. Wang, U. Gohs, N.J. Kang, A. Leuteritz, R. Boldt, U. Wagenknecht, G. Heinrich. Method for simultaneously improving the thermal stability and mechanical properties of poly(lactic acid): effect of high-energy electrons on the morphological, mechanical, and thermal properties of PLA/MMT nanocomposites. Langmuir, 2012, 28, 12601-12608.

[118] V. Thakur, A. Leuteritz, U. Gohs, B. Kretzschmar, U. Wagenknecht , A.K. Bhowmick, G. Heinrich. Montmorillonite nanocomposites with electron-beam modified atactic polypropylene. Applied Clay Science, 2010, 49, 200-204.

[119] K. Naskar, U. Gohs, G. Heinrich. Influence of molecular structure of blend components on the performance of thermoplastic vulcanisates prepared by electron induced reactive processing. Polymer, 2016, 91, 203-210.

[120] M. Mondal, U. Gohs, U. Wagenknecht, G. Heinrich. Efficiency of high energy electrons to produce polypropylene/natural rubber-based thermoplastic elastomer. Polymer Engineering and Science, 2013, 1696-1705.

[121] U. Gohs, L. Girdauskaite, L. Peitzsch, S. Rothe, C. Zschech, G. Heinrich, H. Rödel. Crosslinked continuous glass fiber-reinforced toughened polypropylene composites. Advanced Engineering Materials, 2016, 18, 409-416.

[122] A. Jorge, B.S. Sugranes, M.C. Bsic. Basic operating principles and validation of electron beam irradiation systems. Journal of Validation Technology, 2005, 64-69.

[123] J.G. Drobny. Radiation technology for polymers, CRC Press, 2010, ISBN: 9781420094046 - CAT# 94041.

[124] M.K. Mishra, Y. Yagci. Handbook of vinyl polymers: radical polymerization, CRC Press. 2008, ISBN: 9 9780824725952 - CAT# DK3074.

[125] K. Naskar. Dynamically vulcanized PP/EPDM thermoplastic elastomers: Exploring novel routes for crosslinking with peroxides. Ph.D. Thesis, 2014, ISBN: 9036520452.

[126] X. Chen, J. Yu, S. Guo, Z. Luo, M. He. Effects of magnesium hydroxide and its surface modification on crystallization and rheological behavior of polypropylene. Polymer Composites, 2009, 30, 941-947.

[127] H. Dong, Z. Du, Y. Zhao, D. Zhou. Preparation of surface modified nano-$Mg(OH)_2$ via precipitation method. Powder Technology, 2010, 198, 325-329.

[128] C.M. Liauw, G.C. Lees, S.J. Hurst, R.N. Rothon, S. Ali. Effect of silane-based filler surface treatment formulation on the interfacial properties of impact modified polypropylene/magnesium hydroxide composites. Composites Part A: Applied Science and Manufacturing, 1998, 29, 1313-1318.

[129] M. Shafiq, T. Yasin. Effect of gamma irradiation on linear low density polyethylene/magnesium hydroxide/sepiolite composite. Radiation Physics and Chemistry, 2012, 81, 52-56.

[130] H. Liu, Z. Fang, M. Peng, L. Shen, Y. Wang. The effects of irradiation cross-linking on the thermal degradation and flame-retardant properties of the HDPE/EVA/magnesium hydroxide composites. Radiation Physics and Chemistry, 2009, 78, 922-926.

[131] F. Costa. Mg-Al layered double hydroxide: a potential nanofiller and flame-retardant for polyethylene. Ph.D. Thesis. 2007, URN: 14119548181199227563.

[132] C.H. Hong, Y. B. Lee, J.W. Bae, J. Y. Jho, B. U. Nam, G.J. Nam, K.J. Lee. Tensile and flammability properties of polypropylene-based RTPO/clay nanocomposites for cable insulating material. Journal of Applied Polymer Science, 2005, 97, 2375-2381.

[133] V. Thakur, U. Gohs, A. Leuteritz, U. Wagenknecht, G. Heinrich. Polymer nanocomposites with layered minerals, and method for producing same. 2011, EP 2643389B1.

[134] UL 94, The standard for safety of flammability of plastic materials for parts in devices and appliances testing. Underwriters Laboratories Inc. 1996.

[135] The international organization for standardization. ISO 5660-1.2002.

[136] V. Babrauskas, R.D. Peacock. Heat release rate: the single most important variable in fire hazard. Fire Safety, 1992, 18, 255-261.

[137] G. Camino, L. Costa, L. Trossarelli. Study of the mechanism of intumescence in fire retardant polymers: Part V-Mechanism of formation of gaseous products in the thermal degradation of ammonium polyphosphate. Polymer Degradation and Stability, 1985, 12, 203-211.

[138] Y. Tan, Z.B. Shao, X.F. Chen, J.W. Long, L. Chen, Y.Z. Wang. Novel multifunctional organic-inorganic hybrid curing agent with high flame-retardant efficiency for epoxy resin. ACS Applied Materials & Interfaces, 2015, 7, 17919-17928.

[139] Y.W. Yan, L. Chen, R.K. Jian, S. Kong, Y.Z. Wang. Intumescence: an effect way to flame retardance and smoke suppression for polystryene. Polymer Degradation and Stability, 2012, 97, 1423-1431.

[140] B. Krause, D.Voigt, Haeussler, L, H. Auhl, D. Muenstedt. Characterization of electron beam irradiated polypropylene: Influence of irradiation temperature on molecular and rheological properties. Journal of Applied Polymer Science, 2006, 100, 2770-2780.

[141] B. Schartel, M. Bartholmai, U. Knoll. Some comments on the use of cone calorimeter data. Polymer Degradation and Stability, 2005, 88, 540-547.

List of figures

List of tables

List of publications

Publications:

Dan Xiao, Zhi Li, Uwe Gohs, Udo Wagennecht, Brigitte Voit, De-Yi Wang. Functionalized allylamine polyphosphate as novel multifunctional highly efficient fire retardant for polypropylene. Polymer Chemistry, 2017, DOI:10.1039/C7PY01315A.

Dan Xiao, Zhi Li, Sergio De Juan, Uwe Gohs, Udo Wagenknecht, Brigitte Voit, De-Yi Wang. Preparation, fire behavior and thermal stability of a novel flame retardant polypropylene system. Journal of Thermal Analysis and Calorimetry, 2016, Volume 125, pp 321-329.

Xiaomin Zhao, Dan Xiao, Juan Picón Alonso, De-Yi Wang. Inclusion complex between beta-cyclodextrin and phenylphosphonicdiamide as novel bio-based flame retardant to epoxy: Inclusion behavior, characterization and flammability. Materials & Design, 2017, Volume 114, pp 623-632.

Dan Xiao, Zhi Li, Xiaomin Zhao, Uwe Gohs, Udo Wagennecht, Brigitte Voit, De-Yi Wang. Functional organoclay with high thermal stability and its synergistic effect on intumescent flame retardant polypropylene. Applied Clay Science, 2017, Volume 143, pp 192-198.

Preparation and burning behavior of novel flame retardant polypropylene nanocomposites based on allylamine polyphosphate and montmorillonit. (Preparation)

Fire behavior, thermal stability and tensile properties of a novel efficient flame retarded polypropylene containing allylamine polyphosphate and pentaerythritol. (Preparation)

The high energy electrons effect of flame-retardant polypropylene nanocomposites on reduced heat and smoke toxicity release. (Preparation)

Development of flame-retardant polypropylene nanocomposites by eco-friendly electron induced reactive processing. (Preparation)

Patents:

Preparation of novel polyphosphate and its use as flame-retardant crosslinker to polymers under electron beam treatment. (Application Nr. EP 16200748.8)

Conferences:

Oral presentations

Dan Xiao, Uwe Gohs, Udo Wagennecht, Brigitte Voit, De-Yi Wang. Development and Investigation of High Performance Fire Retardant Polypropylene Composites. PPS Europe/Africa Conference. June 26-29 2017, Dresden.

Dan Xiao, Uwe Gohs, Udo Wagennecht, Brigitte Voit, De-Yi Wang. Novel Flame Retardant Polypropylene Based Nanocomposites. 7th Asia-Europe Symposium on Processing and Properties of Reinforced Polymers (AESP7). February, 4-6 2015, Madrid.

Posters

Xiaomin Zhao, Dan Xiao, Udo Wagennecht, Gert Heinrich, De-Yi Wang. Novel Eco-friendly Flame-retardant Coating to Cotton Textile. Aachen-Dresden-Denkendorf International Textile Conference. November 24-25 2016, Dresden.

Versicherung

Hiermit versichere ich, dass ich die vorliegende Arbeit ohne unzulässige Hilfe Dritter und ohne Benutzung anderer als der angegebenen Hilfsmittel angefertigt habe; die aus fremden Quellen direkt oder indirekt übernommenen Gedanken sind als solche kenntlich gemacht. Die Arbeit wurde bisher weder im Inland noch im Ausland in gleicher oder ähnlicher Form einer anderen Prüfungsbehörde vorgelegt.

Die Dissertation wurde vom Februar 2014 bis Februar 2017 am Leibniz-Institut für Polymerforschung Dresden e.V. im Rahmen des Projktes zum Thema: “Development and Investigation of High-Performance Fire Retardant Polypropylene Nanocomposites via High Energy Electrons” unter der wissenschaftlicher Betreuung von Herr Dr. Uwe Gohs, Herr Prof. Dr. De-Yi Wang und Frau Prof. Brigitte Voit durchgeführt.

Frühere erfolglose Promotionsverfahren haben nicht stattgefunden.

Ich erkenne die Promotionsordnung der Fakultät Mathematik und Naturwissenschaften der Technischen Universität Dresden vom 23.02.2011, inclusive der Änderungen vom 15.06.2011 und 18.06.2014 durch Beschlüsse des Fakultätsrates, in vollem Umfang an.

Dan Xiao

25.06.2017